Utilizing Inverted Colloidal Crystal Scaffolds to Engineer In Vitro Bone and Bone Marrow

by

Meghan J. Cuddihy

A dissertation submitted in partial fulfillment
of the requirements for the degree of
Doctor of Philosophy
(Chemical Engineering)
in The University of Michigan
2010

Doctoral Committee:

Professor Nicholas A. Kotov, Chair
Professor Scott J. Hollister
Professor Jennifer J. Linderman
Associate Professor Joerg Lahann

© Meghan J. Cuddihy 2010
All Rights Reserved

To my parents, Glenn and Patricia.

ACKNOWLEDGEMENTS

I would like to thank my advisor, Professor Nicholas Kotov, for his support and guidance for the last six years. I thank you for allowing me to pursue a research topic that was practical and applicable. No matter what I was interested in, be it a research topic, conference, internship, business plan, or fun idea for a lab party, your support and encouragement was always outstanding. You have a special way of creating a group that is happy and supportive. I would also like to thank my committee members, Professors Scott Hollister, Jennifer Linderman, and Joerg Lahann. Your advice during our meetings has been especially helpful.

I cannot thank enough the various Kotov lab members that have helped me along the way. I would especially like to thank the most permanent of my office mates, Daniel, Ashish, Christine, Edward, and Peter. We have shared so many laughs, procrastinated, and worked together throughout the years. Special thanks to Jungwoo, who introduced me to the lab, ICC scaffolds, and cell culture. I learned so much from you. Christine, thanks for running many miles with me and being a sounding board for everything on my mind. Paul, your ability to be a winner always inspired me. A big thank you to the undergraduates that have helped me out through out the years, especially Charles, for your help and patience. Many thanks to all of the other Kotov group members, past and present, for being such wonderful, supportive, and inspiring people.

I would not be the person who I am today without the friends in my life. First, I would like to thank the Chemical Engineering Class of 2003 at Cornell University,

especially Regan, Andra, Tracy, Kevin, Drew, Ed, Jen, Herberg, Joe, Cody, Scott, Fernanda, Senra, and Satch. From ChemE 112 to graduation, we really grew up together. I have so many fond memories with everyone. Thank you for getting me through the program, and for being such normal engineers and supportive people to work with. Most importantly, thank you for all leading such inspiring lives with careers, travels, hobbies, and personalities I can look up to. To the Chemical Engineering Graduate Students, their spouses, and other friends at Michigan, I thank you for being such fun and supportive people. I am excited to see where we will all end up and the lives we will lead.

I am sincerely grateful to have had Tom in my life for the last two years. You have been a great listener and source of encouragement while finishing graduate school. I can't wait to see where our lives lead us.

Lastly, I would like to thank my parents. Your support throughout my life has been amazing and unwavering. Thank you for always pushing me to explore and develop myself as a person. Thank you to Mom for always being such a sweet and encouraging person, and for always sticking up for me. Thank you to Dad for always pushing me to be my best, from Friendly's dinners to encouraging me to apply to the best colleges I could. Both of you always saw more potential in me than I did.

TABLE OF CONTENTS

LIST OF FIGURES

Figure

LIST OF TABLES

Table

LIST OF ABBREVIATIONS

2D two dimensional

3D three dimensional

ALP alkaline phosphatase

AMTAC (3-Acrylamidopropyl)trimehtylammonium chloride

APC allophycocyanin

ATCC American Tissue Culture Corporation

BM bone marrow

CB cord blood

CC colloidal crystal

CFSE carboxyfluorescein diacetate succinimidyl ester

cm centimeter

CML Chronic myelogenous leukemia

D diameter

DMAA N,N-dimethylacrylamide

DMEM Dulbeccos modified Eagles Medium

DNA deoxyribonucleic acid

ECM extracellular matrix

EDTA ethylenediaminetetraacetic acid

ELISA Enzyme-linked immunosorbent assay

EPO erythropoietin

FBS fetal bovine serum

FITC fluorescein isothiocyanate

flt-3 fms-like tyrosine kinase receptor-3

GPa gigapascal

GlyA glycophorin A

HA hydroxyapatite

HCl hydrochloric acid

HCP hexagonally close-packed

HF hydrofluoric acid

hFOB Human fetal osteoblast

HSC hematopoietic stem cell

HS human stromal

ICC inverted colloidal crystal

IgG immunoglobulin G

IgM immunoglobulin M

IL-6 interleukin-6

IU international units

lin1 lineage cocktail 1

KPS potassium persulfate

LBL Layer-by-layer

M molar

MBA N,N-Methylenebis(acrylamide)

MPa megapascal

MTX methotrexate

PB peripheral blood

PBS phosphate buffered saline

PDDA poly(diallyldimethylammonium chloride)

PE phycoerythrin

PEG polyethylene glycol

PGA polyglycolic acid

PI propidium iodide

PLA polylactic acid

PLGA poly(lactic-co-glycolic acid)

p-NP 4-nitrophenol

p-NPP 4-nitrophenyl phosphate

RPM rotations per minute

SCF stem cell factor

SEM scanning electron microscopy

SFF solid free-form

TKI tyrosine kinase inhibitor

ABSTRACT

Numerous studies have shown that cells and tissues grown in 2D substrates behave dramatically differently than in the body, and that culturing them in three dimensional (3D) scaffolds can restore some of this lost functionality. 3D scaffolds can provide structural support to an injury site in the body, aiding the growth of healthy tissue. Outside of the body, scaffolds can be used to test pharmaceuticals, collecting data in an environment that represents the body better than traditional 2D cultures. This could potentially save millions of dollars in drug development costs.

For these reasons, this dissertation focuses on the utilization of inverted colloidal crystal (ICC) scaffolds for bone and bone marrow engineering. ICC scaffolds are matrices that have a highly ordered 3D structure of interconnected spherical cavities. This dissertation describes the first ICC scaffold composed of a biodegradable polymer, poly(lactic-co-glycolic acid) (PLGA). Within these scaffolds, the scaffold cavity sizes were controlled on the micro-scale by utilizing different beads sizes, 100, 200, and 330 μm, as the scaffold template. Additionally, the size of the channels that connect the cavities were controlled within the range of 660-710 °C by changing the annealing temperature. The compressive moduli of these scaffolds were in the range of 55-63 MPa. Lastly, biocompatibility with a human osteoblast cell line was demonstrated.

Next, the dissertation utilized polyacrylamide hydrogel ICC scaffolds to engineer a human hematopoietic stem cell (HSC) niche. ICC scaffolds demonstrated significantly greater HSC expansion than 2D cultures. This work was continued by comparing the ICC scaffolds to Matrigel and 2D cultures. Here, it was observed that ICC cultures

demonstrated stable numbers of HSCs throughout 14 days. 2D cultures expanded the number of HSCs 6-8× over 14 days and Matrigel cultures expanded differentiated cells but few HSCs. These results indicated that physical cell-cell interactions cause quiescence or preservation of the HSC phenotype, and the absence of direct cell-cell interactions causes HSC differentiation. Lastly, preliminary data was collected in utilizing ICC scaffolds as a tool for drug testing.

CHAPTER I

Introduction

1.1 Introduction to 3D cell culture

The human body is a complex system of organs and tissues. Within each tissue lies a dynamic environment of many cell types, extracellular matrix (ECM) molecules, ions, soluble proteins, and other soluble signaling molecules. For years, scientists have grown cells *in vitro*, cultures outside of the body, to learn about the functions and interactions between the different cell types. These early cultures were composed of cells growing on two dimensional (2D) surfaces, such as petri dishes, and brought forth a great many discoveries about cellular biology [1] and how to manipulate them to yield commercial products, such as the polio vaccine [2]. An important use for 2D cell cultures has been the testing of efficacy and toxicity of pharmaceuticals.

Despite the many advances that came from 2D cell cultures, cells lose a great deal of functionality when they are grown on flat surfaces. Fig 1.1 demonstrates the obvious differences between cells grown on 2D surfaces and those in the body. For example, bone is composed mainly of ECM, primarily type I collagen and hydroxyapatite, with cells dispersed through the matrix. On the surface of bone, osteoblasts lie in sheets in a cuboidal configuration (Fig 1.1A). *In vitro*, cells lie flat on 2D surfaces (Fig 1.1B). Likewise, hepatocytes, the basic cell type of the liver, form hexagonal lobules separated by connective tissue in the body (Fig 1.1D) [3], but lie flat in 2D (Fig 1.1E). In the thymus, lymphocytes exist in suspension (Fig 1.1G) but lie unnat-

urally when cultured on in 2D (Fig 1.1H).

Many of the architectural and functional aspects of these cell types are regained when they are cultured in a more complex microenvironment. When grown in 3D matrices, also called scaffolds, the cell types in Fig 1.1 regain some of the morphology and function that is seen *in vivo* (Figs. 1.1C, F, and I). T cells [4], breast epithelial cells [5], and ovarian follicles [6] have been shown to regain functionalities in 3D matrices. For these reasons, the applications of 3D cell culture have expanded since its first conception 30 years ago [7].

1.2 Applications of 3D cell cultures

In the most basic sense, scaffolds are 3D porous structures that can support cell attachment and growth. With further engineering, some scaffolds have been tailored to cause cellular organization or differentiation [13–17]. The ultimate goal of utilizing 3D scaffolds for cell culture is to engineer tissues or tissue-like models for either implantation into the body to aid recovery of damaged tissues or to study cells or tissues *ex vivo*.

Tissue engineering, one of the most prominent applications for 3D cell culture, aims to replace or aid the healing of damaged or diseased tissues in the body [18]. One approach to tissue engineering is to utilize a 3D matrix to grow tissues *in vitro* that can be used as an off-the-shelf supply to implant into patients. For example, a readily available supply of skin could be used to save victims with severe burns [19]. Another approach aims to insert the matrix in the body, possibly in combination with cells and/or signals, to support the wound site as body tissue grows into the implant. Such an approach is especially progressed in the areas of bone and cartilage engineering [20–22]. In each case, the matrix would theoretically degrade so that only new healthy tissue remains.

3D cultures can also be used to increase basic understanding of the body. Here,

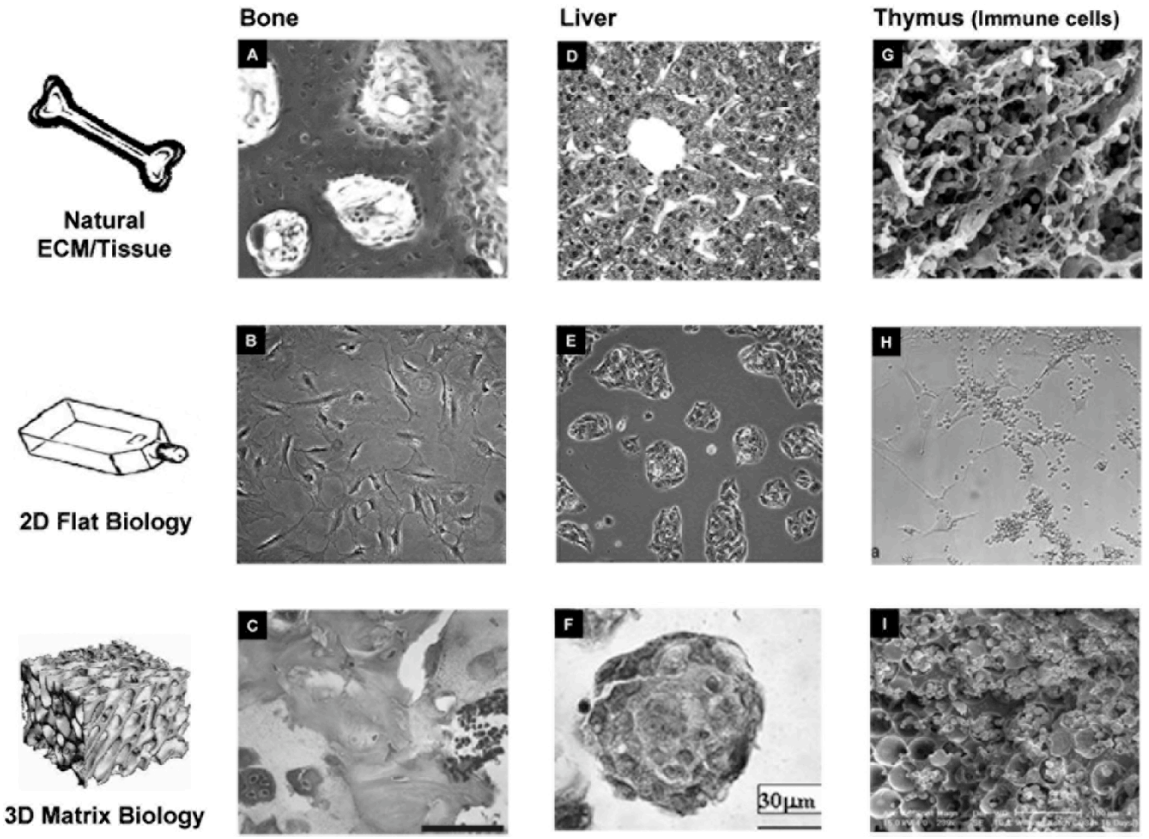

Figure 1.1: Organization of natural tissue, 2D cell cultures, and 3D cell cultures [8]. (A, D) Histological images of (A) bone and (D) liver [3]. (G) Scanning electron microscope image of the thymus [9]. (B, E, H) Optical microscope images of cells grown on 2D substrates. (B) osteoblasts, (E) hepatocytes, and (H) co-culture of lymphocytes and stromal cells [9]. Cellular morphology becomes closer to that of natural tissue when cultured on 3D matrices; different appearance of (C) osteoblasts [10] (F) hepatocytes [11], and (I) mononuclear cells in a 3D matrix [12].

one could isolate one or several cells from the body and study cell-cell or cell-matrix interactions in the scaffold. For example, engineered 3D tumor models gave light to the growth factors that may be involved in the development of new blood vessels in tumors [23]. Similar 3D tumor models have elucidated enzymes that facilitate cancer growth [24].

The last application to be considered is the use of *in vitro* cells and tissues for pharmaceutical drug testing. A major problem with the current drug development

paradigm is that potential drugs are not introduced into humans until late in the testing process. Cells growing in 2D are an oversimplified model of the body, and animal testing is not always accurate. As a result, it is not known whether a drug will be effective until after 10 years and millions of dollars of investment. It is possible that an *ex vivo* 3D model in which cells are behaving more like the human body would be a predictive tool for drug testing, lessening the time and money spent on development. Here, cells or tissues would be cultured in a 3D matrix so that their behavior mimics that of tissues in the human body. Cultured in a well-plate format, healthy or diseased model tissues could be used in a high-throughput environment to predict how the body will react to the drug.

1.3 Introduction to ICC scaffolds

The studies in this dissertation focus on the use of ICC scaffolds for bone and bone marrow engineering. ICCs were developed by the Kotov group as 3D matrices with precise feature size control [8, 25–29]. The ICC manufacturing process is depicted in Fig 1.2. First, a template of tightly-packed array of uniformly-sized microspheres, called a colloidal crystal (CC), is created by slow deposition of beads into a mold under agitation. Next, the microspheres are heated above their glass transition temperature so that the beads slightly connect to one another, forming a solid structure. A liquid polymer solution is then infiltrated into the template and the polymer is solidified, either by evaporating solvent (organic-soluble polymers) or crosslinking (hydrogels). Lastly, the bead template is dissolved, leaving behind an ICC. In this structure, the cavities exist where the microspheres had been, interconnected by channels where the beads were annealed together.

ICC scaffolds have been used in a variety of applications. The first ICC scaffolds were composed of silicate, and were shown to support the growth of hepatocytes and bone marrow stromal cells [26, 28]. Next, the scaffolds were fabricated utilizing

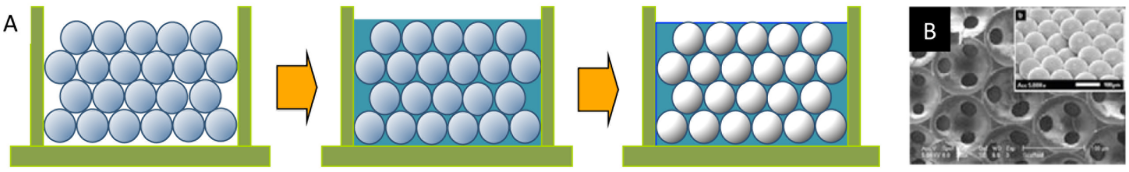

Figure 1.2: Schematic of ICC fabrication process. (A) CCs are produced by sedimenting uniformly-sized microspheres into an ordered array. Next, the microspheres are annealed and the space around the spheres is infiltrated with a liquid solution of the scaffold material. Last, the beads are dissolved, leaving an ordered array of cavities with connections where the beads had touched. (B) SEM image of ICC scaffold and ordered microsphere template (inset).

polyacrylamide hydrogel [27, 29]. The polyacrylamide in these studies held a neutral surface charge and did not facilitate cell attachment. As a result, the scaffolds were coated with Layer-by-layer (LBL) applied films to make possible cell attachment for the cell types mentioned above, as well as HSCs [12, 30] (Fig 1.3A). The neutral properties of polyacrylamide were taken advantage of in ICC scaffolds to grow hepatocyte spheroids (Fig 3B) [8, 31]. The cells assembled into spheroids within the ICC cavities because the cell-cell attractions were stronger than cell-scaffold attractions (Fig 1.3B). Most recently, a cationic polyacrylamide was developed to facilitate cell attachment without LBL surface coatings [32]. In addition to the various hydrogel scaffolds mentioned above, ICC scaffolds were fabricated utilizing a biodegradable polymer for bone tissue engineering that facilitated the attachment of osteoblasts [25].

ICC scaffolds, particularly those that are made of hydrogel, have several major advantages over other matrices. First, the high degree of order yields little scaffold-to-scaffold variation, allowing for more reliable data collection. The matrix is transparent, so that the user can view live cells directly in the scaffold via confocal microscopy. Last, hydrogel matrix is not reorganized by the cells so, unlike ECM-based matrices, the structure does not change or disappear throughout the culture.

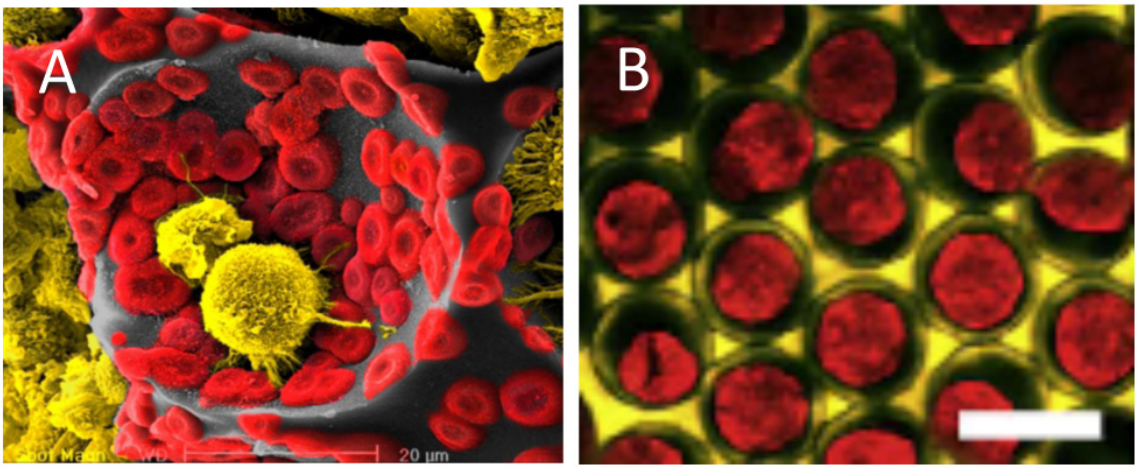

Figure 1.3: Cell cultures in ICC scaffolds. (A) SEM image of HSCs (yellow) cultured with stromal cells (red) in acrylamide ICC scaffolds with an LBL surface coating [12]. (B) Confocal microscopy image of hepatocyte spheroids (red) in acrylamide ICC scaffolds without LBL coating [17].

1.4 ICC scaffolds for bone and bone marrow engineering

The focus of this dissertation is on the engineering of bone and bone marrow. These tissues have essential and complex cell-cell and cell-matrix interactions that are lost in 2D cultures. The application of ICC scaffolds to these tissues is obvious due to the architectural similarity of trabecular bone and ICCs (Fig 1.4). The ability to control the size of architecture features affords the potential for high mechanical properties, which is important when designing an implant for a structural tissue like bone. Within bone, bone marrow is home to intense interactions between HSCs, stromal cells, and the surrounding bone and ECM; these intense interactions can be mimicked utilizing the geometry of ICC scaffolds.

1.5 Organization of the dissertation

This chapter introduced the principles and applications of 3D cell culture. Chapter 2 will review scaffold manufacturing processes, some relevant materials, and close

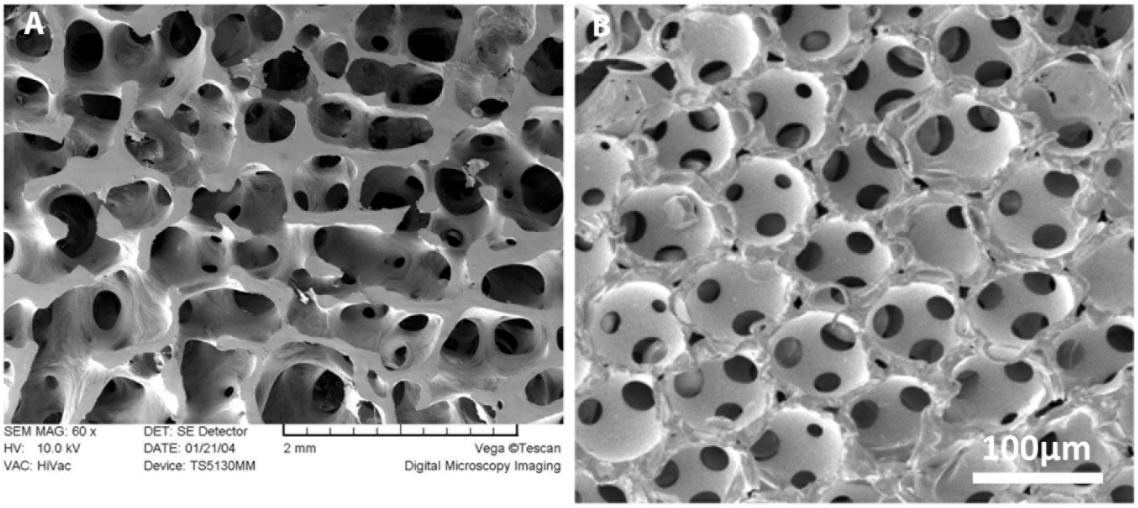

Figure 1.4: Geometrical similarities between trabecular bone and ICC scaffolds. SEM images of (A) trabecular bone and (B) ICC scaffolds [25].

with relevant work in bone tissue engineering, bone marrow engineering and pharmaceutical drug testing in bone marrow. The next chapter discusses the development of biodegradable ICC scaffolds for applications in bone tissue engineering. Chapter 4 presents work on the use of hydrogel ICC scaffolds for bone marrow engineering. Chapter 5 compares three matrices and combinations of stromal cells for bone tissue engineering. The next chapter continues with the use of ICC scaffolds as bone marrow analogs and preliminary drug testing. The final chapter summarizes the work presented in the dissertation and discusses future work.

CHAPTER II

Literature Review and Background

This dissertation focuses on the engineering of bone and bone marrow from two design perspectives: (1) implantable matrices for bone tissue engineering and (2) *in vitro* models of bone marrow for drug testing. These applications have different design criteria for 3D matrices. Tissue engineering targets the creation of functional implants using artificial 3D matrices [18, 33]. Scaffolds are designed to be implanted in a patient wound site to act as a temporary template to restore original tissue function while the natural tissue heals. Accordingly, scaffolds should not only have proper architecture for supporting cell growth, but should also match the shape of the defect site. Materials should be biodegradable and metabolized in the body without causing serious systemic or immunogenic problems [34]. *In vitro* modeling, however, aims to utilize the cell-matrix complex as a tool to improve the understanding of tissue physiology and pathophysiology [35]. The user may want the matrix to be inert so that its shape and organization does not change with time. The 3D matrix should be designed to mimic the organization and function of tissues in the body; thus, geometrical and material property control is extremely important. It is also essential that the matrix is optically accessible to analyze tissue growth and function within the scaffold.

With these applications in mind, this chapter will focus on the different structural design criteria and fabrication methods for 3D matrices. It will also briefly discuss

categories of materials used in 3D matrices relevant to these topics. More detailed information about materials, as well as other considerations and examples of using 3D matrices can be found in a review paper by Lee et al [8]. Lastly, this chapter will summarize relevant work performed in the areas of bone tissue engineering and 3D models of bone marrow.

2.1 Geometrical properties of scaffolds

With a growing variety of available techniques to control the size and shape of materials from the nano- to the micro-scales, scaffold design has become increasingly precise. A multi-scale approach to 3D matrix design is especially important in mimicking living systems, as nature often derives properties from multi-scale or hierarchical design, which previously have been difficult to mimic. For example, much of the toughness of bone originates in the hierarchical structure of interacting nano-scale collagen molecules and hydroxyapatite crystals, collagen fibers and fibrils, micro-scale lamella and osteons [36]. Multiple levels of control allow for the engineering of unique scaffold properties not present in bulk materials, including geometry, porosity, surface texture, cell seeding, signal delivery, and many other matrix characteristics.

2.1.1 Macro-scale

The macro-scale structure, which is defined here to be on the scale of 10^{0} - 10^{-3} m, mainly is engineered to tailor the size and shape of the scaffold (Fig. 2.1A, B). For in-vitro 3D cell culture applications, the size and shape of a matrix can be controlled for convenience and functionality (e.g., fitting to a well plate or bioreactor). In the simplest case, scaffolds can be fabricated directly in a cylindrical mold, such as a vial with the desired diameter. In tissue engineering, it is important to match matrix size and shape to the anatomical defect. For example, a scaffold for bone tissue engineering should have a properly designed macro-scale structure to allow for

integration with adjacent tissues, as well as to generate properly sized tissue [37, 38]. A major challenge is that defect site size and shape vary from patient to patient. One approach to achieving this level of design control is to use computer-based medical imaging tools such as computed tomography and magnetic resonance imaging and design strategies such as computer-aided design, which become useful in customizing the 3D architecture to match a wound site [38]. This design can be manufactured using solid free-form (SFF) fabrication, which will be discussed further in Section 2.1.2. The macroscopic structural design of 3D matrices, along with their fast and individualized production, will become more important with the realization of 3D cell scaffolds in clinical applications [39–41].

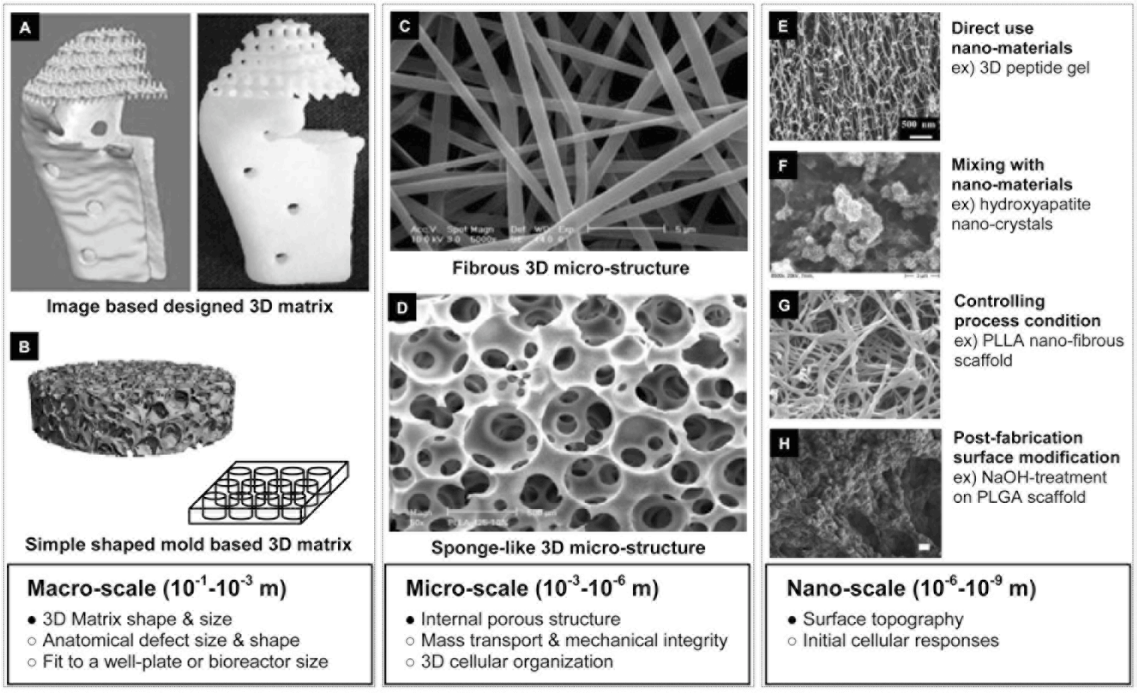

Figure 2.1: Multiple scales of design criteria of 3D cell culture matrices. (A) [38]. (B) [42]. (C) [43]. (D) [44]. (E) [45]. (F) [46]. (G) [44]. (H) [47].

2.1.2 Micro-scale design

Features of interest that are affected by micro-scale ($10^{-3}$$10^{-6}$ m) structure include porosity, pore interconnectivity, pore geometry, pore size distribution, mechanical properties, and topography. These features directly affect the diffusion of nutrients, metabolic wastes, and other soluble molecules. The inclusion of sufficiently sized and well-interconnected pores improves diffusion throughout the scaffold interior. Pore geometry is also a great influence on the scaffold diffusion properties, as different pore shapes can yield different mass transport profiles (Fig. 2.1C, D). As well, a large pore size distribution can lead to areas with poorer accessibility, potentially limiting cell seeding and migration efficiency. The porosity can also affect the mechanical properties of the scaffold. A highly porous scaffold can lose mechanical strength due to the lack of material. Lastly, micro-scale features also are of note because cells are of this scale. Individual cells recognize structures that have comparable dimension to cellular size (10-100 μm) [48]. Micro-scale surface features can activate certain genes and modulate cellular behavior in differentiation or proliferation. For example, microscopic surface patterns and grooves on 2D surfaces guide neuronal cell polarization [48] and myoblast alignment [49].

Traditional scaffold fabrication techniques that impart micro-scale pores include particulate leaching, gas foaming, emulsion freeze-drying, and thermally induced phase separation [50–54]. These techniques are based upon bulk material alteration that yields a random pore structure, leaving the user with little control over the features mentioned above. Specifically, a stochastic micro-structural architecture, such as those resulting from particulate leaching fabrication techniques, yields incomplete scaffold permeability. Consequently, scaffold porosities often approach 95% to ensure complete interconnectivity throughout the scaffold [55]. Such high porosities present a dilemma in bone tissue engineering, where increased porosity enhances interconnectivity but denies the scaffold of sufficient mechanical strength to support the load

of the body until tissue regeneration is complete. Precise design of matrices, where architecture is optimized to provide complete interconnectivity at lower porosities, can improve mechanical strength while preserving effective diffusion [55].

Although there are numerous fabrication methods to make 3D matrices with micro-scale resolution, some manufacturing methods, such as SFF fabrication [56] and ICC fabrication [26, 27, 29], provide precise controllability over 3D matrix architecture at this scale. Computational image-based SFF processes, such as 3D printing, fused deposition modeling, and selective laser sintering, provide precise control over scaffold architecture, including interconnectivity and topography, and can be designed to obtain specific mechanical properties [38]. However, these methods are limited in useable materials and minimum feature size [55, 57–59]. Still, the larger pore sizes can provide room for nutrient and waste diffusion, as well as tissue ingrowth when implanted *in vivo* and SFF-manufactured scaffolds have possessed mechanical properties approaching that of hard tissues [38]. Taboas et al. overcame some of the feature size and material drawbacks of SFF by developing an indirect SFF process [60]. This process involved casting molds manufactured by direct SFF processes with a salt-polylactic acid mixture. Leaching the molds and salt created polymeric scaffolds with controlled global pores from the SFF molds and local porosity from salt particles [60]. Recently, methods such as two-proton polymerization have improved the resolution of SFF techniques to the nano-scale [61]. Continued improvement in accessible feature sizes will make SFF-based fabrication techniques the most realistic for commercial tissue engineering purposes.

ICC scaffolds have emerged as a highly organized 3D environment for cell growth [8, 12, 17, 25–31]. A description of ICC scaffolds and their fabrication is given in Chapter 1. This arrangement of identical spherical cavities offers a uniform cellular environment for differentiation and growth, an ideal setting for understanding the role of cell-cell and cell-scaffold interactions, and for computer modeling of scaffold

properties [62]. Additionally, the complete interconnectivity at low porosities gave hydrogel ICC structures a ten to one thousand-fold greater relative stiffness than those predicted for bulk material alteration techniques in polyethylene glycol hydrogel scaffolds [63]. ICC structures can be prepared of any bulk material, so long as a suitable pair of solvents is found: one to dissolve the mold without affecting the material and vice versa. Ideally, specific design criteria, such as 3D topography resembling that of trabecular bone, mechanical properties, degradation rate, and growth factor release rate, can be met by adjusting scaffold material and sphere size. The ICC structure offers some obvious advantages for bone and bone marrow engineering such as high degree of structural control, complete interconnectivity of cavities,and the possibility of achieving high mechanical strength.

2.1.3 Nano-scale design

Nano-scale design, defined as features in the size range of 10^{-6}-10^{-9} m, is important to consider when mimicking the human body because cells interact with their environment via nano-scale ECM proteins and with other cells via nano-scale receptors. For example, collagen fibrils have a diameter range of 50 to 200 nm, and fibronectin are 60 to 70 nm long and 2 to 3 nm thick. *In vitro*, nano-scale topological features have provided significant influence on cellular functions via cell adhesion, organization, morphology, and differentiation [64].

There are four major methods of imparting nano-sized 3D surface structural features onto a 3D matrix. The first method involves using nano-materials such as 3D peptide hydrogels directly, entrapping cells in a 3D nano-scale fibrous structure (Fig. 2.1E) [45, 65]. The second method incorporates nano-sized materials into bulk materials before matrix manufacture (Fig. 2.1F) [46]. A great deal of research in bone tissue engineering has focused on integrating nano-sized features into scaffolds to improve osteoblast adhesion, proliferation, and calcium deposition. For example,

hydroxyapatite nano-particles incorporated into the matrix of polylactic acid (PLA) scaffolds yielded nano-scale topology that significantly increased protein adsorption [66]. The third method controls processing conditions during fabrication (Fig. 2.1G). A nano-scale fibrous structure can be produced on the surface of a 3D matrix through thermally induced phase separation of PLA solution in organic solvent, followed by a crystallization process during freeze drying [67]. Electrospinning techniques can also reduce fiber diameter to the nano-scale [68]. The last approach is post- fabrication surface treatment or surface coating (Fig. 2.1H). For example, brief exposure of 3D polyester scaffolds to sodium hydroxide created nano-scale surface roughness, which improved the adhesion of osteoblasts and chondrocytes [69]. Although the above techniques are successful at generating nano-scale surface structures, feature controllability on 3D structures continues to present a major challenge.

2.1.4 Geometrical scale conclusions

Proper design of 3D cell culture matrix structure on multiple scales can provide distinct features to the matrix, such as macro-scale shape, micro-scale internal architecture, and nano-scale surface topology. Therefore, all scales should be considered when mimicking natural tissue for either tissue engineering or 3D modeling purposes. The development of processing approaches that allow freedom in choice of macro-, micro-, and nano-scale is one of the most difficult challenges in 3D scaffolds that the materials science and nano-technology communities need to address.

2.2 Material considerations for 3D matrices

2.2.1 Criteria for tissue engineering and 3D modeling applications

The materials that are appropriate for the two applications discussed here vary greatly; however, in both cases the primary consideration is biocompatibility. In

tissue engineering, the most basic goal is to minimize toxicity such that long-term immunological responses, such as rejection or fibrous encapsulation, are avoided. Additional material considerations include the ability to recruit cells from the natural tissue into the implant, and degradability into metabolites that occur naturally in the body. Specifically for bone and other load-bearing tissues, the materials should have mechanical properties that approach those of healthy tissue. For these reasons, in tissue engineering, materials are typically synthetic polymers designed to maximize mechanical properties while undergoing controlled degradation.

The ideal materials of 3D modeling are very different than those of tissue engineering. In this area, the user is growing cells or tissues in a matrix to examine a certain aspect of the human body; for example, to probe the interactions between cells, their reaction to a drug, or the effects of the addition or deletion of a gene, are all uses of *ex vivo* culture [23, 24, 70]. In these applications, one needs to view and track cells and markers, requiring that the matrix is transparent. The matrix should also be inert to its remodelling by cells. For example, biodegradability should be avoided to evade the effects of material metabolites or change in matrix structure.

2.2.2 Relevant materials

The majority of materials utilized in tissue engineering, specifically in bone tissue engineering, are synthetic resorbable polymers. Resorbable polymers, which include poly(α-hydroxyesters), polyanhydrides, and poly(ortho-esters), are useful because their composition can be tailored to obtain certain properties, including degradation rate and mechanical properties. As well, their processability allows for a variety of structural properties such as geometry and porosity.

As 3D modeling requires transparent, nondegradable, materials with properties much like the body, hydrogels, networks of hydrophilic polymer chains, are commonly utilized [71, 72]. Hydrogels are appropriate formats for 3D modeling of many

tissues because ECM is a fully hydrated gel [73]. The hydrogel structure also creates a gradient of soluble signaling molecules within a 3D matrix much like the body, and absorbs mechanical tensions. Three popular types of synthetic gels are used: polyethylene glycol (PEG), peptide, and DNA gels. PEG hydrogel has been used because of its high biocompatibility and precise control of reaction kinetics during rapid photo-polymerization, providing a spatially well-controlled 3D gel for cell entrapment [74]. Peptide gels are composed of macroscopically self-assembled synthetic peptides. Small quantities of elemental peptides (0.1-5.0%) dispersed in water are mixed with a cell suspension, which then undergoes a self-assembling process under the right ionic conditions. Self-assembled peptides generate a stable nano-fibrous structure, entrapping cells. Two types of synthetic peptides currently used in this fashion are amyloid-like fibrils [75] and peptide amphiphiles [76]. Recently, deoxyribonucleic acid (DNA) has been used as a building block to construct hydrogels with the invention of an oligonucleotide synthesizer to design a specific sequence of DNA and polymerase chain reaction to amplify the DNA. Elaborately designed DNA molecules, which have a branched structure with a complementary sticky end, can be hybridized to each other via DNA ligase, self-assembling into a 3D DNA hydrogel [77, 78]. Poor cell adhesion due to the hydrophilicity of hydrogels and the lack of cell binding motifs is a common drawback [72]. These limitations can be overcome by conjugating cell-binding motifs such as arginine-glycine-aspartate on polymer chains [79] or by coating surfaces with bioactive materials post-fabrication [27].

Natural materials tend to show better biocompatibility than synthetic materials, but their animal sources raise concerns about disease transfection. Natural polymers include collagen, gelatin, chitosan, alginate, fibrin, Matrigel. Matrigel is protein gel matrix extracted from Engelbreth-Holm Swarm tumors from mice that has a heterogeneous composition of laminin, type IV collagen, heparan sulfate proteoglycan, entactin, and fibronectin [80, 81]. These soluble proteins undergo self-assembled poly-

merization when incubated at 37 °C, forming a 3D gel [82]. As Matrigel is composed of matrix from *in vivo* sources, cells can digest and restructure the matrix [83]. This feature is useful for migration studies [84], but can be hindering in tissue engineering applications where matrix digestion disrupt the 3D structure. As well, the murine source of Matrigel introduces the potential of viral contamination, such as lactate dehydrogenase-elevating virus.

2.3 Bone Tissue Engineering

The current clinical gold standard in bone replacement is autologous bone, but lack of availability and donor site morbidity severely limits its applications. Similarly, allogenic bone grafts are limited by supply and immunogenic response. Therefore, engineering bone tissue substitutes to regenerate or replace damaged tissue is of great interest.

The major classes of materials used in bone tissue engineering are metals, ceramics, and polymers. Metals and ceramics, e.g. titanium and calcium phosphate, respectively, have had some clinical success as bone implants; however, they do not degrade, which causes loss of strength of natural tissue by shielding local tissue from mechanical stresses [85, 86]. Furthermore, the materials have their own problems, such as wear and brittleness. Ideally, scaffolds should be designed to degrade at the rate that in-growing tissue replaces them. Thus, bone scaffolds generally are composed of syntheitic hydrolytically degradable polymers, which can be tailored to have certain properties, such as compressive modulus or degradation rate. For example, the degradation profile of PLGA scaffolds can be manipulated by adjusting the composition and molecular weight of PLA and polyglycolic acid (PGA) polymers [87].

Bone possesses a range of mechanical properties superior to most of the mentioned synthetic materials (Table 2.1). The organic-inorganic composition of bone is responsible for the combination of strength and stiffness and high fracture toughness.

Inorganic hydroxyapatite, in the form of nano-sized platelike crystals, is thought to contribute to the strength of bone; for example, the Young′s Modulus of cortical bone correlates linearly with its mineral content [88]. Collagen, the main organic component of bone, is said to contribute to the fracture toughness of bone, the energy required to cause matrix failure [89]. Other contributors to the mechanical properties of bone include collagen cross-linking and fibril orientation, mineral crystal size, and microstructural organization [90].

Table 2.1: Mechanical properties of bone components and materials proposed as bone tissue substitutes.

Material	Compressive strength, megapascal (MPa)	Tensile strength, MPa	Elastic modulus, gigapascal (GPa)	References
Cortical bone	130-180	50-151	12-18	[91]
Trabecular bone	4-12		0.1-0.5	[91]
PLGA		41.4-55.2	1.4-2.8	[91]
Hydroxyapatite	>400	40	100-114	[89, 91]

Noting the nano-scale design of natural bone, engineers have attempted to impart nano-scale particles and features into scaffolds. Examples of attempts at mimicking the nanocomposite structure of natural bone include mixtures of silica and apatite, calcium phosphate cement microparticles and PLGA, calcium phosphate and PLGA microparticles, nanostructured titania and PLGA, nano-hydroxyapatite and PLA, and hydroxyapatite (HA) and chitosan-gelatin [66, 69, 92–95]. Specifically, there have been several attempts at improving properties of scaffolds by incorporating HA into polymers. Marra et al. synthesized composite scaffolds with 0-50% HA in poly(caprolactone), PLGA, and blends of both polymers [96]. The Youngs modulus was shown only for strips of 10% HA, but this modulus was five times greater than scaffolds of polymer alone. These results are promising; however, the HA particle size was not given and results could be significantly improved by incorporating nano-

sized HA (size not stated) or varying the inorganic-organic ratio. Nano-sized HA was blended with PLA in ratios of 0-70% HA by Wei et al to obtain 3D structures. A significant improvement of compressive modulus was seen for 30% and 50% HA compared to polymer alone [66]. Kim et al. created 3D scaffolds with HA nanoparticles (100 nm length) and 75:25 PLGA in a 1:1 ratio, but the compressive moduli remained at 2.3-4.5 MPa, most likely due to the 90% porosities obtained from the particulate leaching method used to produce an interconnecting structure [97].

2.4 Bone Marrow Engineering

The interactions between HSCs and the bone marrow niche are incredibly complex and not completely understood. Bone marrow stroma, the tissue surrounding hematopoietic tissue, is composed of a variety of cell types and ECM molecules. Bone cells, such as osteoblasts and osteoclasts, play an important role in HSC maintenance through receptor-receptor contact and calcium concentration regulation [98–101]. HSCs have also been found close to endothelial cells near blood vessels that enter the marrow [102]. Additional stromal cell types include adipocytes and reticular cells. HSCs interact with these cell types directly through cell-cell contacts, or indirectly through secreted growth factors or ECM. The ECM of bone marrow stroma consists of proteins and glycoproteins, such as collagen, osteopontin, and fibronectin [103, 104].

Models of the HSC niche and of bone marrow are desirable for expansion of HSCs and also for testing of drugs within the tissue. Despite the complexity of bone marrow, most models of healthy and diseased HSCs and marrow consist of one or two cell types growing on 2D surfaces. Furthermore, most HSC engineering focuses on their expansion [105–108] and little has been explored in controlled development of HSCs into whole bone marrow.

Traditionally, models of the HSC niche were grown on 2D surfaces, either on

stromal cells [109, 110], supplemented with high concentrations of growth factors [111, 112], or both. The 2D models allowed for the maintenance and expansion of HSC, but lack the dimensionality and ECM components of the HSC niche. With this in mind, 3D models of the bone marrow niche, primarily designed for HSC expansion, were developed. These models ranged from nanofiber scaffolds [105, 108] to porous natural polymers [113] and synthetic polymers [114, 115]. Due to the presence of nanoscale ECM fibers, structures with nanoscale features have been incorporated into 3D matrices for the culture of HSCs; these include electrospun nanofibers [105, 108], nanoridges [4], and nanocomposites [30, 116]. One of the most commonly used nanostructured matrices used in hematopoietic and other stem cell cultures is a commercially available matrix called Matrigel [117, 118].

Most applications of 3D matrices to bone marrow niches are relatively recent. Given the complex cell-cell and cell-matrix interactions in bone marrow, the inclusion of a 3D matrix is likely to elucidate the contribution of many niche components. To accomplish this, much work must be done to determine the necessary signals that should be included to model the bone marrow niche.

2.5 Publications relevant to this chapter

The material in this chapter has been adapted with minor modifications from the following published article:

Jungwoo Lee, Meghan J Cuddihy, and Nicholas A Kotov. Three-dimensional cell culture matrices: state of the art. *Tissue Engineering Part B, Reviews*, 14(1):61-86, 2008.

CHAPTER III

Poly(lactic-co-glycolic acid) Bone Scaffolds with Inverted Colloidal Crystal Geometry

3.1 Introduction

Bone tissue engineering aims to replace traditional autograft and allograft repair strategies with the implantation of mechanically functional biodegradable constructs that support the wound site and hasten the natural repair mechanism until bone has filled the defect [18] [85]. A number of structural criteria for implantable constructs, scaffolds, are agreed upon, including sufficient porosity, interconnectivity, and mechanical properties. Porosity and complete interconnectivity throughout a scaffold are necessary to promote uniform cell loading and migration, eventual tissue and vasculature ingrowth, and sufficient nutrient diffusion and interstitial fluid and blood flow [60, 119]. The ideal bone tissue engineering scaffold should have a precisely-designed structure that provides complete interconnectivity of pores and maximum load bearing capacity [55].

Traditional scaffold fabrication techniques, such as particulate leaching, gas foaming, emulsion freeze-drying, electrospinning, and thermally induced phase separation, are based upon bulk material alteration that yields a random pore structure [50–53, 120]. The random pore distribution risks insufficient scaffold interconnectivity and permeability; consequently, scaffold porosities often approach 95% to ensure complete interconnectivity throughout the scaffold. Such high porosities present a dilemma in

bone tissue engineering, where increased porosity enhances interconnectivity but denies the scaffold of sufficient mechanical strength to support the load of the body until tissue regeneration is complete. Therefore, there is a need for structural engineering of bone scaffolds, providing sufficient control over 3D geometry [38, 91]. A systematic approach to this problem would be the preparation of well-ordered porous materials with tunable geometry. Computational image-based design/fabrication processes, such as Solid Free-Form (SFF) Fabrication, provide precise control over scaffold architecture, including interconnectivity and geometry, but are limited in useable materials and a minimum feature size of 100 μm [8, 38, 59, 60]. A method of producing scaffolds with highly controlled architectural properties on multiple scales would greatly advance scaffold design for bone tissue engineering.

ICC scaffolds have emerged recently as a highly organized three-dimensional (3D) environment for cell growth [26–29, 62, 63]. ICC scaffolds possess a hexagonally close-packed (HCP) geometry, which can be described as closely packed spherical cavities arranged in a hexagonal crystal lattice. The HCP arrangement offers a uniform cellular environment for differentiation and growth, as well as an ideal setting for understanding the role of cell-cell and cell-scaffold interactions, and for computer modeling of scaffold properties [62]. Additionally, HCP geometry guarantees interconnectivity between all neighboring spherical cavities while calculations for the maximum theoretical porosity for HCP structures range from 63-74% [63, 121]. The high interconnectivity and low porosity of hydrogel HCP structures gave a ten to one-thousand-fold greater relative stiffness than those predicted for bulk material alteration techniques in polyethylene glycol hydrogel scaffolds [63]. ICC structures can be prepared of any bulk material, as long as a suitable pair of solvents is found: one to dissolve the mold without disturbing the bulk material, and vice versa. Ideally, specific design criteria, such as mechanical properties, degradation rate, and growth factor release rate, can be met by adjusting scaffold material and the size of spheres

that compose the mold.

Recently, our group has produced ICC scaffolds composed of sol-gel and polyacrylamide hydrogel [26–29, 62]. Several cell types were shown to attach and proliferate on these structures, including human hepatic, bone marrow stromal, thymic epithelial, and premeylote monocyte cells, and mouse fibroblastic and T-cells. The challenges related to cell attachment typical for hydrogels were solved using layer-by-layer coating of their surfaces [27, 122]. The ICC structure offers some obvious advantages for bone tissue engineering such as (1) high degree of structural control, (2) invariably complete interconnectivity of cavities, (3) 3D geometry resembling the morphology of trabecular bone and (4) the possibility of achieving high mechanical strength. Other tangible advantages, which can come into play in future research, are the convenience for tissue development simulation and incorporation of osteoconductive and osteoinductive nanocolloids. From a fundamental point of view, the simplicity of ICC preparation and high degree of structural control provide excellent opportunities for understanding and manipulating cell culture on the scaffold.

Here, we introduce ICC scaffolds from a biodegradable polymer often used in constructing bone implants. The key parameters examined here are the ability to create highly ordered PLGA ICC scaffolds, the potential to control the diameter of the cavities and the channels connecting the cavities, the compressive modulus of the scaffolds, and the biocompatibility of scaffolds *in vitro*.

3.2 Methods

3.2.1 Preparation of CCs

One gram of uniformly-sized soda lime microspheres (Duke Scientific Corporation, Palo Alto, CA) were added to ethylene glycol (Sigma, St. Louis, MO) in a dropper bottle. Molds were assembled by securing a glass Pasteur pipette to a glass vial (7

mm inner diameter) so that the pipette tip hung centered within the vial. Each mold was filled with ethylene glycol and positioned in an ultra-sonic bath. Two drops of the microsphere solution was dropped into the pipette every 15 min, so the microspheres slowly settled onto the bottom of the vial and assembled into a CC under gentle sonication. After the desired volume of microspheres was added to the mold, the pipette was detached, and the microspheres and vial were left under sonication for an additional hour. The vial was then heated at 160 °C overnight to evaporate all ethylene glycol before heating for 3 hours to anneal the microspheres together, forming a solid CC. CCs were constructed of 100, 200, and 330 μm microspheres to yield ICCs with three different cavity sizes.

The annealing temperatures were adjusted in two separate experiments. In the first experiment, the annealing temperature was varied to explore the controllability of the diameter of interconnecting channels. Here, 100 μm microspheres were annealed at 660, 670, 680, and 690 °C, 200 μm microspheres were annealed at 670, 680, 690, and 700 °C, 330 μm microspheres were annealed at 690, 700, and 710, and 720 °C. Based on the result from the first experiment, six combinations of microsphere size and annealing temperatures were chosen to produce scaffolds with different sized cavities and interconnecting channels for cell culture. Microspheres with a 100 μm diameter were annealed at 670 and 690 °C, while 200 and 330 μm microspheres were annealed at 690 and 700 °C. These temperatures were chosen based on stability of CCs and the variety of resulting channel sizes.

3.2.2 Preparation of ICC scaffolds

CCs were removed from vials, and placed into a 0.1 g/mL solution of 85/15 PLGA (Lactel Absorbable Polymers, Pelham, AL) in methylene chloride. The CCs were centrifuged for 10 min at 5900 rotations per minute (RPM) to infiltrate PLGA solution. The infiltrated CCs were allowed to dry at room temperature overnight, and then

placed under vacuum for 24 h. The edges of each infiltrated CC were scraped lightly with a razor blade to remove surface PLGA and expose the microspheres. Next, the infiltrated CCs were stirred in a 5% hydrofluoric acid (HF) solution for 2 days, changing HF solution once, and then stirred in a 1.0 N hydrochloric acid (HCl) solution for one day. The HF/HCl cycle was repeated, rising with distilled H_2O in between cycles. To ensure all HF was rinsed from the scaffolds, resulting ICCs were washed in phosphate buffered saline (PBS), changing solution until the pH remained stable at 7.4.

3.2.3 Characterization of ICCs

The order, overall structure, and diameter of interconnecting channels were characterized for scaffolds of 100, 200, and 330 μm cavity diameters. The HCP order of CCs for each microsphere size was observed with scanning electron microscopy (SEM). In the first annealing temperature experiment, ICCs were characterized with scanning electron microscopy (SEM) to observe overall order and how the interconnecting channel size varied with microsphere annealing temperature. For each microsphere size, two ICCs resulting from each microsphere size and annealing temperature combination were examined, and 10 interconnecting channels were measured on each scaffold. The diameters of interconnecting channels were analyzed using SEM images using the public domain National Institutes of Health (NIH) Image program (developed at the U.S. NIH and available on the Internet at http://rsb.info.nih.gov/nih-image/).

3.2.4 Mechanical Properties

Four ICCs constructed from 100, 200, and 330 μm microspheres with annealing temperatures of 670, 690, and 700 °C, respectively, were mechanically tested in compression using a 100Q Universal Test System Mechanical Properties Tester (TestResources Inc, Shakopee, MN). ICCs were tested in a dry state at room temperature.

The specimens were compressed at a rate of 0.01 mm/s, and the compressive modulus was defined as the slope of the linear portion of the stress-strain curve.

3.2.5 Cell culture

Human fetal osteoblast (hFOB) 1.19 (CRL-11372) was purchased from American Tissue Culture Corporation (ATCC) (Manassas, VA) and grown as recommended by ATCC in 45% Ham's F12 medium, 45% Dulbeccos modified Eagles Medium (DMEM) and 10% fetal bovine serum (Gibco, Frederick, MD) supplemented with 1% antibiotic. Cells were grown at 37 °C and 5% CO_2, changing medium every 2-3 days.

3.2.6 Cell Loading and Culture on Scaffolds

Twelve ICCs, 7 mm in diameter and 1.2 mm in height, were constructed for each of the six cavity size and annealing temperature combinations mentioned above. Scaffolds were sterilized and wetted with ethanol for one hour. Scaffolds then were centrifuged twice in fresh PBS at 900 RPM for five minutes before placing in a well of a 12-well plate. hFOB 1.19 cells were stained with trypan blue (Sigma, St. Louis, MO) and counted before suspending in medium and distributing into wells at $4.6\text{x}10^4$ cells/scaffold. Cells and scaffolds were incubated at 37 °C and 5% CO_2. Three scaffolds of each cavity size and annealing temperature were removed at 1, 5, 9, and 12 days for viability staining and three scaffolds were removed for double stranded DNA (dsDNA) quantification.

In a second set of cell culture experiments aimed at quantifying and examining the osteoblast phenotype, twenty scaffolds of the following cavity sizes and annealing temperatures were utilized: 100 μm, 670 °C; 200 μm, 690 °C; 330 μm, 700 °C. Scaffolds were prepared as described above with ethanol and PBS treatment, and then were placed into wells of a 96-well plate before cells were seeded at densities of 2.0×10^4 cells/scaffold. Scaffolds were inserted to 96-well plates because the scaffolds

would cover the entire bottom area of the wells, increasing the consistency of cell seeding into the scaffolds, rather than onto the bottom of the well plate. Cells were incubated at 37 °C and 5% CO_2. After one day, scaffolds were transferred to a 24-well plate to increase the amount of media surrounding cells. Two scaffolds were removed after three hours, and six scaffolds were removed on days 1, 4, and 7. At all time points, two scaffolds were slated for F-actin and collagen type I staining, and during the later three time points four scaffolds were slated for dsDNA and alkaline phosphatase (ALP) activity.

3.2.7 Staining and Confocal Microscopy for Viability, F-actin, and Collagen Type I

Cells on each of the three scaffolds removed at each time point for viability assessment were stained with 2 μM calcein AM and 4 μM EthD-1 using a Live/Dead Viability/Cytotoxicity Kit (Invitrogen Corporation, Carlsbad, CA).

Scaffolds for F-actin and collagen type I staining were fixed removed at each time point, and fixed with 4% formaldehyde for 10 minutes at room temperature, rinsed in PBS twice, permeablized with 0.1% Triton X-100 for 3-5 minutes, rinsed twice more with PBS, and then immediately treated for visualization of collagen or F-actin. Cells in scaffolds slated for F-actin staining were incubated for 30 min with rhodamine phalloidin (Invitrogen Corporation, Carlsbad, CA). Scaffolds slated for antibody immunohistological staining of collagen were stored in a 40 μg/mL solution of biotin labeled polyclonal goat anti-collagen type I (Millipore, Billerica, MA) at 4 °C overnight. Samples were rinsed twice in PBS, and incubated in a 10 μg/mL solution of FITC-Streptavadin (MP Biomedicals, Solon, OH) for one hour at 37 °C. All samples were viewed immediately or stored at 4 °C protected from light, and were examined using a Leica TCS SP2 Confocal Laser Scanning Microscope with 10× and 20× objectives.

3.2.8 SEM

Samples for SEM were fixed in 2%-volume gluteraldehyde solution overnight, then washed in sodium cacodylate solution for 1 h. Samples were dehydrated through an ethanol series with concentrations of 20, 50, 70, 90, and 100%, rinsing in each for 20 minutes. They were then freeze-dried and gold-coated. SEM observations were performed using a FEI Nova Nanolab Dualbeam Focussed Ion Beam Workstation and SEM at 15 kV.

3.2.9 dsDNA Quantification

Scaffolds slated for dsDNA quantification were washed with PBS, sonicated in 500 μL Passive Lysis Buffer (Promega Corporation, Madison, WI), and stored at -70 °C until quantification, when samples were thawed and centrifuged for 10 minutes at 10,000 rpm. Of the supernatant, 50 μL was prepared for dsDNA quantification using Quant-iT PicoGreen dsDNA Reagent (Invitrogen Corporation, Carlsbad, CA), according to manufacturer protocol. Sample fluorescence was measured at 520 nm by excitation at 480 nm on a Biotek Synergy 2 Multi-Detection Microplate Reader (Winooski, VT).

3.2.10 ALP Activity

ALP activity was assessed using a colorimetric endpoint assay measuring the conversion of colorless 4-nitrophenyl phosphate (p-NPP) (Sigma, St. Louis) to 4-nitrophenol (p-NP) (Sigma, St. Louis) by ALP [123]. Samples were lysed and centrifuged as described above. Of the supernatant, 50 μL was used to quantify dsDNA, and 10 μL was incubated with 40 μL p-NPP (20 M) for 30 minutes at 37 °C. The reaction was stopped by the addition of 50 μL 0.1 N NaOH, and sample absorbance was determined at 405 nm on a microplate reader. The activity of enzyme present was quantified by comparison with a standard curve. ALP activity was normalized

to cell number using dsDNA assay results.

3.2.11 Statistical Analysis

In all graphs, data is represented as the average of the indicated sample sizes ± standard deviation. A Students t-test was performed to determine statistical significance ($p<0.05$).

3.3 Results

3.3.1 Characterization of ICC Scaffolds

The chosen range of annealing temperatures was selected to provide a CC that is stable enough to be handled and provide complete interconnectivity among adjacent microspheres. The upper limit of the temperature range was chosen so that microspheres were not completely melted, which would inhibit the infiltration of PLGA in spaces between microspheres. Highly-ordered CCs were assembled from uniformly-sized soda lime microspheres 100, 200, and 330 μm in diameter (Fig 3.1). For all three sizes, microspheres were arranged in an HCP array, as observed in the structure cross-sections. After infiltration with PLGA, beads were completely removed with HF/HCl, resulting in ICC structures with a similar degree of order to the CC templates (Fig. 3.2). The cavities were uniform in size and showed interconnectivity with all adjacent cavities.

3.3.2 Effects of Annealing Temperature on Channel Size

To explore the degree of control over the diameter of interconnecting channels by CC annealing temperature, each microsphere size was annealed at four temperatures. Several 100 μm CCs annealed above 690 °C were found to anneal to the vial that served as the CC mold, and could not be removed for PLGA infiltration. It was as-

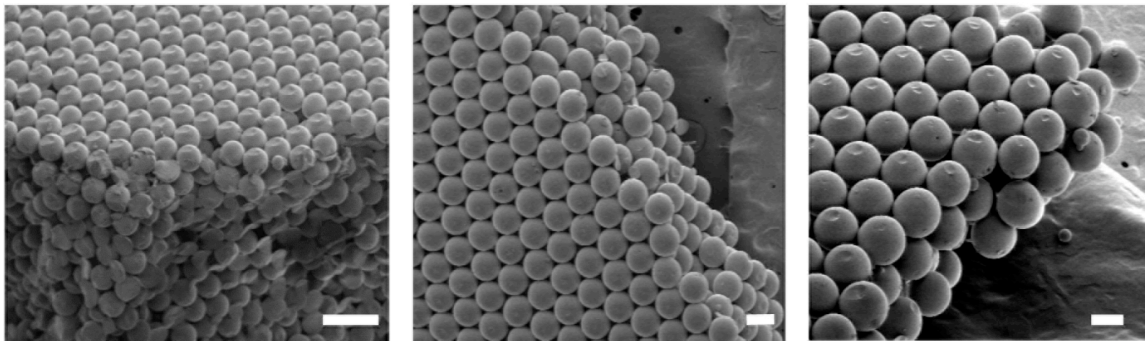

Figure 3.1: SEM images of CCs with various cavity sizes. CCs are made from microspheres of diameter (A) 100 μm, (B) 200 μm, and (C) 330 μm. Scale bar = 200 μm.

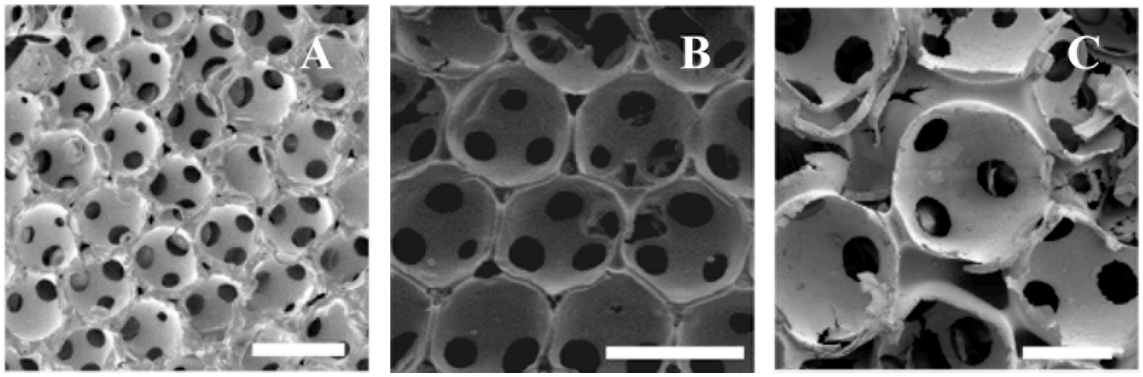

Figure 3.2: SEM images of ICCs with various cavity sizes. SEM images of PLGA ICCs resulting from CCs of microspheres of diameter (A) 100 μm, (B) 200 μm, and (C) 330 μm. Scale bar = 200 μm.

sumed that annealing above 690 °C caused excessive melting of 100 μm microspheres. The edges of 200 μm CCs annealed below 670 °C crumbled when removed from the vial mold; lower temperatures most likely did not cause sufficient annealing to provide a secure structure for handling. For 330 μm microspheres, annealing temperatures of 670 and 680 °C were attempted, but the resulting CCs were not stable enough to be handled without breaking; thus it was assumed that higher temperatures would be explored. Additionally, as 330 μm CCs annealed at 720 °C were melted and cracked, ICCs were not constructed at this temperature. ICCs from CCs of each microsphere diameter and annealing temperature were characterized using SEM. The interstitial

channel diameters were measured to ensure sufficient size to allow cell migration throughout the scaffold. Fig. 3.3 shows the average diameters for ICCs resulting from each microsphere size and annealing temperature.

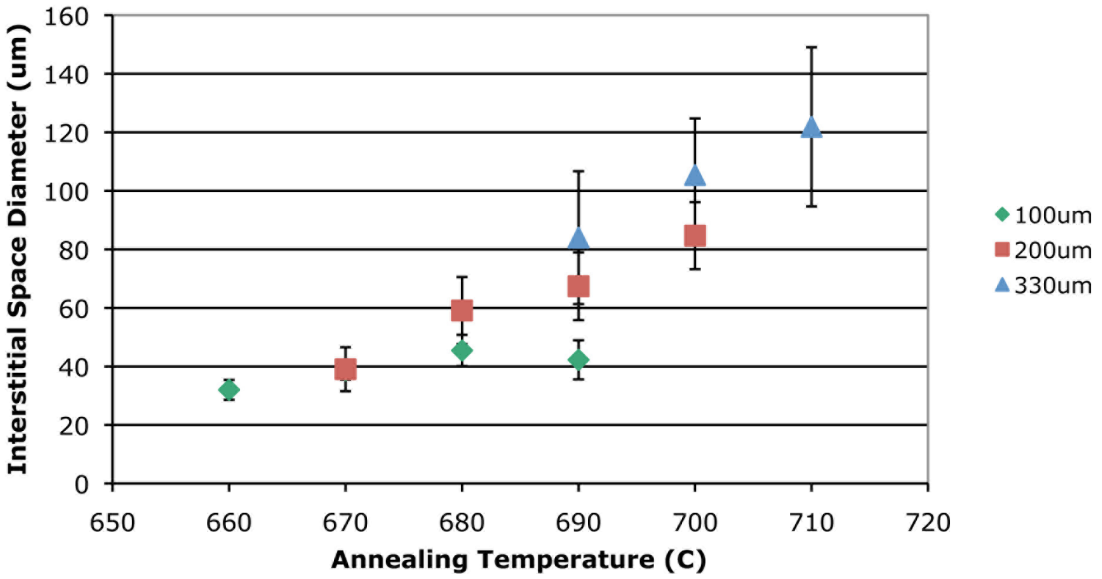

Figure 3.3: Interconnecting channel diameters as a function of microsphere sizes and annealing temperatures.

3.3.3 Mechanical Properties

The compressive moduli of PLGA ICCs resulting from each microsphere size are displayed in Table 3.1. The compressive moduli of ICCs with 100 and 200 μm cavity diameters are slightly higher than those with 330 μm cavities.

Table 3.1: Compressive modulus of PLGA ICCs. PLGA ICCs were constructed using 100, 200, and 330 μm microspheres at the indicated annealing temperatures (n=4).

	100 μm, 670 °C	200 μm, 690 °C	330 μm, 700 °C
Compressive Modulus (MPa)	55.24 ± 17.57	63.63 ± 14.47	54.80 ± 30.98

3.3.4 dsDNA Quantification

Two annealing temperatures were chosen for each cavity size to determine the effects of cavity and channel diameter on osteoblast cell culture. dsDNA quantification for each of these six scaffold cavity and annealing temperature sizes is displayed in Fig. 3.4 for up to 12 days. There is a trend towards greater cell numbers with increased cavity diameters, and proliferation does not seem significant over the culture period.

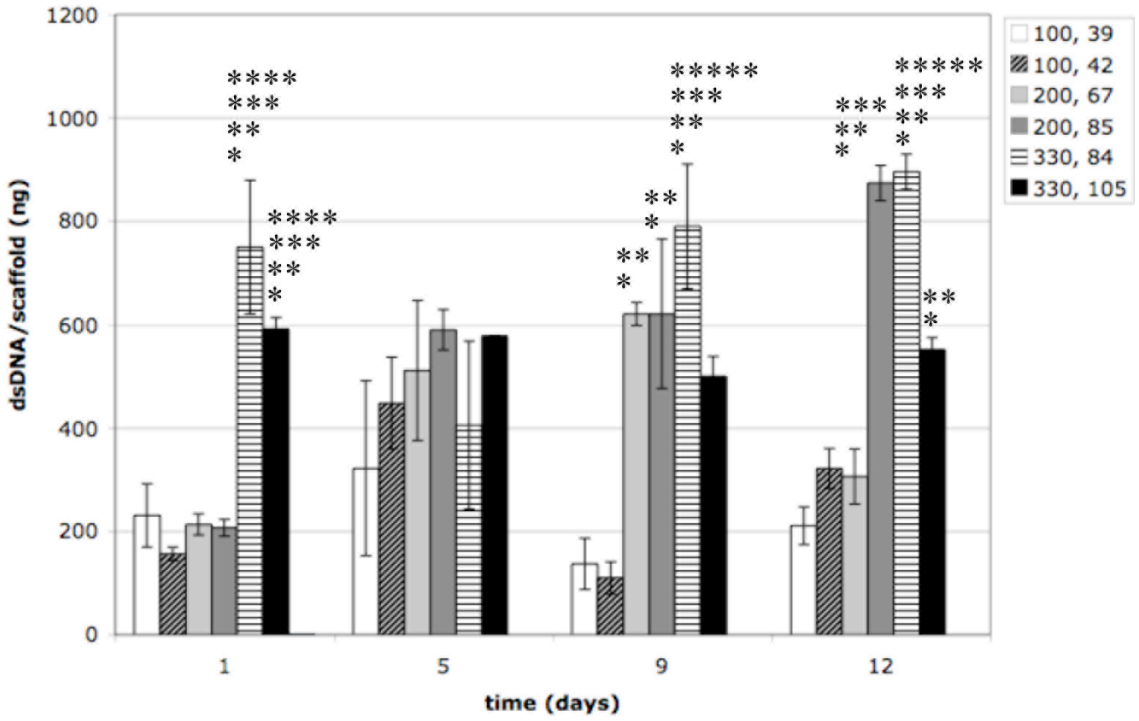

Figure 3.4: dsDNA content in scaffolds. dSDNA present in scaffolds (n=3) of different cavity and interconnecting space diameters for culture up to 12 days. (*Statistically significant ($p<0.05$) as compared to 100, 39 for the indicated culture period; **Statistically significant ($p<0.05$) as compared to 100, 42 for the indicated culture period; *** Statistically significant ($p<0.05$) as compared to 200, 67 for the indicated culture period; **** Statistically significant ($p<0.05$) as compared to 200, 85 for the indicated culture period; ***** Statistically significant ($p<0.05$) as compared to 330, 105 for the indicated culture period.)

3.3.5 Biocompatibility of PLGA ICC Scaffolds

Confocal microscopy and SEM images of hFOB 1.19 cultures on scaffolds 1, 5, 9, and 12 days after seeding onto the scaffolds revealed attachment, viability and proliferation of human osteoblasts for up to 12 days on the scaffolds, as displayed in Fig. 3.5. Most cells retained viability for the duration of the culture period. SEM images, Fig. 3.6, reveal variety in cell morphologies, ranging from fully spread and attached cells, to rounded cells with less area of attachment. Confocal microscopy images of F-actin staining by rhodamin phalloidin for cell cultures of 3 hours, and 1 and 4 days are shown in Fig. 3.7. F-actin staining reveals that at 3 hours cells are rounded, as they have likely not attached to the scaffold, and most F-actin is localized near the cell membrane. After one day, cells have attached to the scaffold and show more uniform F-actin distribution, as their cytoskeletal structure is spread, indicating interaction and contact with the scaffolds.

3.3.6 Maintenance of Osteoblast Phenotype

Anti-collagen antibody staining is displayed in Fig. 3.8. Collagen type I antibody staining did not reveal any collagen in the structure at day 1, but by day four a presence of collagen was observed within or outside of cells, indicating an osteoblast phenotype. ALP activity for each scaffold cavity size at 1, 4, and 7 days are displayed in Fig. 3.9. ALP activity, however, seems slightly higher for greater cavity sizes, and an upregulation was observed over time.

3.4 Discussion

The internal architecture of a scaffold defines the fundamental characteristics of the construct. For example, the surface area for cell migration and proliferation, void volume for tissue and vascular invasion *in vivo*, and bulk scaffold, i.e. mechanical,

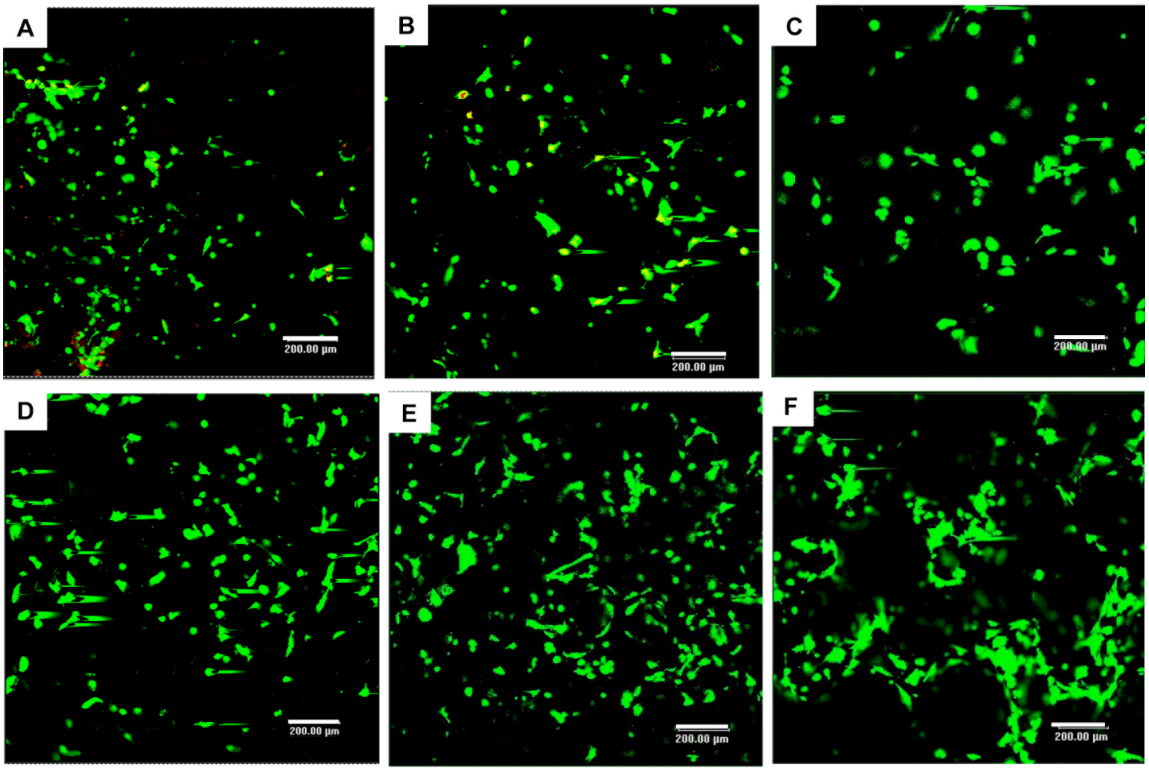

Figure 3.5: Confocal microscopy images of ICC cell cultures. Confocal microscopy images of hFOB 1.19 culture on ICCs of cavity and annealing temperatures of, (A) 100 μm, 670 °C (B) 200 μm, 700 °C (C) 330 μm, 700 °C, (D) 100 μm, 690 °C, (E) 200 μm, 700 °C, (F) 330μm, 700 °C. Images (A) (C) are of cultures after 1 day, and (D) (F) are images taken after 12 days of culture. Scale bar = 200 μm.

properties are all defined by the geometry of a scaffold [56, 124–126]. Control over scaffold internal architecture is important to meet specific design criteria [127, 128]. Principally, we aimed to prove control over scaffold cavity size and the size of the interconnecting channels between cavities, which directly relate to surface area, void volume, and mechanical properties.

The cavity and interconnecting channel sizes of ICCs primarily are controlled by microsphere size, HCP arrangement, and CC annealing temperature. Unlike hydrogel, PLGA does not significantly expand into cavities when microspheres are removed; therefore, the microsphere diameter accurately defines the resulting cavity diameter. The combination of HCP structure and microsphere annealing provides full intercon-

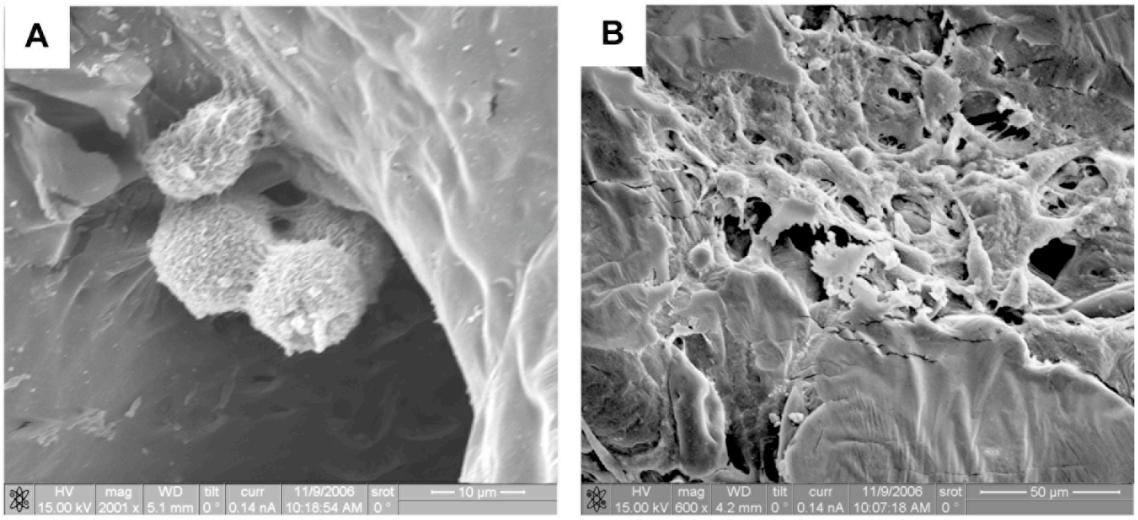

Figure 3.6: SEM images of cells on ICCs. SEM images of hFOB 1.19 on ICCs demonstrating variety of cell morphologies. Cavity diameters and annealing temperatures for pictured scaffolds are (A) 200 μm 690 °C, (B) 330 μm, 690 °C. Both images are after 5 days of culture.

nectivity throughout the ICC scaffold. The highly ordered structure of CCs guarantees connectivity of each cavity to 12 neighboring cavities. Annealing not only gives stability to the CC structure, but also provides the sites of connection between cavities in ICCs. Annealing temperature regulation is essential to ensure complete PLGA infiltration, scaffold interconnectivity, and to regulate the interconnecting channel size.

Pore size is of interest in controlling tissue growth, particularly bone, into scaffolds [129, 130]. *In vivo*, it is generally believed that bone ingrowth and vascularization is maximized over fibrous or connective tissue ingrowth in scaffolds in pore diameters greater than 100 μm [131, 132]; however, this has been debated with research indicating that smaller pore diameters encourage bone growth [133]. Others have shown that bone growth occurs via chondrogenesis in 100 μm pores within hydroxyapatite scaffolds, yet with 350 μm pores osteogenesis directly occurs [134–136]. *In vitro*, it has been shown that larger pore sizes correlate with earlier osteoblast differentiation [125]. There is a need for a systematic method of varying pore diameters to determine optimal bone growth conditions.

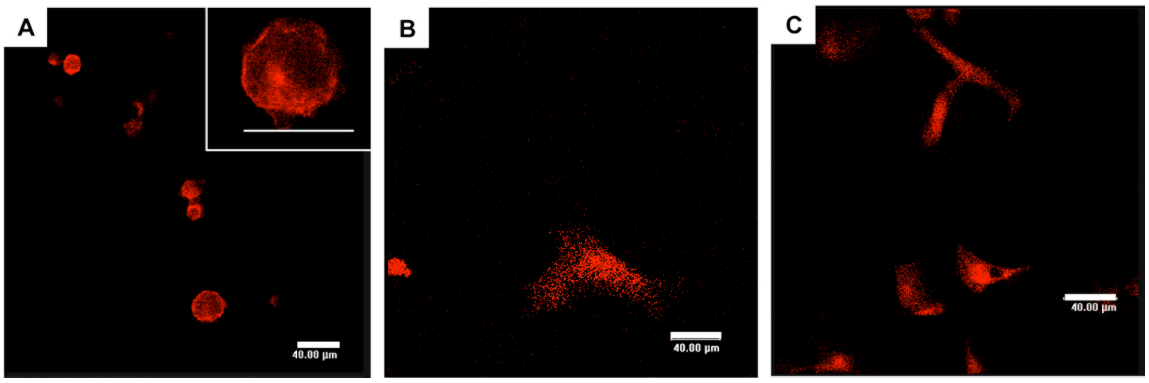

Figure 3.7: Confocal microscopy images displaying actin cytoskeleton. Confocal microscopy images of hFOB 1.19 on ICCs stained for actin after (A) 3h (inset, greater magnification of bottommost cell in image), (B) 1 day, and (C) 4 days.

In this study, diameters of 100, 200, and 330 μm were chosen to demonstrate the ability to construct PLGA ICCs with a range of cavity diameters that would support nutrient and waste diffusion and convection *in vitro* and *in vivo*, as well as tissue and vascular in-growth *in vivo*. Additionally, architectures in this range have been shown to promote osteoblast or bone growth [94, 137].

For each cavity size, the interconnecting channels were large enough to facilitate cell migration throughout the scaffold. Although there is some overlap in the size of interconnecting channels at different annealing temperatures, there is an obvious trend of increased annealing temperature causing increased interconnecting channel diameters. This is important for this type of scaffolds because this experiment demonstrates that both the diameter of the cavities and the diameter of channels connecting them can be controlled during the preparation of the scaffold. The increase of channel diameters is caused by greater melting of microspheres at higher temperatures, providing a greater void space between cavities. It is noted that a slightly greater range of channel diameters exists for each temperature with 330 μm microspheres. This is most likely due to the increased size distribution of 330 μm microspheres (4.9%) over that of 100 μm (3.1%) and 200 μm (2.9%) microspheres, which will cause less-

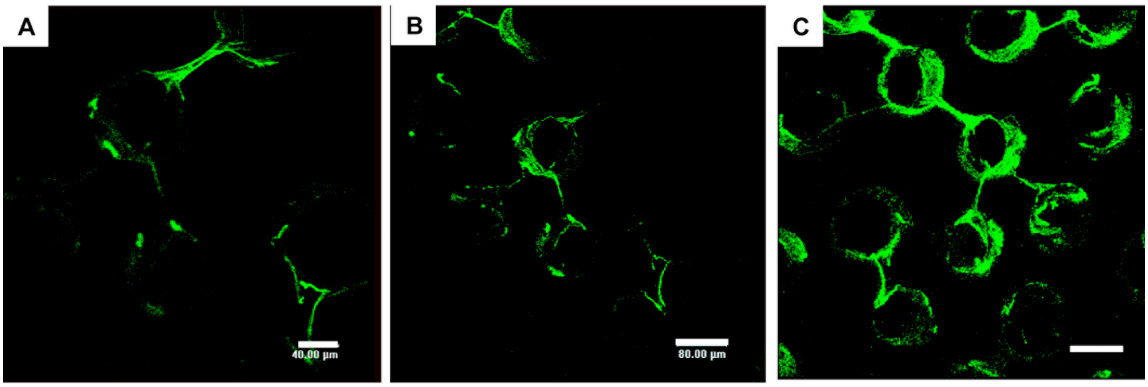

Figure 3.8: Confocal microscopy images displaying collagen type I secretion. Confocal microscopy images of hFOB 1.19 on ICCs stained for collagen type I after four days of culture. (A) Scale bar = 40 μm. (B), (C) Scale bar = 80 μm.

ordered packing and a less consistent degree of contact between microspheres in CCs. Additionally, the increased microsphere size causes faster settling of microspheres during CC construction, which may hinder ordered packing, despite sonication. In each case, the range of interconnecting channel diameters may also be attributed to uneven heat distribution throughout the CC. Adjusting the time of annealing may increase the control over degree of annealing to decrease the variation in interconnecting channel diameters. Despite the range of interconnecting channel diameters, the general linear increase in channel diameter with increased annealing temperature demonstrates an additional level of control over ICC scaffold properties that has not been demonstrated in many other scaffold fabrication techniques.

The targeted functional outcome of bone tissue engineering is to produce a scaffold-cell construct that has mechanical properties supporting the loads of daily life [138]. Overall, the ICC geometry possesses an advantage over traditional porous scaffolds because of its complete interconnectivity at lower porosities. The compressive moduli are greater than those of other porous PLGA scaffolds fabricated using a stochastic arrangement of porogens [139, 140]. In fact, the compressive moduli of the scaffolds are in the range of other polymer scaffolds fabricated using SFF, which can be designed

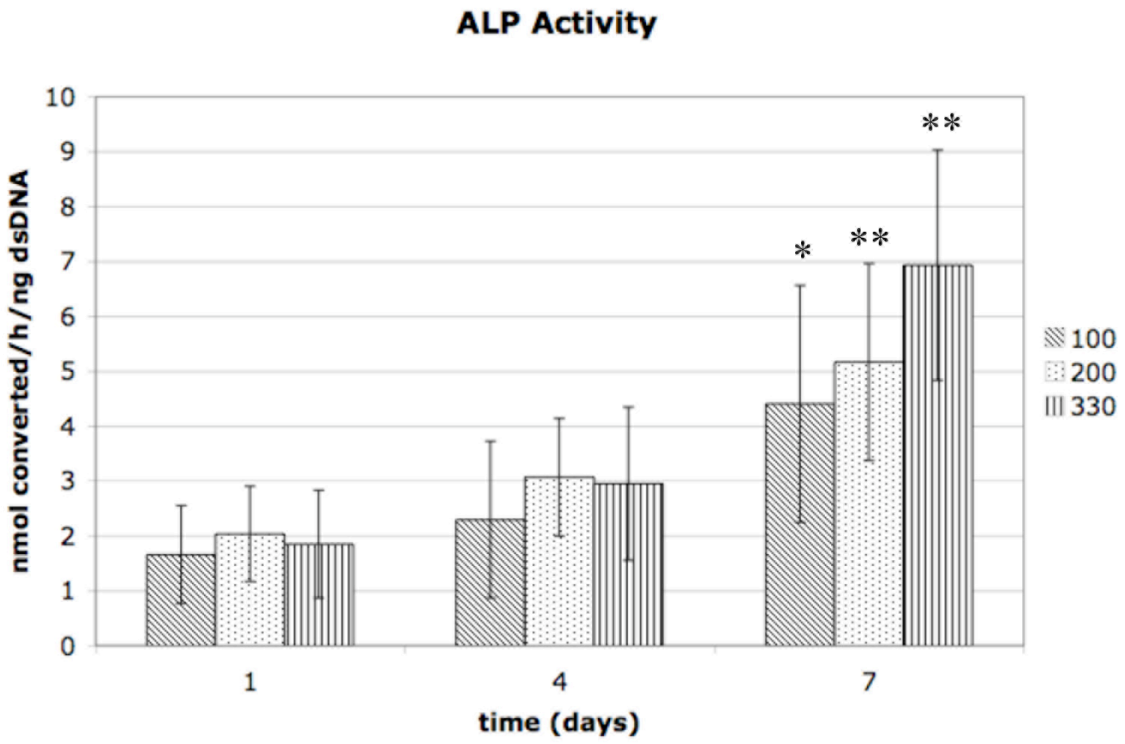

Figure 3.9: ALP activity in scaffolds. ALP activity measured in scaffolds (n=4), normalized by dsDNA levels in scaffolds. (*Statistically significant ($p<0.05$) as compared to day 1; **Statistically significant ($p<0.05$) as compared to days 1 and 4 for the indicated cavity diameter).

to meet specific mechanical properties [56, 141]. Considering the majority of current scaffolds are now composed of composite materials to increase mechanical properties, the ICC scaffolds have great potential to approach the mechanical properties of bone. Improved mechanical properties may be obtained by additional infiltration steps or infiltrating with a stronger biodegradable composite material. An additional infiltration step for the 330 μm or greater CCs may be especially advantageous in obtaining morphological similarity to trabecular bone, which has trabeculae of 80-280 μm in thickness and over 450 μm separation between trabeculae [142].

Confocal microscopy images reveal that cells were able to attach and inhabit the ICC scaffolds for up to 12 days, and the abundance of calcein AM stained cells (green) indicate viability was strong. Cell survival over several weeks is especially important

to establish because of the harsh acid treatment required to remove the microspheres. Note in Figs. 3.5(E) and (F) how cells have begun to coat the cavity walls and appear to have infiltrated beyond the outer layer of cavities.

The variety of cell morphologies displayed in Fig. 3.6 indicates that although cells adhere to the PGLA ICC scaffold, cell adhesion could be improved to achieve more consistently spread morphologies. Increased cell attachment will also encourage cell migration within the scaffold, yielding a more uniform population throughout the structure. F-actin staining revealed that the rounded morphologies with actin localized to the cell membrane were demonstrated at times close to seeding, and that flattened morphologies with a uniform cytoskeleton were observed after a day. The rounded morphologies observed in SEM images may be cells that have recently attached, migrated, or replicated. Still, collagen was not observed at 3 h or 1 day after seeding, indicating that surface modification that enhances or speeds cell spreading may be beneficial in increasing bone production within the scaffold.

The dsDNA assay revealed a trend that greater cell numbers could be found on scaffolds of greater pore sizes, likely because as the pore sizes and interconnecting channel sizes are increased, the cavity openings on the surface of the scaffold are larger, leading to greater cell seeding efficiency. Additionally, there was a trend toward greater ALP activity with greater cavity sizes, as well as increased ALP activity over time. ALP activity was normalized to dsDNA, indicating that cells were more active over time and the increased activity was not due to greater numbers of cells present. As more cells could be seeded into larger pores, perhaps their proximity within spherical pores signal osteogenesis. Additionally, the greater pore sizes likely allow for greater circulation of nutrients, signaling factors, and metabolites. The theoretical porosity should remain the same despite scaffold pore size, but the degree of order may vary slightly with the different size distribution of beads. As well, the permeability of the different cavity sizes was not measured here. These measurements

may further explain the increased viability of the cells in larger pore sizes.

As the quantity of dsDNA did not increase greatly over time for most cavity and interconnecting channel sizes (Fig. 3.4), it is likely that cells were in an osteogenic state, rather than a proliferative state. Low proliferation, increasing ALP activity over time, and the presence of collagen type I are important parameters to consider particularly when utilizing the hFOB 1.19 pre-osteoblast cell line, as these parameters are indicators of osteoblast differentiation and mineralization [123, 143, 144]. As this cell line has a temperature dependent phenotype, meaning that at 33.5 °C cells rapidly replicate, and at 39.5 °C cells display little or no cell division [145]. In these studies, it was indicated that at the incubation temperature used, 37 °C, there low cell replication as well as indicative factors of bone production.

These studies support conclusions that cavity sizes greater than 100 μm are ideal for bone growth, but further study must be performed. Still, one must also remember that with greater pore sizes, mechanical properties are likely to decrease. *In vivo* studies may be more indicative of effects of scaffold feature sizes, as greater quantities of cells, tissues, and circulating fluids are in contact with the scaffold than during *in vitro* studies.

3.5 Conclusions

A new geometry of biodegradable ICC scaffolds was demonstrated with consistent geometries and cavity sizes of 100, 200, and 330 μm. These studies indicated trends that greater pore sizes may increase cell growth and bone production. PLGA ICC scaffolds have great potential for bone tissue engineering applications because they possess a regular structure for high mechanical properties and uniform cell loading and retention. The spherical cavities also provide maximal surface area and variable diameters to support tissue and vascular invasion.

The ICC structure has broad applications in bone tissue engineering in that it can

be incorporated into molds with more complex geometries designed to fit anatomical shapes, for robust mechanical properties, or with architectures ideal for tissue invasion. For example, the ICC structure can be incorporated into molds designed with complex internal architecture for increased mechanical functionality and made using SFF fabrication methods. This incorporation can take advantage of the mechanical and geometric functionality of the SFF scaffold, while increasing its surface area and topography. For this application, CC construction with smaller microspheres might be desired to facilitate increased order when depositing microspheres into molds with their own internal architecture, while providing larger pores in between struts with ICC internal geometries.

3.6 Publications relevant to this chapter

The material in this chapter has been adapted with minor modifications from the following published article:

Meghan J Cuddihy and Nicholas A Kotov. Poly(lactic-co-glycolic acid) bone scaffolds with inverted colloidal crystal geometry. *Tissue Engineering Part A*, 14(10):1639-49, 2008.

CHAPTER IV

In vitro Analog of Human Bone Marrow from 3D Scaffolds with Biomimetic Inverted Colloidal Crystal Geometry

4.1 Introduction

The expansion of human hematopoietic cells *ex vivo* is vital for their use in cellular therapies, as well as in the development of immune therapeutics such as human monoclonal antibodies. As well, as most information on HSC renewal and lineage commitment has been based primarily on mouse models, which do not entirely accurately represent the human body, artificial analogs of the HSC niche can contribute to knowledge of interactions between HSCs and the surrounding stromal cells and matrix. These understandings can be extremely valuable in the situation of pharmaceutical drug testing, where one could observe any effects on HSCs or the niche before testing *in vivo*.

Construction of such *ex vivo* analogs is quite challenging due to the complexity of the human bone marrow microenvironment [146]. Here, stromal cells play a critical role in both presenting membrane-bound ligands and secreting soluble signaling molecules. HSC differentiation is strongly dependent on cellular interactions with stromal tissue and appropriate levels of signal proteins [116, 146–153]. Although the native bone marrow environment can be recreated on 2D culture to some extent by the addition of proper cytokines and growth factors and/or by the presence of co-

cultured stromal or feeder cells [109, 110, 147, 148, 152, 153], it is inefficient for the purpose of replicating hematopoiesis in lacking the dimensionality and ECM components of the HSC niche. Furthermore, 2D cultures have cell-cell contacts only in one direction. Utilizing 3D cell cultures that induce more intensive cell-to-cell contacts between HSCs and stromal cells appears promising to produce the appropriate developmental niches for stem cells [8]. For example, generation of human T lymphocytes from human $CD34^+$ cells *in vitro* was made possible without exogenous cytokines or stromal cells due to 3D organization of the cell scaffold [4].

A 3D matrix ideal for mimicking the HSC niche in bone marrow, specifically for drug testing, must be porous, have a controllable structure, and be made of a transparent material. Porosity and complete interconnectivity allows for cell migration, as well as nutrient, waste, and cytokine diffusion. A controllable structure allows the user to design the intensity of cell-cell contacts, as well as minimizes variation between scaffolds, thereby reducing experimental variability. Transparency is useful in observing the cells through microscopy. With these characteristics in mind, the Kotov group developed the hydrogel ICC scaffolds. ICC scaffolds have a geometry of highly-ordered and uniformly-sized spherical cavities. The cavity size can be easily changed to vary the degree of cell-cell contacts. Each cavity is connected to twelve surrounding cavities, which allows for cell migration and diffusion of cytokines and media. The transparent hydrogel allows the user to view cells within the scaffolds using a simple optical microscope or by tagging the cells with a fluorophore and viewing with a fluorescent microscope.

Our approach for the replication of bone marrow utilized hydrogel ICC scaffolds with feeder cells to demonstrate substantial expansion of $CD34^+$ HSCs. Here, the feeder cells chosen were the human stromal (HS)-5 bone marrow stromal cell line. HS-5 cells were developed from bone marrow specifically for the support of HSCs [109, 110]. HS-5 cells were shown to produce high levels (¿1000 pg/mL) of

growth factors interleukin-6 (IL-6), IL-8, granulocyte colony-stimulating factor (G-CSF), and macrophage-inhibitory protein-1 alpha and also produced detectable levels of granulocyte-macrophage-CSF (GM-CSF), macrophage-CSF (M-CSF), Kit ligand (KL, also called stem cell factor (SCF)), IL-1α, IL-1β, IL-1RA, IL-11, and leukemia inhibitory factor (LIF) [109]. Next, B lymphocyte differentiation was demonstrated with the production of functional B cells and their expression of key signal proteins, class switch of cells from immunoglobulin M (IgM) to immunoglobulin G (IgG). Further evidence of production of functional B cells, such as secretion of influenza A specific antibody, and production of human immune cells in SCID mice after subcutaneous implantation of the designed scaffolds, are presented in a paper by Nichols et al [30], but are outside of the realm of this dissertation.

4.2 Methods

4.2.1 ICC scaffolds fabrication

CCs were prepared as previously reported [27]. Briefly, a plastic mold (diameter (D) = 6.5 mm) was connected to a long Pasteur glass pipette and was partially immersed in an ultrasonic water bath. Two to three drops of polystyrene beads (D = 100 μm, Duke Scientific) suspended in ethanol were released through the Pasture pipette in 20 min time intervals under gentle agitation generated by the ultrasonic water bath until the thickness approximately reached 0.5-1 mm. The beads were completely dried at 60 °C overnight, and then the CCs were annealed at 120 °C for 4 h. Final dimensions of freestanding CCs were 6.5 mm in diameter and 0.5-1 mm in thickness. Scaffolds were manufactured composed of either silicate or hydrogel. For silicate scaffolds, sodium silicate solution (14% NaOH, 27% SiO_2) (Sigma) was diluted with water to a 1:1 ratio with deionized water, and then infiltrated into the CCs by centrifugation at 5800 RPM for 30 min. After that, the composite CCs were

dried overnight in the air to let the sol become a gel. Final silicate ICC scaffolds were obtained after removing the CC template either burning out at 600 °C for 30 min or dissolving by tetrahydrofuran (THF) [33]. For hydrogel scaffolds, hydrogel precursor solution composed of 30% (w/w) acrylamide monomer, 5% (w/w) bis-acrylamide cross-linker, and 0.1% (v/v) N,N,N,N-tetramethylethylene-diamine accelerator was prepared with nitrogen gas purged deionized water. The precursor solution was infiltrated into the CC by centrifugation at 5800 RPM for 10 min, and 1% (w/w) potassium peroxide initiator solution was added. After complete polymerization within 2-3 h at room temperature, the CC containing hydrogel was cut out and immersed in tetrahydrofuran for 24 h to remove the template. Finally the hydrogel ICC scaffolds were washed and equilibrated in deionized water. All chemicals were purchased from Sigma.

4.2.2 LBL surface modification

The surface of polyacrylamide hydrogel ICC scaffolds was coated with sequential layers of negatively charged 0.5% (w/w) clay platelets (average dimension of 1 nm thickness and 70-150 nm in diameter, Southern Clay Products) and positively charged 0.5% (w/w) poly(diallyldimethylammonium chloride) (PDDA) (MW = 200,000) (Sigma) solution utilizing a LBL surface coating technique. The LBL coating was started with a PDDA layer. At first, hydrogel ICC scaffolds were immersed in PDDA solution for 15 min and rinsed in deionized water for 30 min. Then the scaffolds were immersed in clay solution for 15 min and rinsed with deionized water for 30 min. This LBL coating cycle was repeated five times. The outermost layer was clay nanoparticles. To demonstrate 3D LBL coating on hydrogel ICC scaffolds, fluorescein isothiocyanate (FITC) conjugated albumin (Sigma) which has negative charge was used instead of clay nanoparticles. A hydrogel ICC scaffold coated with ten bilayers of FITC-albumin and clay nanoparticles was imaged using the confocal

microscope with 10× objective. Confocal series images taking 160 μm depth were three-dimensionally reconstructed using imaging software.

4.2.3 Bone marrow stromal cell culture

HS-5 (CRL-11882) and hFOB 1.19 cell line (CRL-11372) were purchased from ATCC (Manassas, VA). Culture media for HS-5 was composed of Dulbeccos modified Eagles medium (DMEM) with 4 mM L-glutamine, 4.5 g/L glucose, 1.5 g/L sodium bicarbonate, 10% (v/v) fetal bovine serum (FBS), and 1% (v/v) penicillin-streptomycin (all reagents purchased from ATCC). The hFOB cells were cultured with 45% Hams F12 medium, 45% DMEM, 10% FBS and 1% antibiotic. The cultures were maintained in a T-25 culture flask at 37 °C with 5% CO_2 in high humidity condition. Once cell growth reached approximately 80% confluence, they were detached from the culture flask using 0.25% (v/v) trypsin-EDTA solution and 10^5 cells were seeded on top of UV sterilized scaffolds which were placed in a 96-well plate. Culture volume was maintained 250 mL and media was changed every other day.

In order to characterize stromal cell growth in 3D scaffolds, HS-5 cells were stained with 5 mM carboxyfluorescein diacetate succinimidyl ester (CFSE) (Molecular Probes) [34]. 10^5 pre-stained HS-5 cells were seeded on silicate scaffolds and cultured for 5 days. The cells growing within silicate scaffolds were imaged under a Leica SP2 confocal microscope with 20× objective. A 488 nm laser was used for excitation and emission signals were collected within 515-550 nm window. Transmission image was over-laid with fluorescent image to designate the location of cells within pores.

4.2.4 Human $CD34^+$ HSCs isolation

Peripheral blood buffy coats were obtained from Gulf Coast Blood Bank or from donors (18-50 years of age) after informed consent under protocols that were re-

viewed by the Institutional Review Board of The University of Texas Medical Branch. Cord blood and bone marrow were purchased from Lonza Inc. (Allendale, NJ). The mononuclear leukocyte fraction was isolated from these three $CD34^+$ HSC sources using Ficoll density gradient separation medium as described by the manufacturer (Amersham-Biosciences, Piscataway, NJ). $CD34^+$ HSCs were enriched by counter current centrifugal elutriation of mononuclear leukocytes in a Beckmann J6M elutriator (Beckman Instruments, USA) using a Sanderson chamber. A Masterplex peristaltic pump (Cole Parmer Instruments) was used to provide the counter current flow. RPMI 1640 supplemented with 2 mM glutamine, 100 units penicillin G and 100 mg/mL streptomycin and 10% heat inactivated defined fetal calf serum (Hyclone, Logan, UT) was used as elutriation medium. 3-6 $\times$ 10^6 cells were loaded at 3000 RPM and HSCs were isolated using a step-wise reduction of rotor speed until the appropriate cell diameter population, 6-7 mm, of $CD34^+$ enriched cells was collected.

Immunophenotypic analysis of elutriation with 5-7 μm diameter HSCs at the time of isolation and seeding of the scaffold showed that these cells were lineage cocktail 1 (lin1) mature marker negative, $CD34^+$ cells were further purified by negative selection of any remaining lin1 positive or mature cell types using Dynall magnetic beads or by flow cytometric cell sorting using a FACSaria cell sorter.

4.2.5 Human $CD34^+$ HSCs expansion

$CD34^+$ cells were labeled with the CFSE dye as previously described [34]. Scaffolds were then seeded with 1-4$\times 10^4$ CFSE-labeled $CD34^+$ HSCs in 50 mL of DMEM containing 5% pluronic F-127 on the bottom of a 24-well tissue culture plate. A total of 3-5 scaffolds were placed in a standard 2-10 mL plastic bioreactor chambers mounted on a rotary bioreactor (Synthecon, Houston, TX) with a rotational speed of 5 RPM in the same media. In a subset of experiments matrices were seeded with stromal support cells from human bone marrow aspirates and non-autologous HSCs

were added after 2 days of stromal culture. HSC/stromal cell cultures were also incubated in plastic Petri dishes in order to allow us to evaluate 2D versus 3D cell culture.

4.2.6 Inducing B cell differentiation

To induce HSC differentiation, a co-culture of HS-5 and hFOB1.19 cell line was initially used. Although differentiation was successful these cell lines quickly overgrew the matrix without irradiation and thus were somewhat inconvenient. Later, primary cell lines were created from bone marrow aspirates which included cells positive for CD105 (100%), CD166 (100%), CD44 (95%), CD14 (1%), CD34 (1%) and CD45 (<1%) suggesting they were part of the stromal cell population; at least one cell type in the support cell mix was of osteoblast lineage as it was positive for osteonectin. These primary support cells formed densely populated layers similar to natural bone marrow and replicated the actual bone marrow environment better than the feeder layer made from a single cell type. Growth factors used to promote hematopoiesis included: interleukin IL-2 (5 ng/mL, Calbiochem), IL-7 (20 ng/mL, R&D Systems), Flt3 ligand (20 ng/mL, Chemicon), stem cell factor-1 (SDF-1, 20 ng/mL, Calbiochem), BMP-4 (4 ng/mL, R&D Systems), and IL-3 (10 ng/mL, Chemicon). Additives used to promote development of a B lymphocyte lineage included: soluble CD40L (5 ng/mL, Invitrogen), IL-4 (10 ng/mL, Calbiochem), IL-5 (10 ng/mL, Chemicon), IL-6 (10 ng/mL, Calbiochem), IL-10 (10 ng/mL, Chemicon), IL-2 (5 ng/mL, Calbiochem), IL-7 (20 ng/mL), Flt3 ligand (20 ng/mL), stem cell-derived factor (20 ng/mL, Chemicon), IL-3 (10 ng/mL) and agonist anti-CD40 mAb (5 mg/mL, clone HM40-3; BD Biosciences).

Cultures were exposed to 3.5 mg/mL lipopolysaccharide (Sigma-Aldrich) to activate B lymphocytes and induce plasma cell formation. Secreted IgM was quantitated for all B cell cultures using a total human IgM ELISA assay (Diagnostic Automaton,

Inc.) as described by the manufacturer. Supernatant fluids were removed from 3D and 2D cultures and levels of secreted IgM were determined. All samples were run in triplicate and averaged optical densities at 450 nm were compared to a standard curve using optical densities obtained for each of the standards.

4.3 Results

4.3.1 ICC scaffolds

The matrices described here are ICC scaffolds, which were recently introduced [33,38]. The template for the ICC scaffolds were hexagonally-packed lattices of uniformly-sized (110 μm) microspheres (Fig. 4.1A). The resulting ICCs presented a similar structure of a hexagonally-packed lattice of cavities, with hydrogel filling in the spaces in between the microspheres of the template Fig. 4.1B). The channels that connected the cavities measured approximately 10-20 μm.

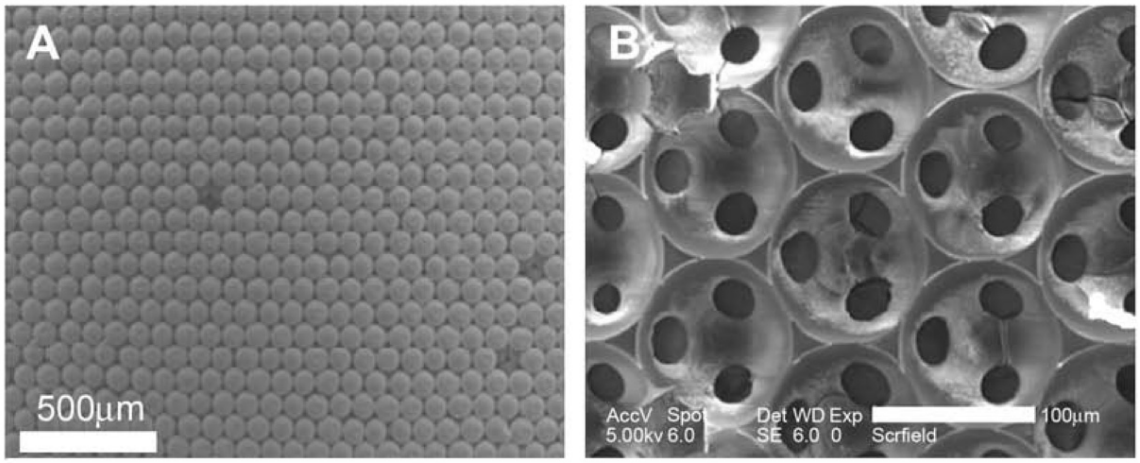

Figure 4.1: SEM images of (A) a CC composed of polystyrene microspheres and (B) an ICC composed of silicate hydrogel.

To provide adequate adhesion of bone marrow support cells, hydrogel matrices were coated by clay and PDDA multilayers via LBL technology [154], which results in a thin layer of nanocomposite on the walls of the scaffold [27] (Fig. 4.2). Fig. 4.2A

presents the overall concept of LBL, where a substrate is dipped first into a charged aqueous solution, and then rinsed so that only one monolayer of the charged substance remains. The solution may be of any charged substance that can form a solution in water; e.g. polymers, nanoparticles, or proteins. Next, the substrate is dipped into an aqueous solution of the opposite charge, which is then rinsed so that one monolayer adheres. This cycle completes one bilayer, and it can be repeated until as the desired number of bilayers have adsorbed onto the surface. Fig. 4.2B is a schematic of the clay/PDDA layers, and Fig 4.2C is an atomic force microscope (AFM) image of the clay/PDDA layers on a silicon wafer [154]. Fig 4.2D demonstrates LBL on an ICC scaffold through 5 layers of FITC-labeled albumin and PDDA.

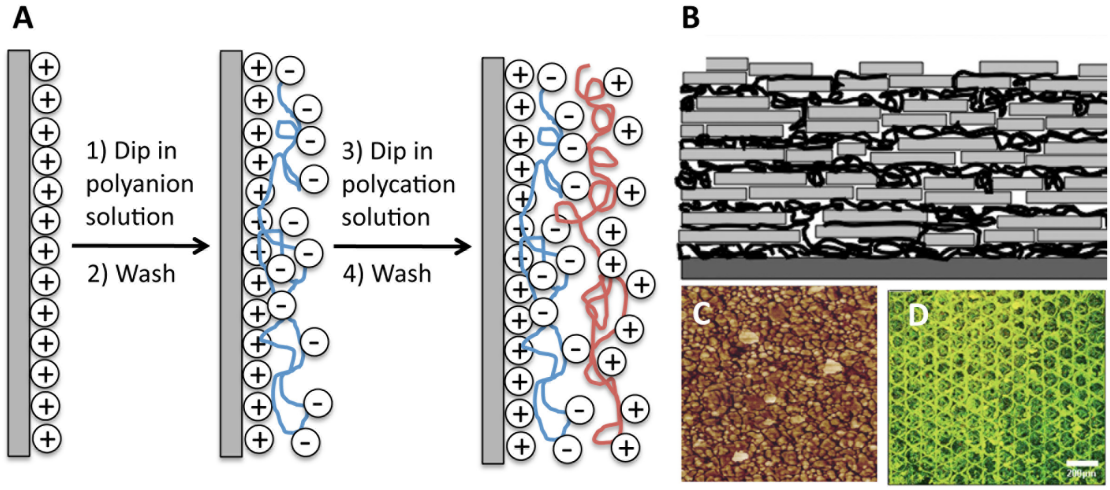

Figure 4.2: Schematic of LBL surface coatings and its applications on ICC scaffolds. (A) Schematic of LBL on a flat substrate. (B) Illustration of clay/PDDA LBL on a flat substrate [154]. (C) AFM image of PDDA/LBL on a silicon wafer. (D) 3D reconstruction of an ICC scaffold coated with five layers of FITC-labeled albumin and PDDA. Scale bar = 100 μm.

4.3.2 HSC niche

Human bone marrow stromal cells were seeded on scaffolds and cultured for 3 days to allow the formation of a support cell layer on the scaffold surface prior to

the addition of $CD34^+$ HSCs. Bone marrow stromal cells were stained for expression of the cell marker CD105 to allow for visualization of the stromal cell network that was formed by day 3 (Fig. 4.3A). On day 3 $CD34^+$ were then seeded onto stromal cell/ICC constructs (Fig. 4.3B). HSCs were isolated from human peripheral blood (PB), umbilical cord blood (CB) or bone marrow (BM). All cells were positive for CD34 and were lin1 negative when seeded onto the scaffolds. Analogous cultures were also made on 2D plates to establish the importance of the 3D geometry in ICC scaffolds. Examination of ICC cultures on day 28 showed the continued presence of $CD34^+$ HSCs (red) (Fig. 4.3C); $CD34^+$ antibody-labeled cells (red) are shown interacting within the scaffold with $CD105^+$ stromal cells (green).

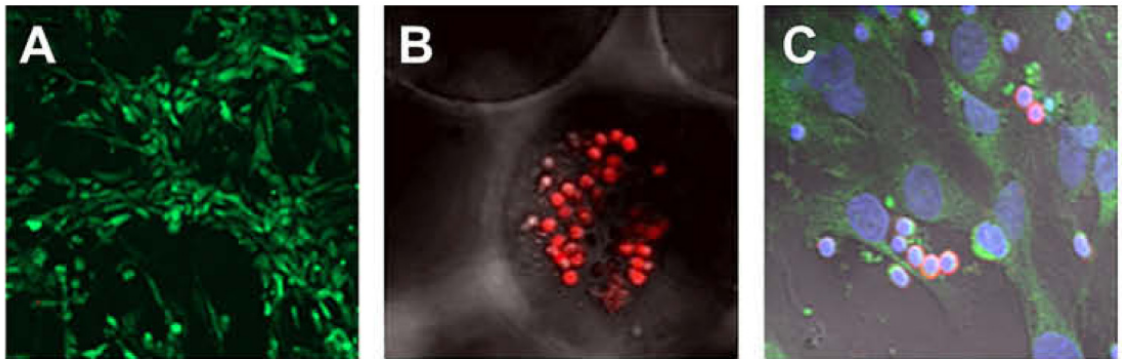

Figure 4.3: Confocal microscopy images of stromal- HSC interactions. (A) Stromal cells after 3 days of culture, stained for CD105 (green). (B) $CD34^+$ cells (red) interacting with stromal cells (green) after 1 day of culture. (C) Interactions between $CD34^+$ cells (red) and stromal cells (green) after 28 days of culture.

Data from flow cytometry show that there were significantly higher percentages of $CD34^+$ cells in ICC cultures after 28 days, regardless of the original cell source, when compared to 2D plate cultures (Figs. 4.4A-F). Figs. 4.4A-C correspond to 3D ICC cultures, while Fig. 4.4D-F correspond to 2D plate cultures. Cells in cultures Fig. 4.4A and D, B and E, and C and F were isolated from bone marrow, cord blood, and peripheral blood, respectively. A significantly greater percentage of cells in ICC scaffolds expressed CD34 (red) over the isotype control (green line). These data are

summarized in Fig. 4.4G. This demonstrates that an undifferentiated population of $CD34^+$ cells was maintained over time and demonstrates the importance of the chosen 3D ICC organization of the cell cultures for replication of reproductive functionality of bone marrow. This is also supported by the loss of CFSE fluorescence intensity (Fig. 4.4H), where the percentage of CFSE loss corresponds to the proliferation of the cells labeled with it ($CD34^+$).

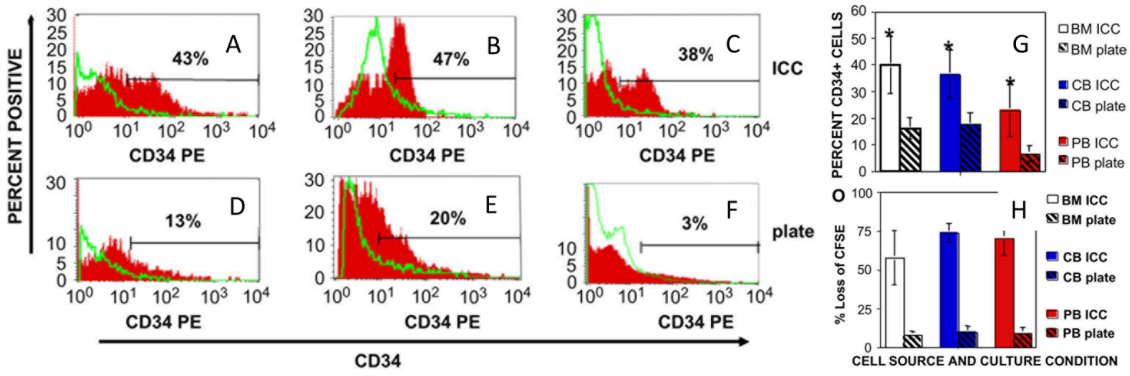

Figure 4.4: Flow cytometry results from $CD34^+$ expansion after 28 days. (A-F) Histograms representing cells stained for CD34. Red histograms represent cells that stain positive for CD34, green represents the isotype controls. (A-C) 3D ICC cultures. (D-F) 2D plate cultures. Cells in A and D, B and E, and C and F were sourced from bone marrow, cord blood, and peripheral blood, respectively. The percentages indicated on each plot are the percentage of cells that express higher intensity for the CD34 marker when compared to the isotype control. (G) Summary of percentages of cells positive for CD34. (H) Loss of CFSE fluorescence intensity.

To assess the ability of the artificial bone marrow constructs to produce functional immune cells, we focused on B lymphocyte production since B cells normally undergo the process of differentiation (as well as negative and positive selection) in the bone marrow [148, 153, 155, 156]. After 3 days of culture, ICC/stromal cell constructs containing growth factors to drive the B cell differentiation were seeded with $CD34^+$ HSCs isolated from umbilical cord blood. Cell cultures were examined for stage-specific markers of development and functionality on days 1, 7, 14, 28 and 40. ICC cultures showed nuclear specific expression of recombination activating gene-1 protein

(RAG-1), which is expressed in developing B and T lymphocytes, by day 7 (Fig. 4.5A). Also seen by day 14 (Fig. 4.5B) was cell surface expression of IgM (green) and CD19 (red), indicating differentiation of the $CD34^+$ HSC into B cells. Co-expression of IgM (green) with IgD (red) was seen by day 28 (Fig. 4.5C) confirming differentiation of $CD34^+$ into mature antigen-naive B lymphocytes. Averaged data for cells from six different donors evaluating expression of CD40, IgD, IgM as well as co-expression of IgD and IgM are displayed in Fig. 4.5D and show the comparison between 3D and 2D cultures. Expression of CD40 ($P = 0.0002$) and IgM/IgD co- expression ($P = 0.021$) was significantly higher in donor matched ICC cultures than in 2D cultures (Fig. 4.5D).

4.4 Discussion

The open geometry of the ICC lattice, high porosity (74% free space), full interconnectivity, and large surface area made ICC scaffolds an attractive structure for the studies of 3D effects in cell cultures. The ICC structure (Fig. 4.1) is geometrically similar to that of trabecular bone, which is important for creation of the microenvironmental niches that maintain stem cell survival and promote maturation [157–159]. As the beads provide a template for the scaffold cavities, the diameter of the beads is directly proportional to the diameter of the resulting cavities. Similarly, the size of channels connecting the cavities can be tuned by the bead diameter, as the degree of contact upon annealing is greater for larger beads, and also by annealing temperature and time [25]. This bead diameter was chosen because it provides efficient contacts between adhesion and dispersion cells [62], and allows for natural cell migration through the channels between the cavities, which is imperative for replication of hematopoietic tissues. The materials of a typical ICC scaffold used here can be either silicate or polyacrylamide hydrogel, both of which were demonstrated to be compatible with human cell cultures [26, 27, 29]. Lastly, dynamic culture within a rotary

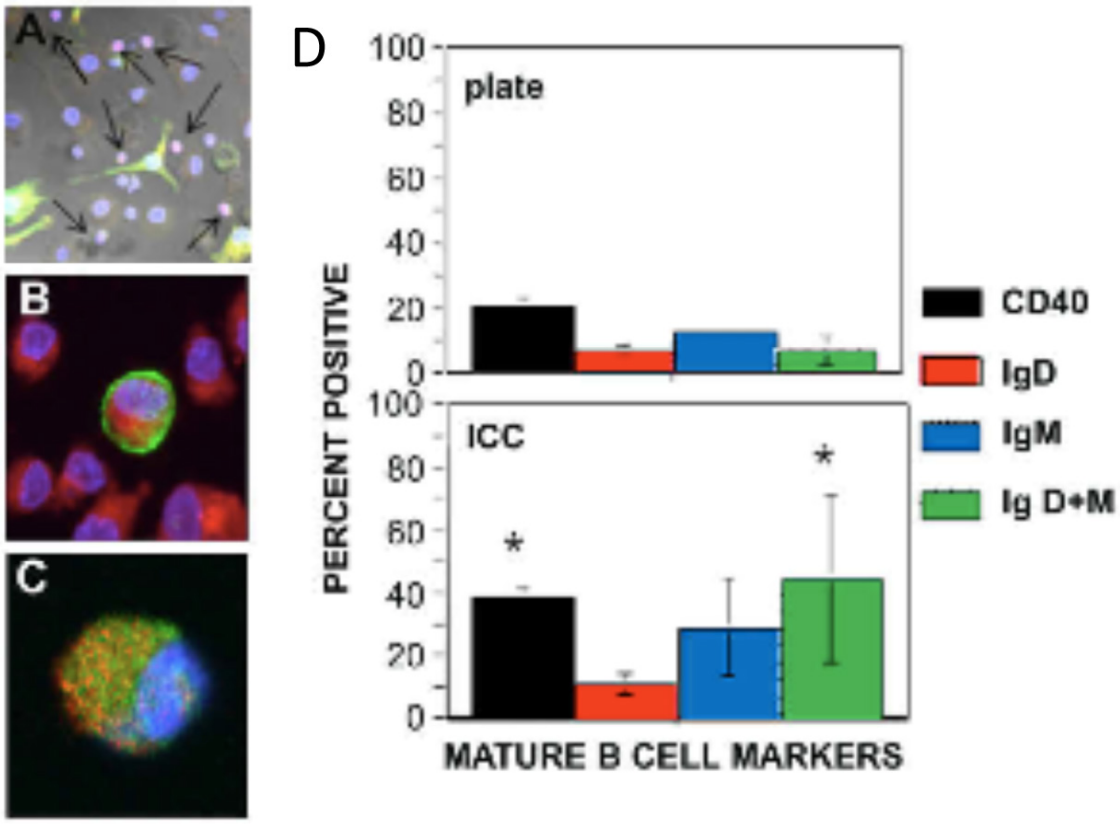

Figure 4.5: Results of B cell differentiation. (A-C) Confocal microscopy images of cultures in ICC scaffolds. (A) Expression of Nuclear RAG-1 (red) and surface expression of IgM (green) on day 7. (B) Cell surface expression of CD19 (red) and IgM (green) on day 14. (C) Expression of IgM (green) and IgD (red) on day 28. In all images, blue indicates DAPI nuclear stain. (D) Flow cytometry results quantifying percentage of cells expressing IgM, IgD, and CD40 for plate and ICC cultures.

cell culture vessel was beneficial not only by creating a more realistic physiological environment but also by maximizing the role of specifically designed ICC geometry by generating continuous convective media flow into ICC pores.

To facilitate cellular adhesion to the hydrogel, ICC scaffolds were coated with a LBL-applied nanocomposite of clay/PDDA (Fig. 4.2). The nanoscale nature of the coating is essential for several reasons. (i) The hybrid organic-inorganic composite is mechanically compatible with the hydrogel and does not delaminate. (ii) It provides high Youngs modulus [29] necessary for successful stromal cell adhesion [16, 160].

(iii) Nanocomposites have minimal light scattering because the characteristic diameter of the inorganic component is smaller than the wavelength of light, which is quite relevant for optical interrogation of biological processes. These features markedly differentiate ICC hydrogel scaffolds from those previously used for bone marrow cultures. In fact, the nanocomposite bilayers add another layer of tunability to the construct related to cell adhesion in that the surface stiffness of the scaffold can be adjusted with the number of bilayers coated on its surface. For example, freestanding films of the same materials were shown to have increased Youngs modulus with increasing numbers of bilayers [29]. The ability to tune mechanical properties and increase surface stiffness by the addition of nanocomposite bilayers is important because substrate mechanics have been shown to influence cell adhesion [15, 161, 162]. Additionally, the bilayers provide a surface charge necessary for cell adhesion. Lastly, multilayer films have also been shown to guide cell differentiation [163, 164]. In the framework of this study, no difference in silicate and hydrogel ICC scaffold performance in terms of bone marrow functionality was observed, although hydrogel scaffolds are preferred due to much higher transparency and ease of confocal microscopy examination.

Self-renewal and maintenance of an undifferentiated population of $CD34^+$ HSCs and production of fully functional immune cells of specific leukocyte lineages are the two basic functions of bone marrow most essential for applications mentioned above. Bone marrow stroma is comprised of a complex reticulum containing hematopoietic precursors, as well as non-hematopoietic cells such as fibroblasts, epithelial cells, nerve cells, reticular cells, adipocytes and osteoid cells [147, 148, 152, 153, 163–165]. It is unknown how many or all of these cell types may be necessary to support the development of fully functional leukocytes. Figs. 4.3 and 4.4 demonstrate the successful expansion of $CD34^+$ cells within the stromal-cell coated ICC scaffolds. The direct interactions between stromal cells and $CD34^+$ cells that can be seen in Fig. 4.3) provided cues for the expansion of $CD34^+$ cells rather than their quiescence

or differentiation. Fig 4.4 demonstrates that the 3D ICC scaffolds induced much greater $CD34^+$ expansion than 2D plates.

The next step taken to demonstrate the functionality of the expanded $CD34^+$ cells was the production of B cells. Growth factors were added to the media to induce differentiation. After seven days of culture (Fig 4.5) , the cells demonstrated nuclear expression of RAG-1, which is a marker for immature B cells. By day 14, cells were expressing IgM and CD19, which are B lymphocyte differentiation markers. By day 28, the co-expression of IgM and IgD indicated the presence of mature B cells. When compared to 2D plates, a significantly greater percentage of cells in ICC scaffolds displayed markers for CD40 and co-expression of IgM and IgD.

4.5 Conclusions

In this work we demonstrated the following key points. The use of 3D ICC cultures allowed for significantly greater production of $CD34^+$ cells when compared to 2D cultures, demonstrating that dimensionality is a key component of the HSC niche. Directed differentiation of the $CD34^+$ cells also demonstrated that 3D culture in ICC scaffolds produced greater expression of key B cell markers. ICC scaffolds allowed for the growth, differentiation and movement of cells in a 3D environment effectively mimicking the natural *in vivo* bone marrow environment normally encountered during hematopoiesis and B lymphopoiesis.

4.6 Publications relevant to this chapter

The material in this chapter was performed in collaboration with the group of Dr. Joan Nichols at the University of Texas Medical Branch. It is presented here with minor modifications. The full study, which includes the stimulation of mature B cells and *in vivo* studies, is found in following published article:

Joan E. Nichols, Joaquin Cortiella, Jungwoo Lee, Jean A. Niles, Meghan Cuddihy, Shaopeng Wang, Joseph Bielitzki, Andrea Cantu, Ron Mlcak, Esther Valdivia, Ryan Yancy, Matthew L. McClure, Nicholas A. Kotov. *In vitro* analog of human bone marrow from 3D scaffolds with biomimetic inverted colloidal crystal geometry. Biomaterials. 30:1071-9. 2009.

CHAPTER V

Replication of Bone Marrow Differentiation Niche: Comparison of Three-Dimensional Matrixes

5.1 Introduction

Many blood and bone marrow diseases, such as chronic myelogenous leukemia, acute myelogenous leukemia, and bone marrow failure syndromes, are characterized by disordered development or production of hematopoietic cells in the bone marrow [166, 167]. The interactions between HSCs and the bone marrow niche are incredibly complex and not completely understood [103, 146]. Bone marrow stroma, the tissue surrounding hematopoietic tissue, is composed of a variety of cell types and ECM molecules [151, 157, 168–170]. HSCs interact with these cell types directly through cell-cell contacts or indirectly through secreted growth factors or ECM. In fact, some of these HSC diseases are thought to be influenced by interactions with stromal cells [171].

Despite the complexities of the HSC niche, current *in vitro* pre-clinical drug testing methods are dependent on HSC culture on 2D surfaces. To provide niche signals to the HSCs, they are cultured either on stromal cells [109, 110], in media supplemented with high concentrations of growth factors [111, 112], or both. The 2D models allow for the maintenance and expansion of HSC, but lack the dimensionality and ECM components of the HSC niche [172]. With this in mind, 3D models of the bone marrow niche, primarily designed for HSC expansion, were developed. These models ranged

from nanofiber scaffolds [105, 108], to porous natural polymers [113] and synthetic polymers [114, 115]. One of the most common 3D matrices used in hematopoietic and other stem cell cultures is a commercially available matrix protein gel called Matrigel [117, 118]. Matrigel is composed of extracellular matrix proteins extracted from Engelbreth-Holm-Swarm mouse sarcomas. The gel has an advantage of being liquid at 4 °C and gelling at 37 °C. With this property, Matrigel can be mixed with cells, proteins, or other desired culture components at the low temperature, and plated or injected into an animal where it will polymerize into a gel. As well, Matrigel contains several growth factors, including transdermal growth factor (TGF)-beta, epidermal growth factor, and fibroblast growth factor, so it can be a source of soluble signals that may be useful for certain applications [24, 173–175]. As Matrigel is composed of matrix from *in vivo* sources, cells can digest and restructure the matrix [83]. This feature is useful for through-tissue migration studies [84], but can be hindering in tissue engineering applications where matrix digestion disrupt the 3D structure. As well, the murine source of Matrigel introduces the potential of viral contamination. The batch-to-batch reproducibility of Matrigel is also a concern.

Recently, a 3D bone marrow analog was designed using ICC scaffolds [30]. ICC scaffolds are hydrogel matrices with uniformly shaped spherical cavities arranged in a hexagonal array where each cavity is connected to twelve adjacent cavities [12, 17, 26–29, 31]. The bone marrow analog utilized a transparent acrylamide hydrogel with 70% water content, coated with clay nanocomposite to allow for cell attachment and to mimic the mineralized surface of bone. $CD34^+$ cells, hematopoietic progenitor cells, were expanded within scaffolds with the support of growth factors and bone marrow aspirates, and the $CD34^+$ cells were then differentiated into functioning B cells. The results showed much greater expansion and directed differentiation of $CD34^+$ cells when compared to 2D cultures, demonstrating that the 3D interactions are necessary for $CD34^+$ cell expansion. The ICC scaffolds demonstrated some intrinsic advantages

with the stromal-CD34$^+$ cell co-culture. The geometry of closely-packed spherical cavities provided 3D interactions between the stromal and stem cells. Physically, the stem cells could contact stromal cells from multiple directions, especially when compared to the unidirectional interactions on 2D well plates. As well, soluble factors are released in all directions from the attached stromal cells, eliminating the steep concentration gradient that is seen in 2D. The interconnectivity also played a large role in stromal-stem cell interactions. As CD34$^+$ cells are not attachment-based, they were free to migrate throughout the scaffold. This is unique to the ICC scaffolds when compared to encapsulation-based 3D matrices such as Matrigel.

An *in vitro* system that represents the interactions between HSCs and their niches has great potential for use in pharmaceutical drug testing. In an *in vitro* HSC niche for pharmaceutical drug testing, one would test drugs that specifically target bone marrow, such as for anti-leukemia drugs, or those that have side effects within bone marrow, like anti-virals [176]. Given that the *in vitro* niche accurately represents the interactions within the *in vivo* HSC niche, the user could obtain information about how the drug may act in the human body long before clinical trials. To learn about the effects of drugs on HSCs and their niche, one should use cells as the source of cytokines and other signals, rather than high doses added to the media. The choice and number of stromal cells types should be highly controlled and simplified to make the environment repeatable. Lastly, the environment should produce a stable number of HSCs to best represent the body and to best see the effects of drugs on the system.

With these features in mind, we chose to compare three intrinsically different cell culture formats: traditional 2D tissue cultured polystyrene, Matrigel, and ICC scaffolds. A direct comparison between these cell culture formats has not been published. The three formats have great potential in bone marrow drug testing but have intrinsically have very different properties; thus, it is important to directly compare the formats in the context of this potential. In addition to dimensionality and feature

scale, it is important to note the differences in cell-cell contacts in each of these formats. In 2D culture, the as $CD34^+$ cells are plated on top of stromal cells so the two cell types are in direct contact. In order to provide a true 3D structure to the Matrigel culture, one must encapsulate the cell cultures in the gel by mixing the gel and cells before plating. With cell encapsulation, cells are surrounded and separated by matrix, limiting cell-cell contact. For cells to have cell-cell contact, they must digest the matrix and migrate to one another. As ICC scaffolds have a porous 3D structure, they can be seeded directly onto the matrix, allowing for them to contact not only the matrix but also each other. Thus, with these three matrices we can compare 2D and 3D matrices, as well as those with intimate and limited cell-cell contact. As well, we chose to examine HSC cultures with two stromal cell types. The first is the HS-5 cell line, which secretes many HSC-supportive growth factors, as mentioned in Chapter 4. The second is the hFOB 1.19 cell line, which has not been characterized as well, but its known cellular products include alkaline phosphotase and osteocalcin [145]. Osteoblasts are important to consider because of the extracellular matrix secreted and also because of osteoblast-HSC contacts that are known to be important for HSC signalling, such as Ang1-Tie2 and transmembrane SCF [99, 103, 157]. In vivo, bone marrow is a 3D tissue with extensive cell-cell contacts, so the distillation of these features to those that are most important in a culture format and cellular microenvironment is significant.

5.2 Materials and Methods

5.2.1 ICC fabrication

Colloidal crystals were prepared in a manner similar to those previously described [25]. One gram of soda lime beads with a diameter of 80 μm (Thermo Scientific) were mixed with approximately 5 mL of ethylene glycol. Under constant sonication, one

drop of beads was added every 20 minutes to the top of the pipet that was inserted into a 4.5 mm diameter vial. Drops were added until the height of beads in the vial was approximately 1 centimeter (cm). Ethylene glycol was evaporated in a furnace at 165 °C overnight, and beads were annealed at 665 °C for 3 h. Annealed colloidal crystals were cracked out of the vials.

Cationic hydrogels were infiltrated and formed in the colloidal crystals as previously described [32]. Briefly, an initiator solution was made by adding 0.1 g potassium persulfate (KPS) to 10 mL of deoxygenated water. Next, an acrylamide precursor solution was made by adding 3.5 g N,N-dimethylacrylamide (DMAA), 0.5 g (3-Acrylamidopropyl)trimehtylammonium chloride (AMTAC), and 0.05 g N,N-Methylenebis(acrylamide) (MBA) to 9 mL of deoxygenated water. Colloidal crystals were added to vials, and enough precursor solution was added to completely submerge the crystals. The colloidal crystals were then centrifuged in precursor solution for 25 minutes at 5500 RPM. Next, 300 μL of initiator was added to each vial, and centrifugation was repeated for an additional 15 minutes. Vials were heated in an oven for 3 h at 75 °C with the caps placed on the vials but not screwed tight, and then overnight at 60 °C with caps screwed tight. Gels were then cracked out of vials, and excess gel was scraped off of the colloidal crystals using a razor blade.

Glass beads were removed as described previously using a series of HF and HCl washes; removal of soda lime was accelerated by ultrasonicating during acid washes. The resultant 1 cm ICCs were washed several times in PBS before cutting. To cut the 1 cm ICCs into thin scaffolds, ICCs were first mounted in HistoGel (Thermo Scientific), and cut into 350 μm thick sections using a Vibratome 3000 series sectioning system (VIbratome, St. Louis, MO). Thin ICCs were then washed sequentially with PBS, pH 10 buffer, calcium chloride, and PBS. Scaffolds were sterilized by washing in 190 proof ethanol, and then were washed twice in sterile PBS.

5.2.2 Stromal cell expansion

hFOB cell line 1.19 (CRL-11372) and bone marrow HS-5 cells (CRL-11882) were purchased from ATCC (Manassas, VA). hFOB 1.19 cells were grown as recommended by ATCC in 45% Hams F12 medium, 45% DMEM, and 10% FBS (Gibco, Frederick, MD) supplemented with 0.3 mg/mL G418. HS-5 cells were grown as recommended by ATCC in DMEM supplemented by 10% FBS and 1% penicillin-streptomycin. Both cell types were grown at 37 °C and 5% CO_2, with the medium changed every 2 to 3 days.

5.2.3 Stromal and CD34$^+$ cell seeding in 2D cultures

For each matrix type, hFOB 1.19 or HS-5 cells were seeded at a density of 40,000 cells per culture. This number was chosen to avoid contact inhibition in 2D 96-well plate cultures. Stromal cells were seeded directly onto the plate, and allowed to attach for three hours before irradiating at 6000 rads. Media was then changed to StemSpan (StemCell Technologies, Vancouver, BC) supplemented with 40 μg/mL low density lipoprotein (Sigma) and 1% penicillin-streptomycin. Frozen bone marrow CD34$^+$ cells (StemCell Technologies) were thawed and washed with StemSpan as directed by the cell supplier. CD34$^+$ cells were added to cell cultures at a density of 10,000 cells/well and cultured at 37 °C and 5% CO_2. Controls were prepared by culturing CD34$^+$ cells without stromal cells in 96-well plates.

5.2.4 Stromal and CD34$^+$ cell seeding in Matrigel cultures

In order to encapsulate irradiated stromal cells with CD34$^+$ cells in Matrigel, hFOB 1.19 and HS-5 cells were irradiated at 6000 rads in 75 cm^2 flasks prior to seeding in gels. Matrigel cultures were prepared according to manufacturers instructions for culturing cells within the matrix. Briefly, three tubes were placed on ice and equal volumes of Matrigel was pipetted into each tube. hFOB 1.19 or HS-5 cells were

counted and placed into Matrigel tubes so that each well would receive 40,000 stromal cells; the third tube was left without cells. $CD34^+$ cells were thawed and washed with StemSpan, and $CD34^+$ cells were added to cell cultures at a density so that 10,000 $CD34^+$ cells would be included in each well. Matrigel, stromal cells, and $CD34^+$ cells were gently mixed by pipetting, and 32 μL of Matrigel-cell mixtures were added to each well. Cells were cultured at 37 °C and 5% CO_2.

5.2.5 Stromal and $CD34^+$ cell seeding in ICC Scaffolds

One scaffold was placed in a well of a 96-well plate. 100 μL of 190 proof ethanol was added to each well. Scaffolds were allowed to equilibrate for 10 minutes before ethanol was removed and replaced with an additional 100 μL of fresh ethanol. After 10 minutes, most of the ethanol was removed and plates were placed in an incubator at 37 °C overnight to evaporate any residual ethanol. The next day, cell solutions of either hFOB 1.19 or HS-5 cells were made at a density of 40,000 cells per 20 μL . 20 μL of cell suspension gently was pipetted directly onto each dehydrated scaffold, and well plates were placed in an incubator for three hours. Wells were then filled halfway with HS-5 media (described above), and cells and scaffolds were irradiated at 6000 rads. Media was then removed and replaced with StemSpan media. $CD34^+$ cells were thawed and washed with StemSpan as described above. $CD34^+$ cells were added to cell cultures at a density of 10,000 cells/well and cultured at 37 °C and 5% CO_2. Controls were prepared by culturing $CD34^+$ cells without stromal cells in ICC scaffolds.

5.2.6 Live/dead staining

After 8 days of culture, cells were incubated in 2 mM of calcein AM and 4mM of ethidium homodimer-1 using a Live/Dead Viability/Cytotoxicity Kit (Invitrogen Corporation, Carlsbad, CA). Images were acquired directly in 96-well plates using a

Leica DM IRB inverted microscope.

5.2.7 Flow cytometric analysis

Enumeration of cells expressing the $CD34^+$ marker was performed by flow cytometry. For 2D and ICC cultures, cells were released through treatment with trypsin-ethylenediaminetetraacetic acid (EDTA) and repeated pipetting. Matrigel cultures were released by treatment with Dispase and repeated pipetting. Cells were washed in ice cold 2% FBS in PBS, and incubated with fluorescently labeled CD34, glycophorin A (GlyA), and lin1 (CD3, CD14, CD16, CD19, CD20, CD56) antibodies (BD Biosciences, San Jose, CA). The combination of lin1 and GlyA are hereafter referred to as lin. Relevant single color, negative, and isotype controls were prepared for compensation and to distinguish specific binding. Flow cytometry was performed on either a Beckman Coulter Quanta SC or a BD FCSCanto II. Regions positive for CD34 and lin1/GlyA were determined based on isotype controls.

5.2.8 Enzyme-linked immunosorbent assay (ELISA)

ELISAs for IL-6 (R&D Systems, Minneapolis, MN), SCF (R&D Systems), and fms-like tyrosine kinase receptor-3 (flt-3) (R&D Systems) were performed according to manufacturer instructions.

5.2.9 Statistical Analysis

In all graphs, data is represented as the average of the indicated sample sizes $\pm$ standard deviation. A Students t-test was performed to determine statistical significance ($p<0.05$).

5.3 Results

5.3.1 Imaging of cultures

Fig. 5.1 highlights the different cell-matrix interactions in each culture type. In all culture formats, stromal-free cultures show a sparse number of rounded $CD34^+$ cells and their progeny. These cultures showed little, if any, expansion. Of particular interest are the cultures that included stromal cells. Figs 5.1B and C display 2D cultures. Here, stromal cells lay flat and $CD34^+$ cells and their progeny remain round on top of the stromal cells. Stromal cells in Matrigel cultures (Fig 5.1E-F) are rounded and isolated from the hematopoietic cells due to encapsulation. Some stromal cells have migrated to the bottom of the plate and lay flat (Fig 5.1F). In ICC cultures stromal cells are difficult to see because they conformably adhere to the matrix and the hematopoietic cells cluster within cavities. Figs 5.1J-L display live/dead stains of the matrices, further illustrating the cell morphologies and viability. In each culture, cells appeared mostly viable.

5.3.2 Enumeration of cells within matrices

The number of cells that could be extracted from each culture type at days 7 and 14 were quantified using a hematocytometer (Fig 5.2A). These cells included both stromal cells and $CD34^+$ cells and their progeny. In all matrices the number of cells in stromal cell-free culture were very low, indicating that these cells did not replicate significantly. The cells extracted from 2D surfaces displayed little growth at day 7 but had expanded by day 14. Conversely, cells grown in Matrigel expanded significantly at day 7 but had decreased by day 14. ICC scaffold cultures displayed consistent cell numbers over the two weeks. All co-cultures produced significantly ($p<0.05$) more cells than the cultures with $CD34^+$ cells alone. In all instances, within the same matrix type and day, the number of cells produced by hFOB 1.19 co-cultures

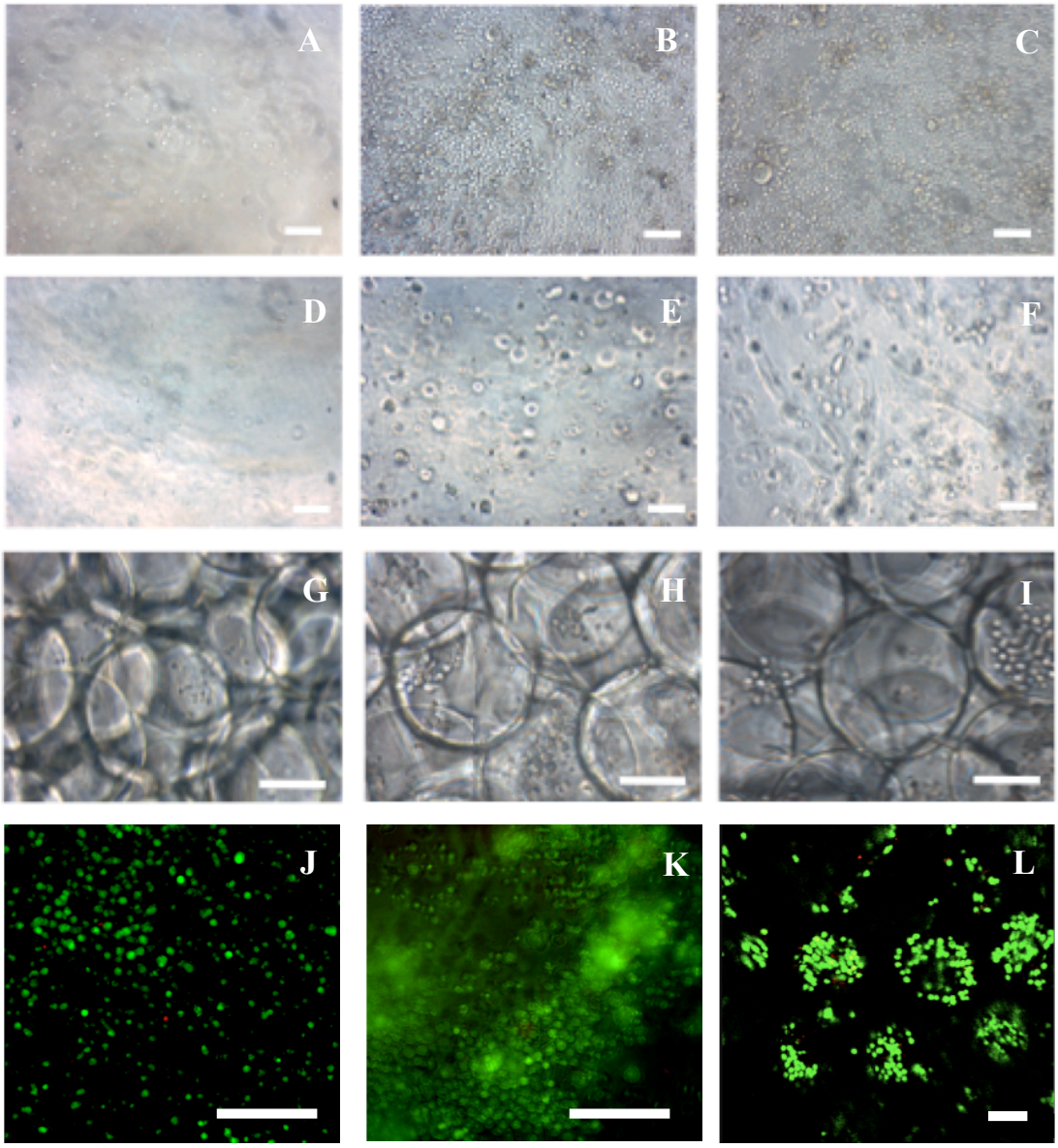

Figure 5.1: Representative images of matrices. (A-I) Inverted microscope images of cells in matrices on approximately day 7. (J-L) Confocal images with live/dead stain. The first row of images (A, B, C) shows cells grown in 2D, the second row (D, E, F) shows cells grown in Matrigel, and the third row (G, H, I) shows cells grown in ICC scaffolds. The first column (A, D, G) displays $CD34^+$ cells grown alone, the second column (B, E, H) displays $CD34^+$/hFOB 1.19 co-cultures, the third column (C, F, I) displays $CD34^+$/HS-5 co-cultures. The fourth row, cells stained with the live/dead assay, shows cells grown in (J) 2D, (K) Matrigel, and (L) ICCs. Green cells are alive, while cells stained red are dead. Scale bar: (A-I) 100 μm, (J-L) 80 μm.

were not significantly different when compared to the HS-5 cultures. The amount of expansion, represented as the number of cells extracted divided by the number of cells initially seeded in the cultures, is displayed in Table 5-1.

Table 5.1: Expansion of cells in different matrices.

		Total cells		$CD34^+/lin^-$ cells	
		Day 7	Day 14	Day 7	Day 14
2D	$CD34^+$ alone	0.42	0.02	0.14	0.01
	hFOB 1.19 / $CD34^+$	0.99	8.57	0.24	0.85
	HS-5 / $CD34^+$	1.02	6.23	0.38	1.05
Matrigel	$CD34^+$ alone	0.30	0.43	0.02	0.01
	hFOB 1.19 / $CD34^+$	5.59	1.79	0.02	0.05
	HS-5 / $CD34^+$	13.50	5.41	0.11	0.50
ICCs	$CD34^+$ alone	0.11	0.15	0.05	0.01
	hFOB 1.19 / $CD34^+$	1.31	0.66	0.43	0.19
	HS-5 / $CD34^+$	0.46	0.86	0.29	0.09

Expansion is calculated by the number of cells extracted divided by the number of cells added to the matrix at the beginning of culture (total cells or $CD34^+/lin^-$ cells).

5.3.3 Flow cytometric analysis

In most matrices stromal cell-free cultures displayed a higher percentage of cells that were $CD34^+/lin^-$ than the cultures with stromal cells (Fig 5.2B). It is important to remember that these cultures began with 100% $CD34^+/lin^-$ cells. In the majority of co-cultures, the percentage of $CD34^+/lin^-$ had decreased from 20% (as seeded) to less than 10% of the total number of cells. For each matrix type, $CD34^+$ cells cultured alone displayed significantly ($p<0.05$) higher percentages of $CD34^+/lin^-$ cells than co-cultures of that same matrix type and day.

The number of $CD34^+/lin^-$ cells (Fig 5.2C) was calculated by multiplying the numbers shown in Fig 5.2A by those in Fig 5.2B. None of the matrices and cell combinations significantly expanded the $CD34^+/lin^-$ population (Table 5.1). 2D co-cultures displayed a recovery of the original number of $CD34^+/lin^-$ cells between 7 and 14 days. Matrigel, in contrast to Fig. 5.2A, produced very few $CD34^+/lin^-$ cells by day

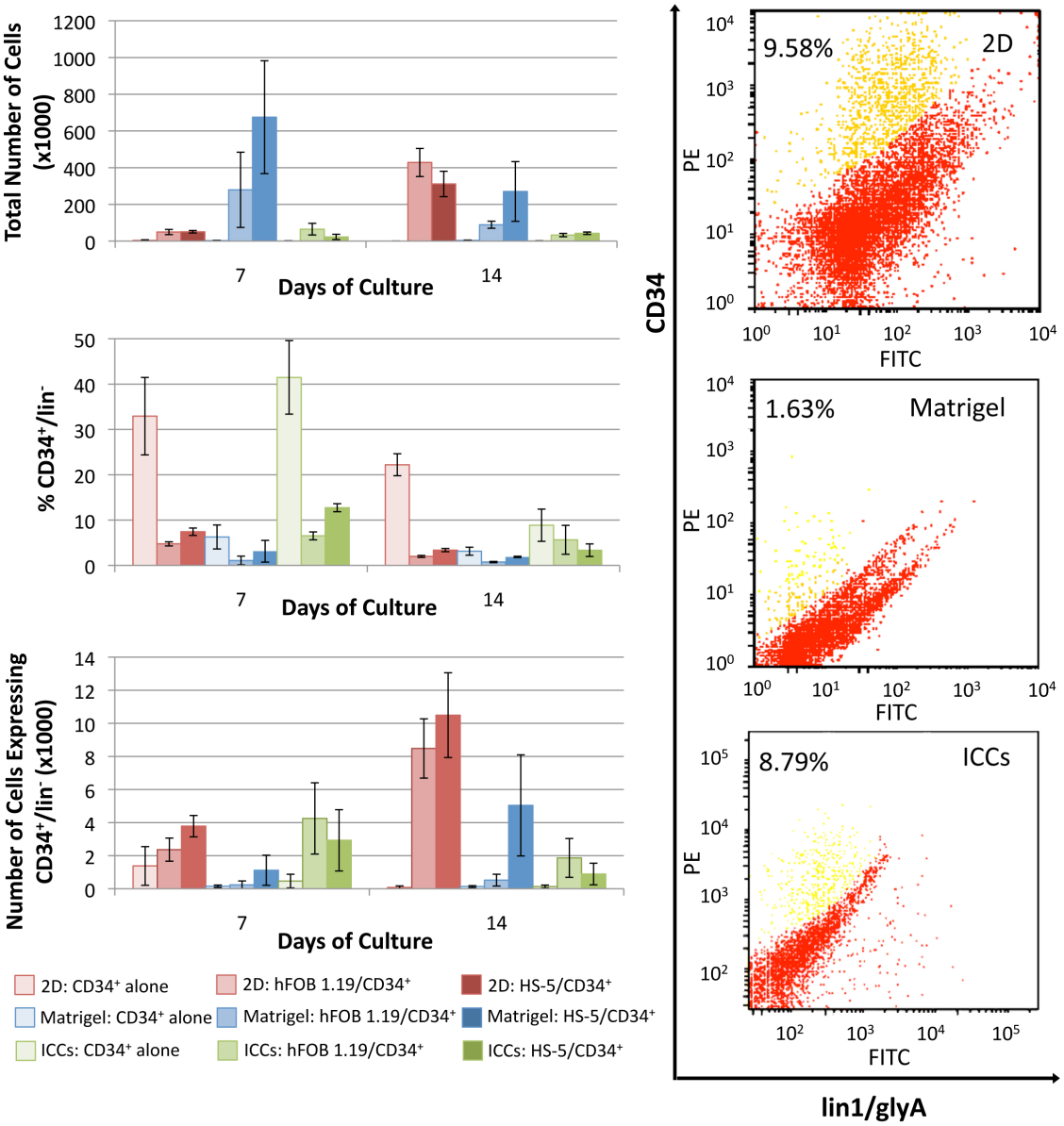

Figure 5.2: Number and phenotype of cells extracted from cultures. (A) Number of cells extracted from culture formats on indicated days. (B) Percentage of cells that displayed the $CD34^+/lin^-$ phenotype. (C) Number of $CD34^+/lin^-$ cells extracted. (D) Representative dot plots of flow cytometry data for HS-5/$CD34^+$ cultures in, from top to bottom, 2D, Matrigel, and ICC cultures at seven days. Percentages on dot plots indicate the percentange that measured $CD34^+/lin^-$; these cells are also indicated by yellow dots.

7, meaning that the expanded population seen in the first seven days was a progeny population. ICC scaffolds displayed a fairly consistent number of $CD34^+/lin1^-$ cells from day 7 to day 14, though the original number had decreased largely by day 14. For all matrices and times, co-cultures produced significantly ($p<0.05$) more $CD34^+/lin^-$ cells than $CD34^+$ cells grown alone. When comparing co-cultures within culture formats, at seven days, hFOB 1.19/$CD34^+$ cultures in 2D produced significantly more $CD34^+$/lin cells than did HS-5/$CD34^+$ cultures in 2D and at 14 days, for hFOB 1.19/$CD34^+$ cultures in Matrigel produced significantly more $CD34^+/lin^-$ cells than did HS-5/$CD34^+$ cultures in Matrigel. Comparing culture formats, 2D and ICC co-cultures produced significantly more $CD34^+/lin^-$ cells than Matrigel at seven days, and at 14 days 2D cultures produced more $CD34^+/lin^-$ cells all 3D matrices. Fig. 5.2D displays representative CD34 versus lin1/GlyA dot plots for the three matrix types.

5.3.4 ELISAs

ELISAs for SCF, flt-3, and IL-6 were performed on media extracted from cultures (Fig 5.3). SCF and flt-3 were found in concentrations much lower than cultures used to expand HSCs [105]. Additionally, the concentrations did not vary between cultures with and without stromal cells. IL-6 was found in concentrations 100 times higher than flt-3 and IL-6. Stromal cell cultures had significantly higher levels of IL-6 than cultures without stromal cells. It appeared that HS-5 cells typically produced significantly more IL-6 than hFOB 1.19 cultures.

5.4 Discussion

We chose three cell culture formats with very different architectures to explore the contributions of dimensionality and cell-cell contacts to engineering an *ex vivo* HSC niche. The traditional 96-well plate was a 2D culture that allowed for communication through direct cell-cell interactions and secreted cytokines, Matrigel was a 3D culture

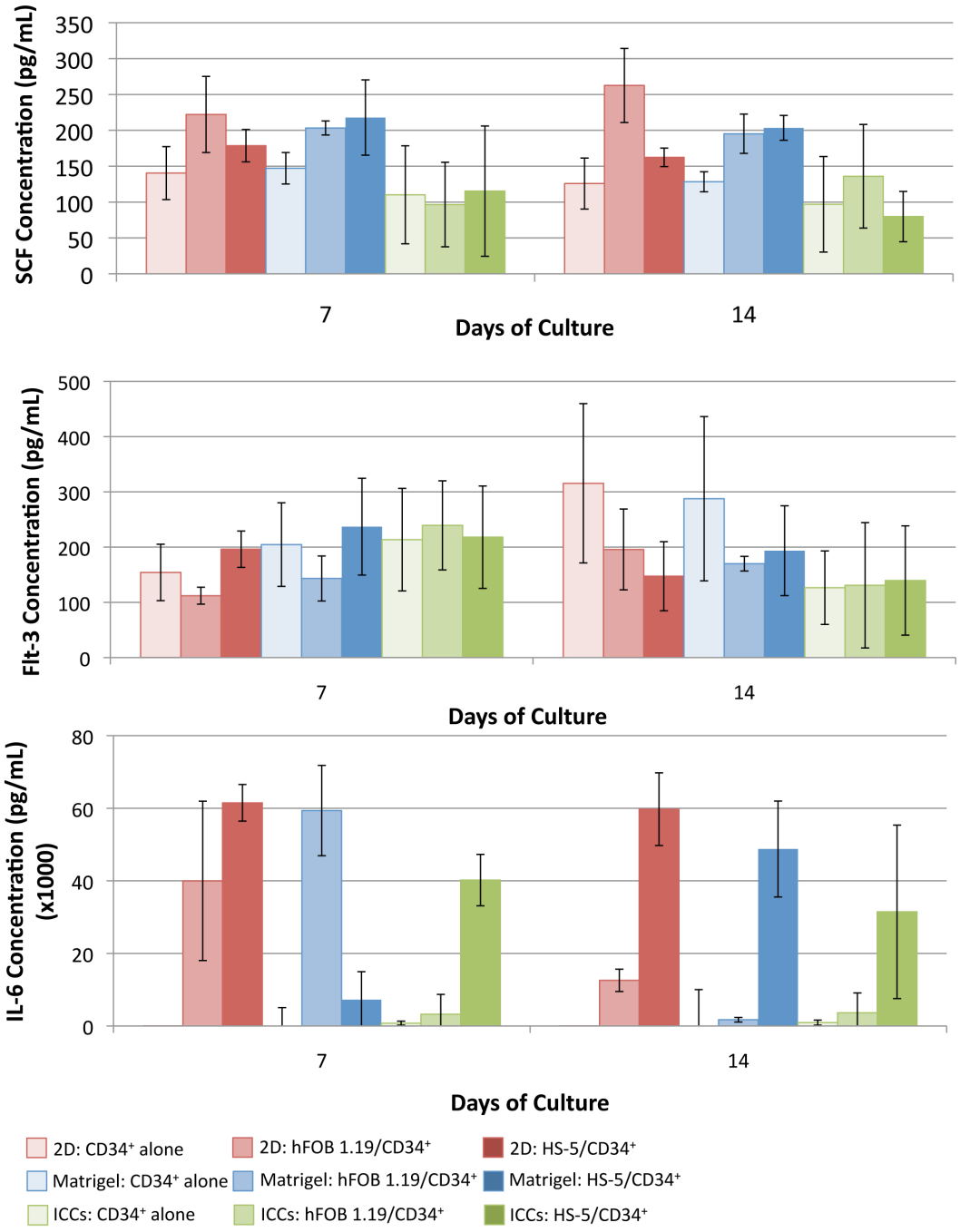

Figure 5.3: Concentrations of relevant cytokines in the media as determined by ELISAs. (A) SCF (B) Flt-3, (C) IL-6. Starred values represent values that are statistically significant ($p<0.05$) when compared to the other stromal cell in that culture format (i.e., 2D, Matrigel, or ICC) for that day ($n = 6$).

that only allowed for communication via secreted cytokines, and ICC scaffolds represented 3D cultures that allow for communication via direct contacts and secreted cytokines. Fig 5.1 demonstrates the diversity of geometries between these matrices. 2D cultures caused the stromal cells to lay flat on the plate surface, and HSCs typically associated with the top of these cells, rarely contacting the well plate, even if a section was exposed. This was one indication that the $CD34^+$ cells showed affinity towards cell-cell contacts. Matrigel began with cells encapsulated through the matrix. After one week, it was observed that the stromal cells had migrated toward the bottom of the plate. ICC scaffolds allowed for direct 3D interactions between stromal cells and $CD34^+$ cells. It was observed that the $CD34^+$ cells and their progeny expanded in the cavities, as if they had formed their own niche. The geometry of ICC scaffolds is much like that of trabecular bone; thus, the directionality of interactions and degree of contact between stromal and stem cells is very similar in ICCs and bone marrow. The cavities where the stem cell expansion was observed (Figs 5.1I and L) are very similar to niches that are seen in the body.

It appeared that Matrigel caused differentiation and expansion, or vice versa, of progeny over seven days. This is likely due to the dominance of cytokine signaling or the lack of cell-cell contact. 2D cells produced the greatest number of $CD34^+$ cells, perhaps because 2D culture allowed for cytokine signaling and cell-cell contact. The ICC culture, which allowed for both contact types in 3D, caused a fairly quiescent population of cells between 7 and 14 days.

We looked into three of the signals that were secreted in the media, and found that IL-6 was secreted at physiologically relevant levels, particularly by HS-5 cells. Furthermore, we found that the pattern of IL-6 secretion in Fig 5.3C followed the pattern of $CD34^+/lin^-$ cell numbers in Fig 5.1C. Thus, it seemed that with the cell types used here, particularly HS-5, IL-6 is the dominant secreted cytokine of those tested. It is also interesting to note that although all three formats presented similar

levels of IL-6, the 2D format showed the greatest expansion of $CD34^+/lin^-$ cells. In 2D, there is a distinct concentration gradient from the source of soluble cytokines at the bottom of the plate to the top of the plate. Therefore, in 2D cultures the HSCs are exposed to very high concentrations of soluble cytokines. In 3D cultures, this gradient is lessened considerably due to the arrangement of stromal cells, and thus the secretion of soluble cytokines, in three dimensions. It is possible that the concentration gradient of secreted cytokines could contribute to the quiescence or expansion of the HSC.

The three cell culture formats allowed for the interaction of cell types by secreted cytokines, though the two matrices that allowed for cell-cell contact did not show the extensive differentiation and expansion seen in Matrigel cultures. It has been hypothesized that the cell-cell contacts at the endosteal surface are important for stem cell quiescence, particularly between HSCs and osteoblasts [99, 103, 157]. Thus, the presence of HS-5 or hFOB 1.19 cells and the ability for HSCs to contact directly the stromal cells may contribute to the data we see here. Additionally, the inclusion of 3D cell-cell contacts may cause quiescence where it is not seen in 2D cultures (Fig 5.2C). Studies have raised doubt in the importance of HSC-endosteal cell contacts [100, 177] and suspected that the endosteal cell influence on HSC quiescence is due to secreted cytokines, but we did not observe that in our *in vitro* cultures.

The data discussed here implies that direct cell-cell contacts are more important than soluble cytokines for the quiescence of HSCs in the context of the osteoblasts and bone marrow stromal cells used here. Additionally, it implies that 3D culture further contributes to the quiescence of $CD34^+$ cells. In vivo, the niche causes HSCs to be quiescent [99], and the source of some HSC-derived cancers is in quiescent stem cells [166, 167]. As the quiescent cancer stem cells are not affected by typical chemotherapy drugs, the ability to keep HSCs quiescent in culture is essential in a drug testing paradigm. When designing an *in vitro* HSC niche for the testing

of drugs one should utilize a 3D matrix that allows for direct cell-cell contact and secreted cytokine communication.

Of the two stromal cell types explored here, neither stood out in best recapitulating the HSC niche by causing HSC quiescence. The specific receptors involved in the contacts observed here need to be elucidated. It is likely that a combination of several cell types may provide the cytokines and receptors necessary to provide the signals that are necessary for an environment for drug testing. As well, the inclusion of other cell types, such as endothelial cells that represent the sinusoidal vascular niche [151, 178] may further contribute to mimicking the HSC niche.

5.5 Conclusions

The ability to organize key aspects of the HSC niche *ex vivo* will provide a tool for studying pathology and potential cures for many blood and bone marrow diseases, including chronic myelogenous leukemia and bone marrow failure diseases. Here, we attempted to recreate the HSC niche while comparing several stromal cell types and matrix types. Well plate cultures, which represent 2D formats, demonstrated the greatest expansion of $CD34^+/lin^-$ cells. These cultures provided permitted both direct cell-cell contacts and soluble cytokine communication. Matrigel cultures, which were 3D cultures where cell encapsulation inhibited cell-cell contacts but allowed for communication through soluble cytokines, exhibited a large expansion of cells that did not have the $CD34^+/lin^-$ phenotype. ICC scaffolds, 3D cultures that permitted both direct HSC-stromal cell contacts and the release of soluble cytokines, seemed to cause quiescence of the $CD34^+/lin^-$ cells, much like what is seen in *in vivo* bone marrow.

The comparision of hFOB 1.19 and HS-5 stromal cells revealed that the dominant soluble cytokine tested was IL-6. The presence of IL-6 correlated with the production of $CD34^+/lin^-$ cells. This was emphasized in 2D cultures, where the local

concentration of soluble cytokines is higher near $CD34^+/lin^-$ cells.

With this evidence, we conclude that 3D culture formats that provide direct cell-cell contacts is essential in designing an *ex vivo* HSC niche. Realizing this is an important step towards creating a niche that mimics the human body such that it can be used for drug testing. In addition to the dimensionality of cell-cell contacts and soluble cytokine gradients, one must also remember that the gradients of drugs, as well as the ability of HSCs to be protected by stromal cells, is much closer to the human body in 3D cultures. Further work needs to be done to elucidate the necessary cell types that cause HSCs to behave as they do in the body. Once this is achieved, the model should also be examined utilizing diseased HSCs, to ensure the model can be used as a disease model. This will give clues to the pathophysiology of many blood and bone marrow diseases.

5.6 Publications relevant to this chapter

The work discussed here is in preparation for submission to the journal Biomaterials.

CHAPTER VI

Preliminary Drug Testing Experiments on Inverted Colloidal Crystal Scaffold Hematopoietic Stem Cell Niches

6.1 Introduction

Drug development for cancer and other diseases is a costly and time consuming process, in part due to the necessity of screening thousands of compounds in order to arrive at a few viable candidates. Worsening this inefficient process is the inability to correctly screen out compounds using 2D culture systems, such as Petri dishes. As well, animal tests are not always accurate, so failures are not recognized until human clinical trials, which could be after up to a billion dollars of investment over almost 15 years [179].

The pharmaceutical industry, as well as drug discovery labs in academia and biotech, lacks an effective early-stage and fairly inexpensive drug testing tool to predict a drugs behavior in the human body. It has been shown that many cell types, such as breast epithelial cells [5, 180, 181], ovarian follicles [6, 182], pancreatic [183], renal [184], display more complex cell-cell and cell-matrix interactions when grown on 3D substrates than when on traditional widely used 2D plates or wells [185–187]. The paradigm-changing drug testing tool would be a 3D human cellular assay that would allow drug testing on human cells organized in a tissue where cells can interact as they would in the body. This is particularly important for many anticancer drugs

that need to target 3D cell bodies/tumors rather than individual cells. In addition, problems of drug transport, cell adaptation, and dormant cancers can be studied substantially more accurately within such a 3D cellular assay than in flat 2D cell systems where dormant stage of cancer and collective cell behavior is difficult if not impossible to realize.

Chronic myelogenous leukemia (CML) is diagnosed in approximately 5,000 people a year in the U.S. In CML patients, the HSCs possess a mutated protein (bcr-abl) that causes rapid cell division and an accumulation of myeloid cells in the marrow and blood. Currently, a class of drugs that inhibit the bcr-abl protein, called tyrosine kinase inhibitor (TKI)s, are available as treatments for CML. TKIs make the disease manageable, but do not cure it. Resistance to TKIs is common as BCR-ABL, the gene that codes for the bcr-abl protein, can mutate and interfere with TKI binding, causing relapse [188]. It is thought that further developments in CML drugs will focus on overcoming resistance to the available TKIs. With the development of new classes of CML drugs in the next decade comes a need for new methods of *in vitro* drug discovery and testing that might increase understanding of the disease and new approaches to curing it. Current pre-clinical drug testing methods, which include 2D *in vitro* assays and *in vivo* transgenic mice, leave a gap in innovation as there are no ex-vivo models that accurately represent the body. Traditional 2D cultures neglect the 3D and complex multicellular aspects of *in vivo* HSC niches in bone marrow. As CML is a disease originating from HSCs, one must take into account the effect of the complex multicellular stem cell niche on the persistence of diseased cells [104, 157, 169, 189–191]. Transgenic mouse models have been used extensively [192, 193], but these animals are extremely expensive and do not always mimic the human body. This leaves room for more advanced co-cultures or 3D methods to fully understand the CML stem cell niche and utilize it in drug development.

For these reasons, we aim to develop a model of the HSC niche for drug testing.

In Chapter 5, we introduced the preliminary work in designing a niche using stromal cells, HSCs, and comparing matrices. Due to the stability and quiescence of the HSCs in ICC scaffolds, we chose to continue to look at these stromal cell/ICC combinations within the context of drug testing. In our opinion, an ideal *in vitro* HSC niche for drug testing should be as like the human body as possible, where the cells only receive cues from other cells, via secreted matrix, soluble signals, and direct cell-cell contacts. When adding a drug to a culture, it is impossible to know whether the reaction to the drug is influenced by signals from high levels of exogenous cytokines. For this reason, we chose to avoid exogenous cytokines in our cultures. In Chapter 5, we looked at several stromal cells within matrices while looking at the replicative ability of $CD34^+$ cells. Here, we take a slightly different approach, in attempting to describe the presence of hematopoietic lineages within the constructs. An ideal drug testing tool utilizing the HSC niche should be simple to use, but it should also include the many cell types that are found in bone marrow, including those that are derived from HSCs.

As discussed in Chapter 5, the hFOB 1.19 and HS-5 cell types contribute differently to the HSC niche; thus, we continue here with several combinations of these stromal cells within ICC to determine if a certain combination will cause the HSCs to create a more marrow-like environment. We continue with looking at several stromal cell combinations within the context of drug testing by adding several simple compounds that should have a positive or negative effect on the cell cultures. The model drugs that we chose were erythropoietin (EPO) and methotrexate (MTX). EPO is a key growth factor involved in the regulation of erythropoiesis [192, 193]. Thus, with the addition of EPO one would expect to see an upregulation of erythroid cell production. Erythroid cell production has been documented at EPO concentrations as low as 1 international units (IU)/mL, though the typical concentration in this context are 3 IU/mL [194, 195]. MTX is a chemotherapy drug known to be cytotoxic to repli-

cating cells by inhibiting DNA synthesis [196] [176]. We expected to see a decrease in cell numbers in our models at a concentration of 10^{-6} M [197, 198]. These tests are performed comparing 2D and ICC cultures. From here, we chose one stromal cell type (hFOB 1.19), and cultured $CD34^+$ cells within 2D and ICC cultures, adding two different doses of EPO and MTX. We expected to see a more dramatic change in cell number and type with increased drug dose.

6.2 Materials and Methods

6.2.1 ICC scaffold fabrication

ICCs were fabricated exactly as described in Chapter 5.

6.2.2 Stromal cell expansion

Stromal cells were expanded exactly as described in Chapter 5.

6.2.3 Stromal and $CD34^+$ seeding in 2D and ICC cultures

In a first experiment, cells were seeded in ICC scaffolds in the following way. One scaffold was placed in a well of a 96-well plate. 100 μL of 190 proof ethanol was added to each well. Scaffolds were allowed to equilibrate for 10 min before ethanol was removed and replaced with an additional 100 μL of fresh ethanol. After 10 min, most of the ethanol was removed and plates were placed in an incubator at 37 °C overnight to evaporate any residual ethanol. The next day, cell solutions of either hFOB 1.19, HS-5 cells, or both, were made at a density of 40,000 cells per 20 μL. 20 μL of cell suspension gently was pipetted directly onto each dehydrated scaffold, and well plates were placed in an incubator for three hours. Wells were then filled halfway with HS-5 media and cells and scaffolds were irradiated at 6000 rads. Media was then removed and replaced with StemSpan (StemCell Technologies, Vancouver, BC) media with

40 μg/mL low density lipoprotein (Sigma) and 1% penicillin-streptomycin. $CD34^+$ cells (StemCell Technologies) were thawed and washed with StemSpan as directed by the cell supplier. $CD34^+$ cells were added to cell cultures at a density of 10,000 cells/culture and cultured at 37 °C and 5% CO_2. Controls were prepared by culturing $CD34^+$ cells without stromal cells in ICC scaffolds.

In the experiments that followed, ICC scaffolds were seeded in the same way, but with only 1,000 $CD34^+$ cells. 2D wells were seeded as follows. hFOB 1.19 or HS-5 cells were seeded at a density of 40,000 cells per culture. Stromal cells were seeded directly onto the plate, and allowed to attach for three hours before irradiating at 6000 rads. Media was then changed to StemSpan supplemented with 40 μg/mL low density lipoprotein (Sigma) and 1% penicillin-streptomycin. $CD34^+$ cells were added to cell cultures at a density of 10,000 cells/culture and cultured at 37 °C and 5% CO_2. Controls were prepared by culturing $CD34^+$ cells without stromal cells in the 96-well plate.

6.2.4 Cell extraction and enumeration

Cells in both 2D and ICCs were extracted in the same way. First, all media was removed from cultures and set aside. Wells were rinsed briefly with approximately 20 μL of trypsin/EDTA, and the trypsin/EDTA were added to the media. Next, cells were left in another 20 μL of trypsin/EDTA, and the trypsin/EDTA for approximately 10 minutes, until stromal cells were visibly detached. Liquid was removed and added to the media; when removing liquid from ICC scaffolds, the liquid was pipetted several times to dislodge any cells that may be in the center of the scaffold. Of the media and trypsin that had been removed from each culture, 30 μL were set aside for counting using a hemocytometer, and the rest was used in staining for flow cytometery.

6.2.5 Flow cytometric analysis

Cells were washed in ice cold 2% FBS in PBS, and incubated with a phycoerythrin (PE)-labeled antibody for CD34, and a FITC-conjugated antibody to GlyA, a FITC-labeled antibody cockatil, lin1 (CD3, CD14, CD16, CD19, CD20, CD56), and allophycocyanin (APC)-labeled antibodies to CD3, CD19, and CD56 (BD Biosciences, San Jose, CA). With these labels, the $CD34^+$ cells that are negative for FITC or APC would be undifferentiated HSCs, the $FITC^+/APC^-$ cells are lymphoid cells, and the $APC^+/FITC^-$ cells are myeloid cells. The combination of lin1 and GlyA are hereafter referred to as lin. Relevant single color, negative, and isotype controls were prepared for compensation and to distinguish specific binding. Flow cytometry was performed on a BD FCSCanto II. Regions positive for CD34 and lin1/GlyA were determined based on isotype controls.

6.2.6 ELISAs

ELISAs for IL-6 (R&D Systems, Minneapolis, MN), SCF (R&D Systems), and flt-3 (R&D Systems) were performed according to manufacturer instructions.

6.2.7 Addition of drug

In each of the two experiments above, cells were cultured for three days, changing 75 μL media each day. On the third day of the first experiment, either EPO or MTX was added. In the first experiment, 75 μL of media was replaced with media with drug so that the entire volume of media per well (250 μL) would contained either 10^{-6} M MTX or 3 IU/mL EPO (Table 6.1). On each day thereafter, 75 μL of media with drug was exchanged with fresh media with drug at the concentration of either 10^{-6} M MTX or 3 IU/mL EPO. Control samples did not have any drug added.

In the second experiment, two doses of either EPO or MTX were added (Table 6.2). In the first experiment, 75 μL of media was replaced with media with drug

so that the entire volume of media per well (250 μL) would contained either 10^{-6} M MTX, 10^{-5} M MTX, 3 IU/mL, or 5 IU/mL EPO. On each day thereafter, 75 μL of media with drug was exchanged with fresh media with drug at these concentrations. Control samples did not have any drug added.

Table 6.1: Drug testing experiment 1: cell types and drug doses.

	Drug and dose added		
	control	EPO (IU/mL)	MTX (M)
hFOB 1.19/CD34$^+$	-	3	10^{-6}
1:1 hFOB 1.19: HS-5/CD34$^+$	-	3	10^{-6}
HS-5/CD34$^+$	-	3	10^{-6}

Table 6.2: Drug testing experiment 2: drug doses.

	Drug and dose added		
	control	EPO (IU/mL)	MTX (M)
Dose 1	-	3	10^{-6}
Dose 2	-	5	10^{-5}

6.2.8 Annexin/propidium iodide (PI) assay

In the second experiment, after one and seven days of adding drug cells were removed as described in Section 6.2.4 and stained with the FITC Annexin V Apoptosis Detection Kit I (BD Biosciences). Staining and flow cytometry was performed as described by the manufacturer. Analysis was performed on a Beckman Coulter Quanta SC flow cytometer.

6.2.9 Statistical Analysis

In all graphs, data is represented as the average of the indicated sample sizes $\pm$ standard deviation. A Student's t-test was performed to determine statistical significance. In graphs, significance ($p<0.05$) is indicated by a star.

6.3 Results

6.3.1 Combinations of different stromal cells for the production of bone marrow

The first set of experiments here explored different combinations of the hFOB 1.19 and HS-5 stromal cell types within ICC scaffolds to determine if a certain combination would best mimic the HSC niche. Fig 6.1 demonstrates the percentage and total number of $CD34^+$ cells that were extracted from the matrices. As well, the concentration of IL-6 is displayed. Concentrations of SCF and flt-3 were also determined, but there was no appreciable production of these growth factors (data not shown). As seen in Chapter 5, the concentration of IL-6 was dependent on the presence of at least 50% HS-5 cells. Still, at this point there was no data that gave an obvious combination to be used in drug testing.

The next experiment utilized several combinations of stromal cells to determine whether the stromal cells caused differentiation into the types of cells present in bone marrow. Fig 6.2 displays the results for flow cytometric analysis of the different lineage markers described above. Fig 6.2 demonstrates the presence of HSCs, myeloid cells, and lymphoid cells. At day three of culture, 2D cultures showed a greater percentage of cells that were of the myeloid lineage than ICC cultures.

6.3.2 Dosing experiment 1: Total cell enumeration and lineage presence

These experiments were continued in the context of drug testing. One dose each of EPO and MTX were administered for up to seven days to co-cultures with combinations of hFOB 1.19, HS-5 and $CD34^+$ cells. The results of enumerating the cells that were extracted from 2D and ICC cultures are shown in Fig 6.3. None of the cultures showed a change in cell number after one day of treatment, except for the 1:1 hFOB 1.19:HS-5 cultures in 2D treated with EPO, which showed a decrease with

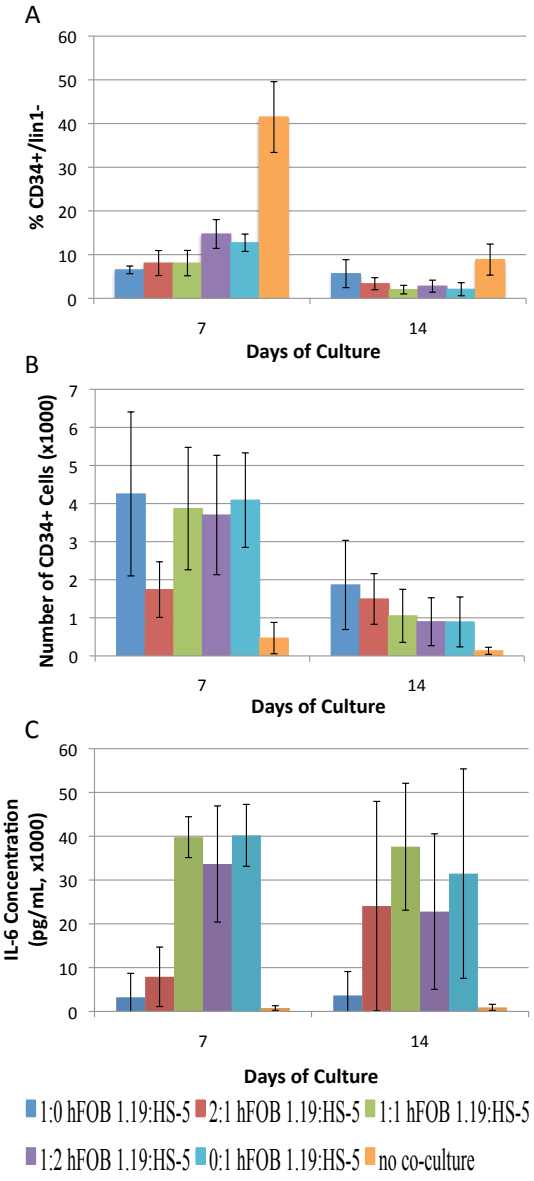

Figure 6.1: Total cells extracted from cultures after seven and 14 days of culture. (A) Percentage of cells positive for CD34 cell marker and negative for all other markers. (B) Number of $CD34^+$ cells as determined by multiplying the percentage positive for CD34 and the total number of cells extracted (data not shown). (C) Concentration of IL-6 growth factor as determined by ELISA.

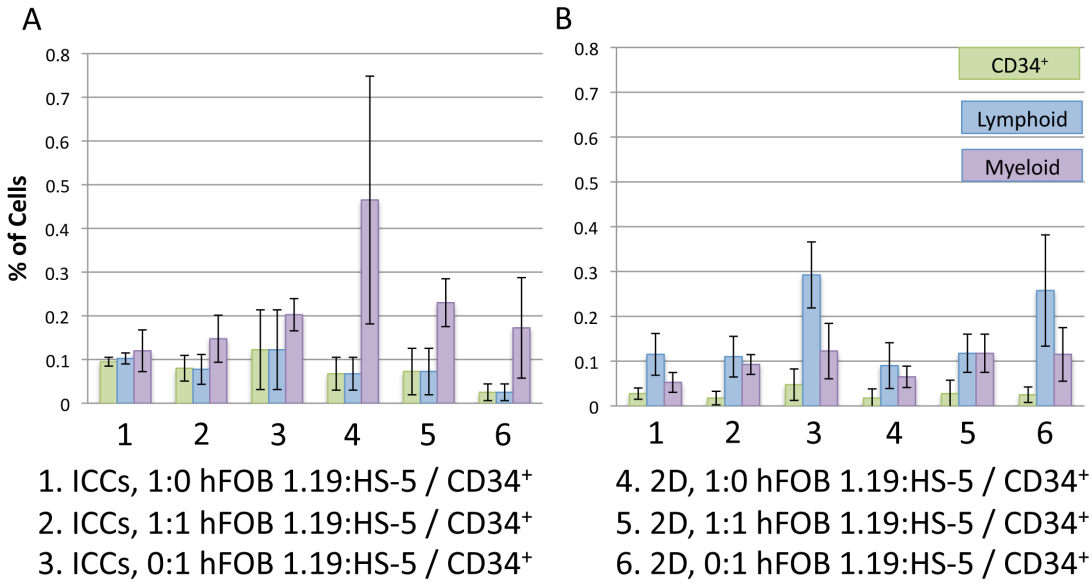

Figure 6.2: Percentage of cells displaying various lineage markers. Each plot displays two different culture formats: ICC scaffolds (1, 2, and 3), and 2D well plates (4, 5, and 6). Each culture format was utilized for different stromal cell combinations. Columns labeled 1 and 4 contained only hFOB 1.19 and $CD34^+$ cells. Columns labeled 2 and 5 contained a 1:1 ratio of hFOB 1.19 and HS-5 cells and also $CD34^+$ cells. Columns labeled 3 and 6 contained HS-5 cells and $CD34^+$ cells. (A) Three days of culture. (B) Ten days of culture.Starred values represent values that are statistically significant ($p<0.05$) ($n = 4$).

EPO treatment, and the 1:0 hFOB 1.19:HS-5 cultures in ICCs treated with MTX, which showed an increase in cell number with MTX treatment. Both of these were the opposite of the predicted effects. In all three co-cultures, generally all cell cultures increased in cell number after treatment with EPO for seven days. This is expected, as EPO should promote the growth of myeloid cells. After seven days of treatment with MTX, most cultures showed no significant change in cell number, but hFOB 1.19/HS-5 2D co-cultures (Fig 6.3E) showed an increase in cell number.

This data was elaborated by looking at the effects of the drugs on the specific lineage types. The most interesting aspect of this data would be whether or not myeloid cells were increased with the presence of EPO. After seven days of drug

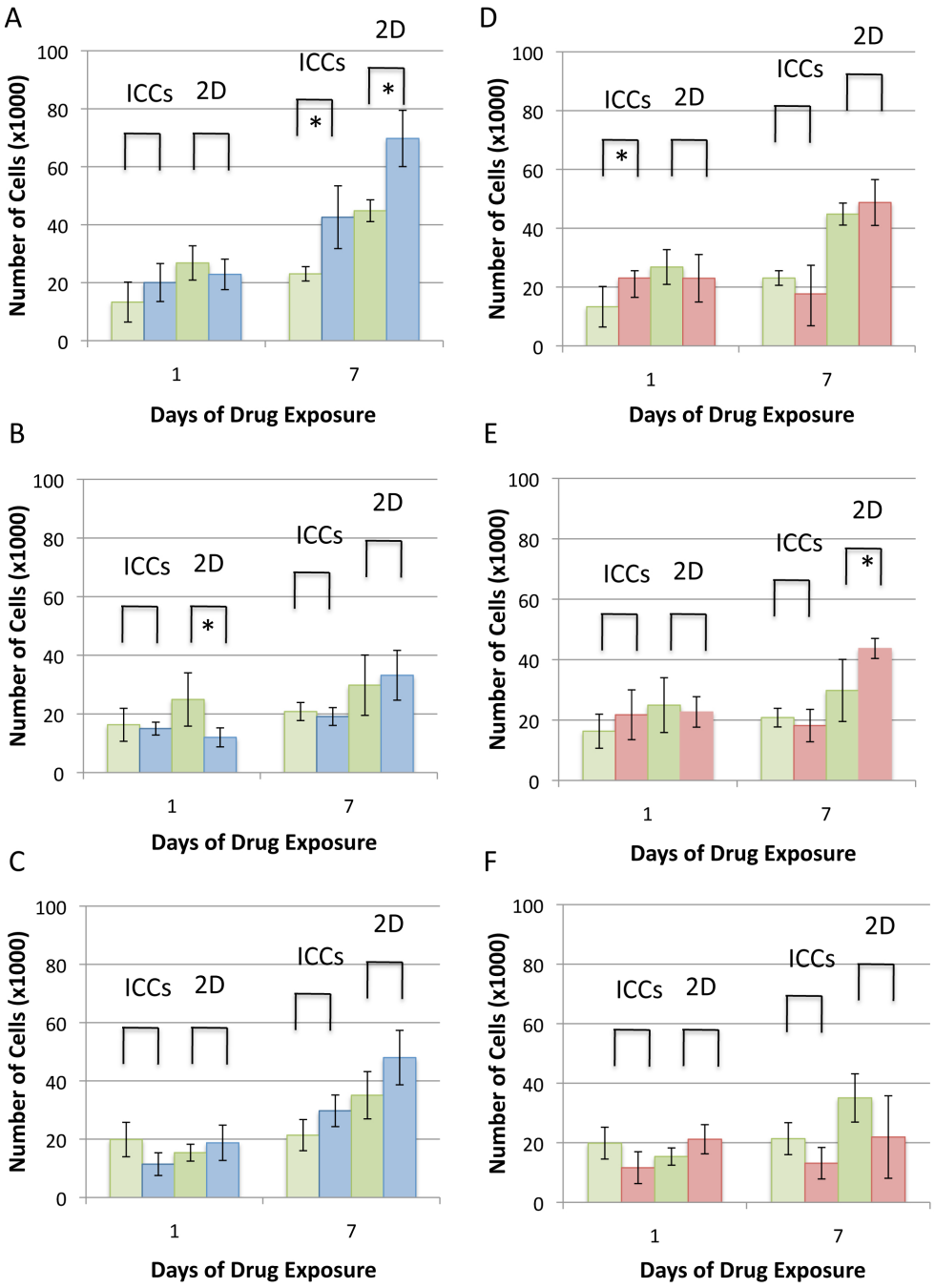

Figure 6.3: Total cells extracted from cultures after one and seven days of drug treatment (Dosing experiment 1). (A-C) Treated with 3 IU/mL EPO. (D-F) Treated with 10^{-6} M MTX. (A), (D) hFOB 1.19/CD34^{+} cultures. (B),(E) 1:1 hFOB 1.19:HS-5/CD34^{+} cultures. C),(F) HS-5/CD34^{+} cultures. Stars represent values that are statistically significant ($p<0.05$) (n = 4).

treatment, however, there was no difference between controls and treated cells in any of the groups (Fig 6.4).

6.3.3 Dosing experiment 2: Total cell enumeration and lineage presence

The changes in cell number as a response to EPO were as expected in the hFOB 1.19 cultures above; thus, this cell type was used to test an increased dose of each drug. In the second experiment, the doses in Table 6.2 were administered to co-cultures of hFOB 1.19 and $CD34^+$ cells. The results of enumeration of cells extracted from 2D and ICC cultures are given in Fig 6.5. Here, one-day doses of EPO showed no change in cell number (Fig 6.5A), and no trend after seven days (Fig 6.5C). Interestingly, both 2D and ICC cultures showed a trend after one day towards less cells with MTX treatment (Fig 6.5B). By seven days, both cultures were significantly limited by MTX treatment (Fig 6.5C).

The lineages present in the cells in Fig 6.5 were examined via flow cytometry. The data for EPO-treated cultures is presented in Fig 6.6. Between two and seven days of drug treatment, the percentage of $CD34^+$ increased for all groups. The predicted increase in myeloid cell numbers was not seen with EPO treatment. In fact, all myeloid cell percentages decreased over seven days. The data for the MTX-treated drugs is presented in Fig 6.7. There is no difference between control and treated groups.

6.3.4 Annexin/PI assay

The results of PI exclusion are given in Fig 6.8. No significant association by annexin was shown (data not shown). It is likely that this is because for both days the latest dose given was a day prior to the assay; thus, any apoptosis that may have occurred at the time of adding the drug could not be measured at the time of the assay. Figs 6.8A and C show little difference in cell death, as measured by PI

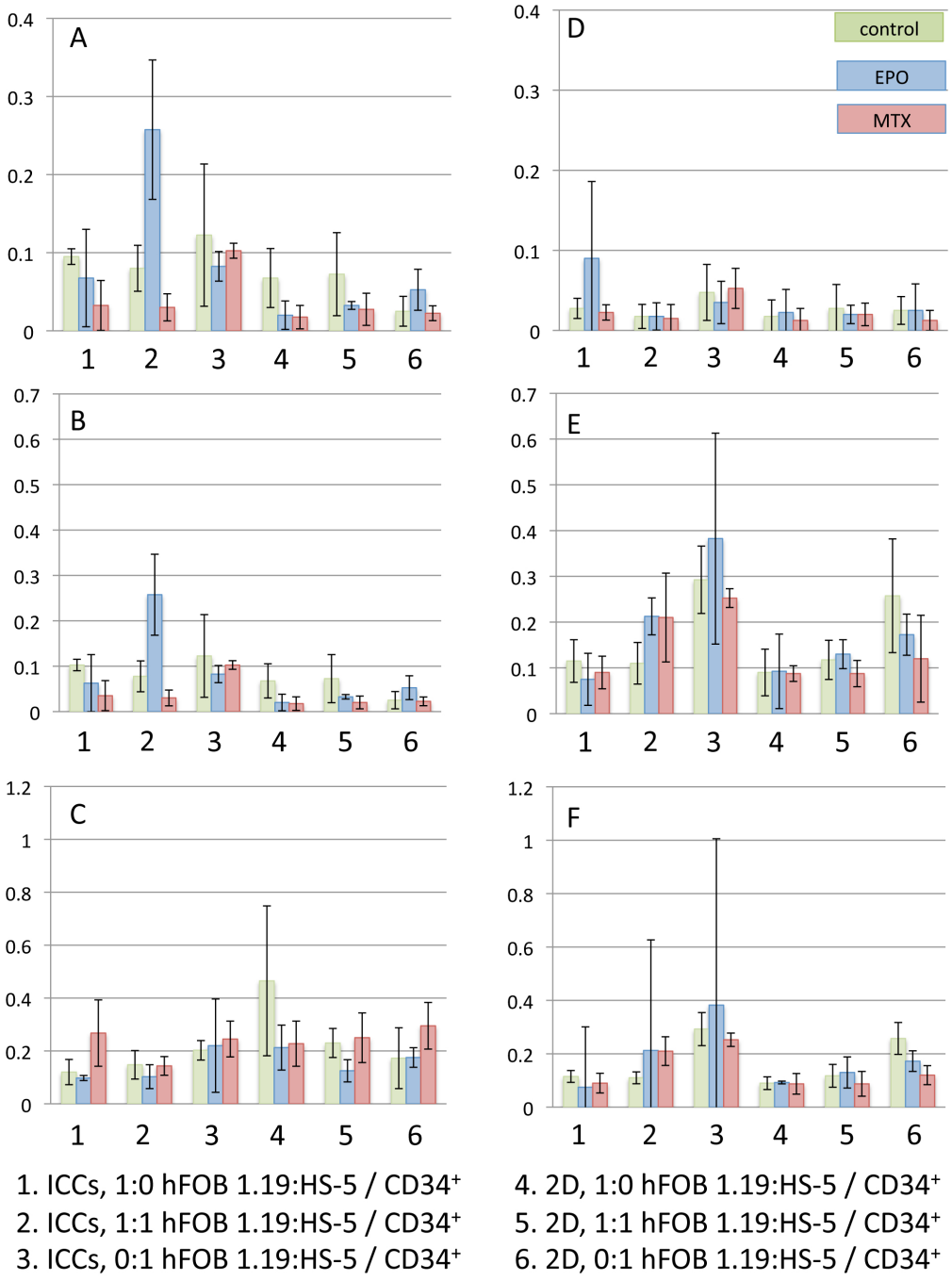

Figure 6.4: Percentage of cells expressing lineage markers after extraction from cultures after one and seven days of drug treatment (Dosing experiment 1). (A-C) Two days of drug treatment. (D-F) Seven days of drug treatment. (A), (D) Percentage $CD34^+$/$lineage^-$. (B), (E) Percentage positive for lymphoid markers. (C), (F) Percentage positive for myeloid markers.

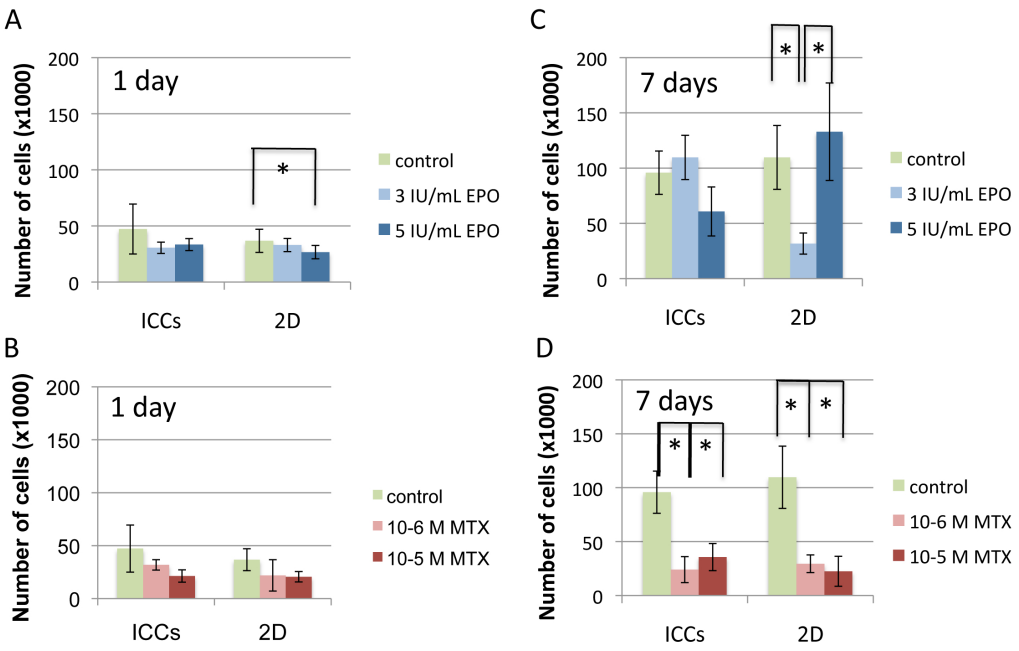

Figure 6.5: Total cells extracted from cultures after one seven days of drug treatment (Dosing experiment 2). (A), (C) Treated with EPO. (B),(D) Treated with MTX. (A), (B) Results after one day of treatment with drug. (C), (D) Results after seven days of drug exposure. Starred values represent those that are statistically significant ($p<0.05$) ($n = 4$).

staining of DNA. In fact, of EPO-treated cultures, the only difference between treated cultures and control cultures is seen in the 2D cultures on day 7 (Fig 6.8C), where the EPO-treated cultures showed less cell death than controls. This means that EPO does not cause cell death, as expected.

6.4 Discussion

We wished to explore the use of traditional well plate cultures and newer 3D ICC cultures. In order to reduce any potential exogenous influences, we decided to utilize stromal cells that are found in bone and bone marrow as a source of soluble and insoluble signals, rather than adding growth factors to the media. As discussed Chapter 5, osteoblasts and bone marrow stromal cells contribute uniquely to the

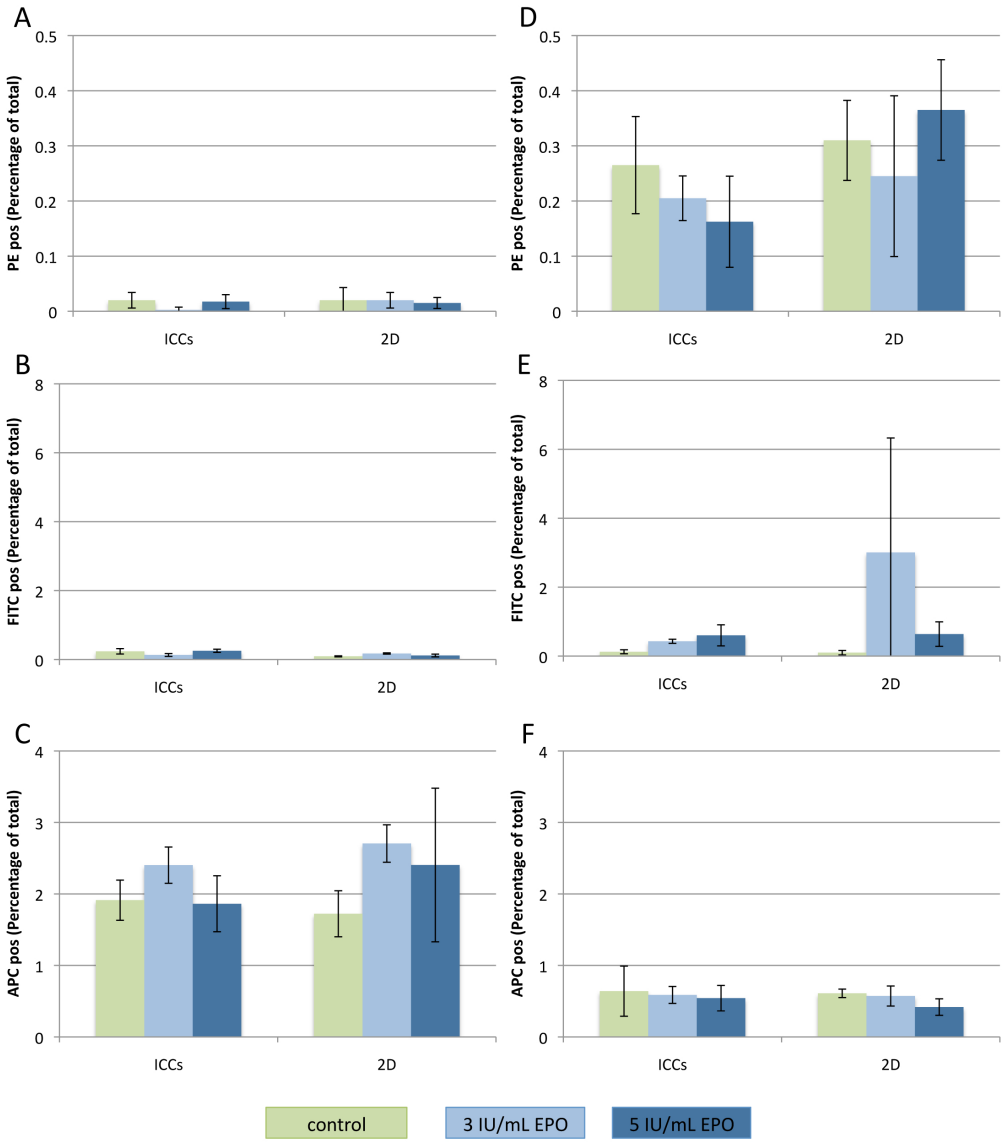

Figure 6.6: Lineages present in EPO-treated cultures (Dosing experiment 2). (A-C) Two days of drug treatment. (D-F) Seven days of drug treatment.(A), (D) Percentage $CD34^{+}$/$lineage^{-}$. (B), (E) Percentage positive for lymphoid markers. (C), (F) Percentage positive for myeloid markers.

cultures. As such, we decided to explore whether either of these cell types, or a combination, represents the body in the context of drug testing by exhibiting the responses to drugs that we expected.

Fig 6.1 confirms the data in Chapter 5 that the presence of HS-5 cells increases

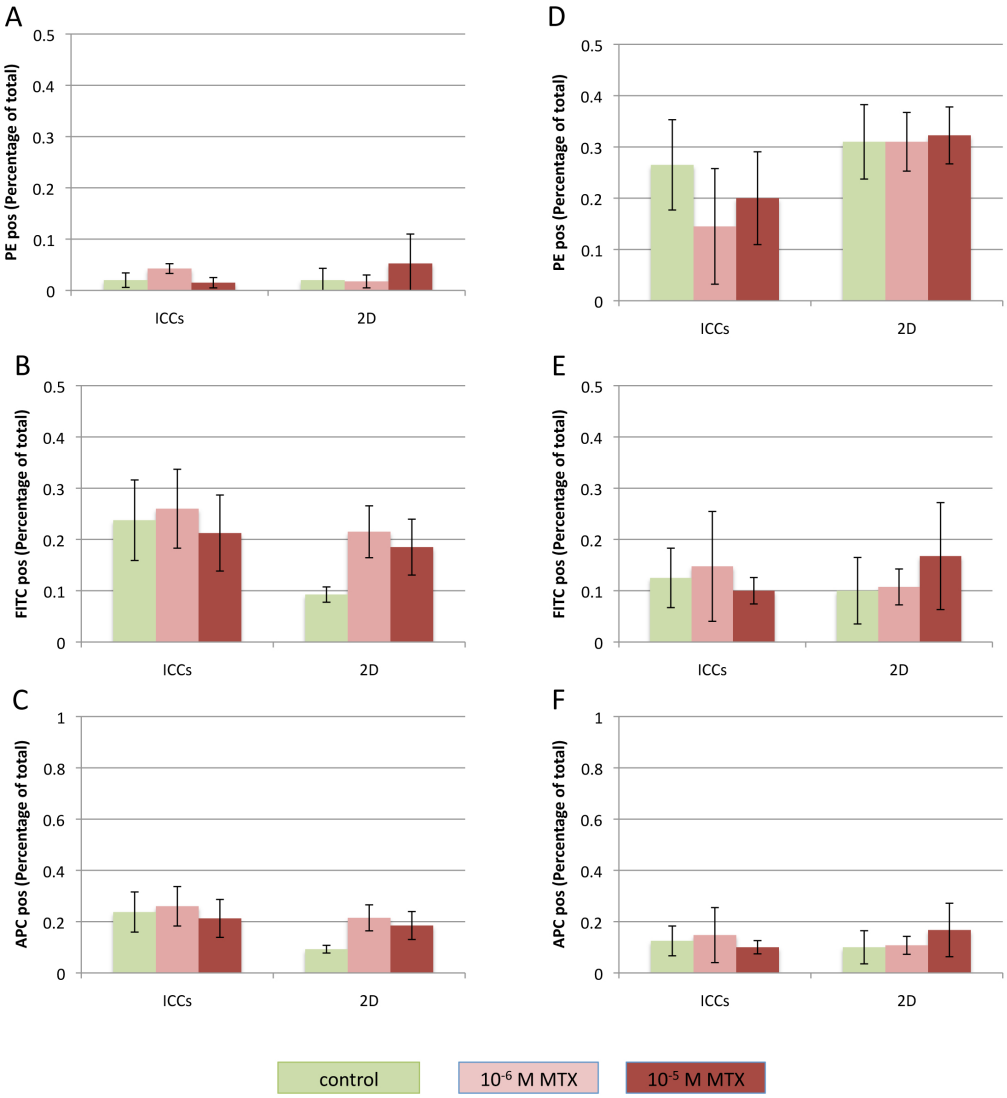

Figure 6.7: Lineages present in MTX-treated cultures (Dosing experiment 2). (A-C) Two days of drug treatment. (D-F) Seven days of drug treatment. (A), (D) Percentage $CD34^+$/lineage$^-$. (B), (E) Percentage positive for lymphoid markers. (C), (F) Percentage positive for myeloid markers.

the secretion of IL-6, particularly at 7 days. Still, the number of stem cells present did not vary with stromal cell type, meaning that each stromal cell type has unique contributions to the cultures. In Fig 6.2, there was no trend indicating that a certain lineage of cells was influenced by a specific stromal cell type. With this data, we could not discern whether a single cell type could be chosen for drug testing uses. Thus, in

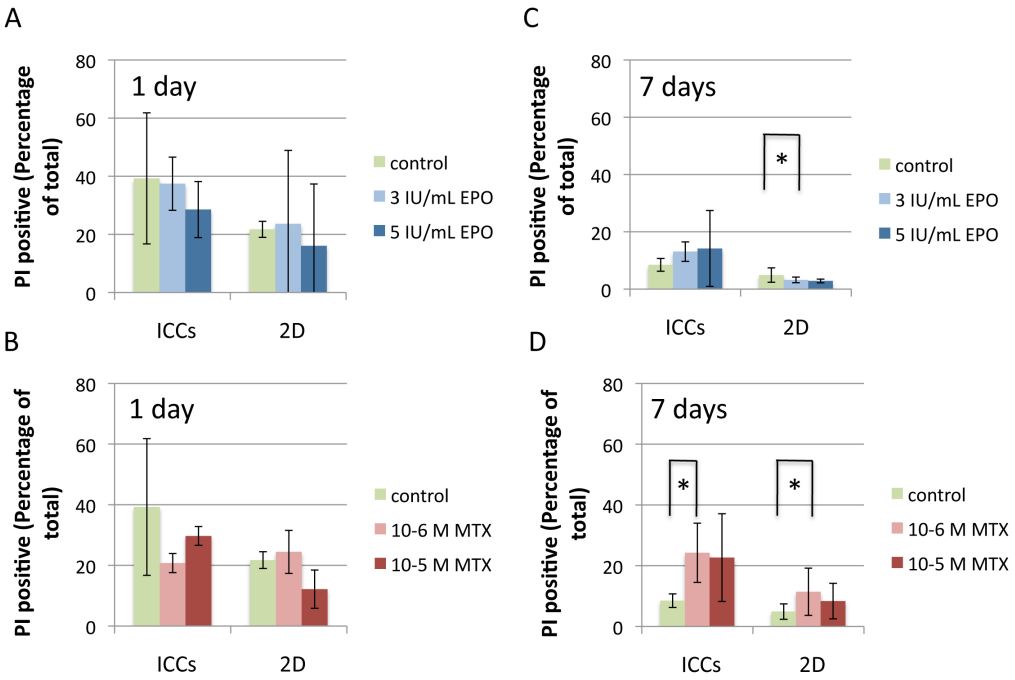

Figure 6.8: PI exclusion assay (Dosing experiment 2). (A) Treated with 3 IU/mL EPO. (C) Treated with 5 IU/mL EPO. (B) Treated with 10^{-6} M MTX. (D) Treated with 10^{-5} M MTX. (A), (B) Results after one day of treatment with drug. (C), (D) Results after seven days of drug exposure. Starred values represent values that are statistically significant ($p<0.05$) ($n = 4$).

drug testing experiments we continued with a combination of stromal cells.

Fig 6.3 displays the data for dosing of these cell combinations with EPO and MTX. Here, one can see that in hFOB 1.19/CD34$^+$ cells, the response to seven days of treatment with EPO is as predicted in both 2D and ICC cultures. HS-5/CD34$^+$ and 1:1 hFOB 1.19:HS-5/CD34$^+$ cultures treated with EPO were no different from the control cultures. This is further confirmed in Fig 6.4, where there is not an increase in the percentage of myeloid cells in EPO-treated cultures.

We expected cultures treated with MTX to show a decrease in the total number of cells or inhibit production of cells. In Fig 6.3, one can see that hFOB 1.19/CD34$^+$ cultures had no significant change in cell number when compared to control cultures. The cells extracted from 1:1 hFOB 1.19:HS-5/CD34$^+$ cultures in 2D increased with

seven days of MTX exposure, which is the opposite result to what was expected. HS-5/CD34$^+$ cells displayed no difference when compared to controls.

As the results of the experiments in Fig 6.3 did not reveal any differences between 2D and ICC cultures or stromal cell combinations, we decided to look into whether increased concentrations of these drugs would elicit a more obvious response. We chose to utilize hFOB 1.19 cells because of their ease of expansion and appropriate response to EPO treatment in Fig 6.3.

Fig 6.5 displays the results of treating hFOB 1.19/CD34$^+$ cultures with the drugs and doses in Table 6.2. Again, EPO did not cause significant increases in cell numbers. MTX cultures showed the expected response of a decrease in cell numbers in both 2D and ICC cultures after seven days of treatment; however, there were not further decreases in cell number with increased MTX dose. It should be noted that the number of cells in the MTX-treated cultures remained similar when comparing Fig 6.3 and Fig 6.5, but the number of control cells increased significantly in Fig 6.5. Thus, the experiment should be replicated to determine whether the responses are repeatable.

The percentage of extracted cells that were labeled as dead is displayed in Fig 6.8. Figs 6.8A and C show the percentage of dead cells in EPO cultures. It should be noted that there is some cell death upon the inoculation of CD34$^+$ cultures; CD34$^+$ have approximately 80% viability upon arrival. As well, stromal cell cultures naturally have some cell death with irradiation and aging of cells. There is a decrease in the percentage of dead cells between days 1 and 7. This can be explained by the overall increase in cell numbers (Fig 6.5), indicating that the CD34$^+$ or their progeny had expanded. In summary, EPO treatment did not cause any significant cell death in any cultures or doses.

Figs 6.8B and D display the percentage of dead cells after MTX treatment. There is more cell death observed in MTX-treated cultures than in control cultures. This

confirms the data seen in Fig 6.5 where less cells were observed in MTX-treated cultures. In fact, the decrease in cell numbers is not only due to the lack of cell replication, but due to increased cell death, meaning the MTX treatment causes more cell death than control cultures.

The cultures did not show increased response to increased doses of either drug. With respect to EPO treatment, as the hormone regulates erythrocyte production, we would expect to see an increase in cell number. However, many growth factors are involved in the up-regulation of erythroid cell production [194, 199]. As this is a simple model with only two cell types, some of the necessary growth factors, such as SCF are not present (Chapter 5). In future experiments, a chemical should be chosen that up-regulates the production of a hematopoietic cell type without working in cooperation with another growth factor. As well, the model needs to be adjusted to include additional cell types that make the model more physiologically relevant.

6.5 Conclusions

The creation of an *in vitro* method of drug testing could revolutionize the pharmaceutical industry, allowing companies to collect information about how the drug will act in the body long before it is introduced into human clinical trials. As well, such a collection of assays could significantly reduce the amount of animal testing in the industry.

Here, we looked at two culture formats, 2D well plates and 3D ICC scaffolds, as well as different stromal cell types. Varying stromal cell types did not show significant differences in drug response, though this deserves greater exploration as stromal cells contribute to disease and drug response. Similar responses were seen in both 2D and 3D cultures. This is encouraging, in that the simplistic mechanisms of EPO and MTX may not be affected by dimensionality. Future work with drugs that are used to specifically treat $CD34^+$ cells, such as those that are used against CML, may show

more significant responses when looking at stromal cells or dimensionality due to the affects of stromal cells on disease pathology.

CHAPTER VII

Summary and Future Directions

7.1 Summary

ICC scaffolds have great potential in the applications of tissue engineering for several reasons. First, the unique and highly controllable structure allows one to control the size of cavities and interconnecting channels, affording the possibility of studying the effects of feature size on such characteristics as cell seeding and migration, diffusion of drugs and other molecules, and mechanical properties. As well, ICC scaffolds can be fabricated out of any material that can be made into a liquid and later solidified or gelled. One can also image cells directly within hydrogel scaffolds.

This dissertation presented work utilizing ICC scaffolds within the context of bone and bone marrow engineering. The first part of this dissertation presented the first work to create this structure out of a biodegradable polymer. Here, we demonstrated microscale control over cavity and interconnecting channel sizes, and that the mechanical properties were higher than scaffolds with stochastic structures. The scaffolds were also shown to be biocompatible. Next, the structure was fabricated out of polyacrylamide hydrogel, which was used to grow a HSC niche that supported HSC expansion and directed differentiation. The scaffolds were further explored for HSC engineering in a study that compared the scaffolds to Matrigel and 2D cultures. This demonstrated that ICC scaffolds provided an environment where HSCs remained quiescent, similar to the human body. Last, this dissertation presented initial work

in utilizing the matrices for drug testing.

7.1.1 Bone tissue engineering

The ultimate goal of bone tissue engineering is to design implantable scaffolds to promote and guide bone growth into a wound site. Ideally, the scaffold should degrade at the same rate that bone grows into the scaffold. With this design, eventually the wound site will be filled with healthy bone. The material chosen for the ICC scaffolds discussed here was PLGA, which is a well-characterized biodegradable polymer that hydrolytically degrades over months in the body into lactic acid and glycolic acid, which are naturally found in the human body [200, 201].

In order to facilitate bone and vasculature ingrowth, cell and/or cytokine seeding, and nutrient and waste diffusion, the scaffolds must be porous. As well, the scaffold geometry should be completely interconnected, meaning that there are no areas of the scaffold that are isolated, so that the scaffold is a consistent growth environment and also so that tissue grows in evenly. A major problem with traditional scaffold design, which imparts random porosity into the bulk material, is that the scaffolds must have high porosities, as high as 95%, to ensure complete connectivity. With such high porosities, the mechanical properties of the bulk material are sacrificed. Due to the ordered structure of ICC scaffolds, ICCs have complete interconnectivity at porosities as low as 63-74% [63, 121]. In Chapter 3, we demonstrated that the scaffolds have compressive moduli that are much greater than typical scaffolds with a stochastic pore geometry.

In addition to the mechanical property advantages of the highly ordered structure of ICC scaffolds, we demonstrated that their fabrication methods allowed for control over several microscale properties of the scaffolds. The cavity diameter could be controlled by changing the diameter of the beads used as a CC template; this was demonstrated with beads with diameters of 100, 200, and 330 μm. Additionally, by

changing the annealing temperature of the beads, we showed that the interconnecting channel diameter can be controlled. At the time that these scaffolds were developed, there was no other way to obtain precise control on a scale as low as 30 μm. More recently, SFF-based fabrication methods have improved to provide control on a similar or better scale [61].

7.1.2 Bone marrow engineering

Next, the dissertation focused on the use of the ICC scaffolds to create hydrogel structures for bone marrow engineering. In contrast to the PLGA scaffolds, here the goal was to create a stable environment mimicking the HSC niche, with the ultimate application to be in pharmaceutical drug testing. A nonbiodegradable hydrogel was chosen so that the matrix environment would not change over time. The matrix was seeded with stromal cells, and without exogenous cyokines was able to support the expansion of $CD34^+$ HSCs for up to 28 days while being cultured in a rotary reactor. In comparison to 2D plates, ICC scaffolds produced approximately twice the percentage of cells that were $CD34^+$. As well, loss of CFSE showed that $CD34^+$ cells in ICCs replicated approximately 10 times more than those in 2D plates. These data together demonstrate that the expansion of $CD34^+$ HSCs was much greater in ICC scaffolds than in 2D plates. The identity of the $CD34^+$ cells was confirmed through flow cytometry and the ability to direct the lineage of differentiation HSC. The addition of cytokines to cause the differentiation of the $CD34^+$ cells into B-cells resulted in surface expression of markers characteristic of B-cells. Markers were several times more frequent in ICCs than in 2D plates. This was functionally characterized by exposing cells to lipopolysaccharide, which stimulated the production of IgM, demonstrating that the cells produced from $CD34^+$ cells functioned as B-cells. Concentrations of IgM in media were 10-20 times higher in ICCs. The data presented here demonstrated that the contacts presented by 3D cultures were important in HSC expansion

and retention of function.

The ultimate goal of the bone marrow engineering described here is to apply the matrices for *ex vivo* drug testing. With this in mind, we wished to simplify the use of the matrix so that it could be used in a drug testing format. The next project utilized the ICC scaffolds within 96-well plates, and compared it to the traditional 96-well plate cultures and a well-known commercially available matrix, Matrigel. Here, several stromal cells were compared to determine if the HSC niche could be replicated with just one stromal cell type. It was found that the 2D 96-well plate caused the greatest expansion of $CD34^+$ cells over 14 days. This is likely due to signals both released into the media and also from cell-cell contacts. Matrigel, which inhibited cell-cell contacts, had a great degree of total cell expansion, but a low percentage of $CD34^+$ over 14 days. It was suspected that this is due to the lack of direct cell-cell contacts. ICC scaffold cultures demonstrated little change in the number of $CD34^+$ cells over 14 days. This behavior is observed in human bone marrow, and is described as HSC quiescence. The quiescence seen in ICC scaffolds were thought to be because the matrix provided soluble and direct cell-cell communication, and also provided contacts in 3D, much like the structure of human bone marrow. The 3D communication minimizes gradients of soluble signals, and allows for HSC-stromal cell contact with directionality, much like contacts in the body.

The last section utilized the ICC scaffolds in the context of drug testing. Here, stromal cell-HSC cultures were performed in 2D 96-well plates and in ICC scaffolds. The cultures were treated with model drugs, EPO and MTX at several doses. It was found that there was an expected response of decreased cell number with MTX treatment, but no significant increase in cell number with EPO treatment.

7.2 Future directions in bone tissue engineering

This work presented here on PLGA ICC scaffolds was the first step in a larger project of multiscale bone tissue engineering. Here, we demonstrated control on the micro-scale by varying the cavity and interconnecting channel size. In particular, there are several ways to impart macro- and nano-scale control on the ICC scaffolds discussed here.

7.2.1 Macro-scale control

As mentioned above, a major consideration in bone scaffold engineering is to ensure sufficient permeability of nutrients and waste, as well as space for vasculature ingrowth. SFF fabrication-based techniques could be combined with the ICC structures to create the ordered and controllable structure over a larger scale (Fig 7.1). The macro-scale design of the SFF fabricated matrices could be designed to ensure the matrices have high mechanical properties and sufficient pore space for nutrient and waste diffusion. As well, the scaffolds should have sufficient space for bone and vasculature ingrowth. The micro-scale porosity donated to the scaffold structure by the ICC geometry will increase the surface area of the scaffolds for greater cell attachment. Lastly, the implantation of the scaffolds into an animal model could reveal further clues as to the ideal pore size to facilitate bone and vasculature growth into the scaffolds.

7.2.2 Nano-scale control

One of the most important future directions of bone tissue engineering is to further control the structure of scaffolds on a smaller scale, and to integrate this control into the micro-scale. Bone is composed of collagen fibrils and nanostructured HA, so the inclusion of calcium phosphate nanoparticles may improve the mechanical properties of the bulk polymer. As well, the precise arrangement of the nanoparticles may

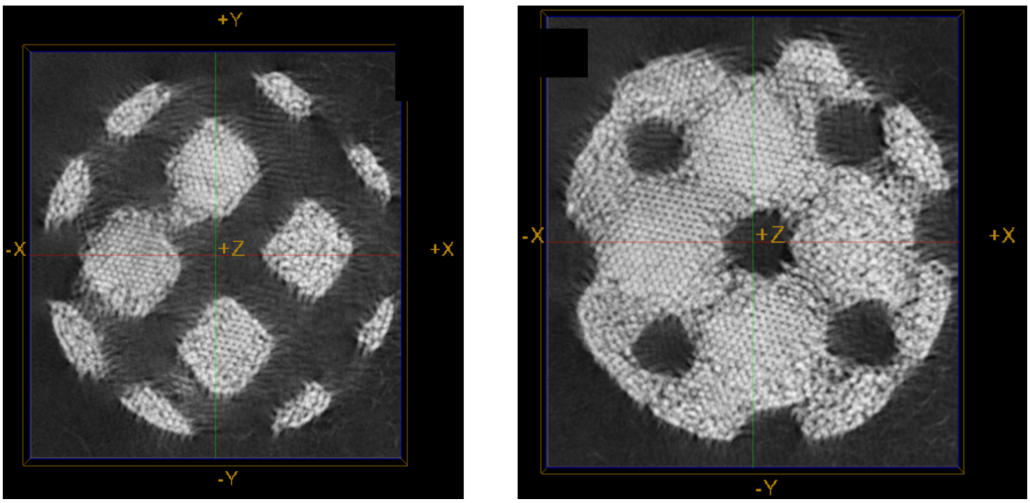

Figure 7.1: Micro-computed tomography images of CCs in a crossbar arrangements. CCs were fabricated by depositing glass beads under sonication into a mold fabricated by SFF techniques. Beads were annealed, and the mold was subsequently dissolved.

increase these mechanical properties. Currently, the Kotov group is attempting to construct a 3D structure out of nano-structured calcium phosphate [202] and a polymer (e.g., PDDA) via LBL synthesis. In addition to potential increases in mechanical properties, the inclusion of nano-structured materials can impart nano-sized surface properties. As cells have been shown to attach to nano-structured surfaces, these properties can aid the attachment and migration of cells within the matrix.

7.3 Future directions in bone marrow engineering

7.3.1 Choice of cell types in bone marrow engineering

The concept of bone marrow engineering for drug testing is new and not thoroughly explored. One complexity in this task is the balance of functionality and simplicity of the model. As discussed in Chapter 2, bone marrow is an incredibly complex environment of many cell types that contribute to the fate of HSCs through direct cell-cell contacts, ECM production, and soluble cytokine production. To fully

recapitulate bone marrow, an *ex vivo* model should incorporate all cell types in the proper ratios to produce signals that properly mimic those in the body. To make this model practical and reproducible, however, calls for simplicity in the number of cell types included in the model. Distilling the bone marrow microenvironment to several key components will be a difficult task. In addition to the bone and stromal cells explored in this dissertation, endothelial cells and adipocytes may be necessary to provide the most realistic cellular environment.

It is necessary to explore bone marrow models that utilize cells that represent a disease. Most importantly, the inclusion of primary disease cells, such as those extracted from the bone marrow of a CML patient, could provide clues about how cells interact with stromal cells, the pathology of the disease, or how cells react to certain drugs. As well, cell lines could be included. K-562, HL60, and Kasumi-6 are cell lines that mimic leukemias [203]. Comparing the replication, function, and reaction of these cell lines to chemotherapeutic drugs in 3D and 2D environments could provide basic information about the pathology of leukemias.

7.3.2 Choice of drugs used to validate the model

The models discussed in Chapter 6 did not demonstrate a difference between 2D and 3D cultures in the context of drug testing. Once the cell types have been deemed appropriate to mimic human bone marrow, different classes of drugs should be explored, including those that directly affect bone marrow, such as anti-virals. A wide range of drug concentrations should be explored to elucidate whether one culture exhibits greater sensitivity due to diffusion or arrangement of cells within the microenvironment.

7.4 Future directions in ICC scaffold development

7.4.1 Cell extraction from hydrogel ICC scaffolds

There are several developments that could be improved in the ICC scaffolds themselves. The most important issue that was observed through the course of this dissertation work is the extraction of cells from the scaffold for counting or flow cytometric analysis. Some 3D matrices, such as Matrigel, are composed of a material that degrades when exposed to the enzyme dispase. This allows for ease of removal of cells that are in the center of the matrix. The current polyacrylamide ICC scaffolds cannot be degraded, so all cells must be removed from the scaffold via repeated pipetting. As the scaffold geometry is tortuous, it is difficult to extract cells from the center of the matrix. An ideal improvement to the scaffold would be to include chemistry within the polymer that could cause degradation of the scaffold upon the addition of an enzyme or a cellularly benign chemical.

7.4.2 Assay development

An ideal scaffold for drug testing would be integrated with current assays and instrumentation. Current assays and protocols are developed for use with 2D cell cultures. In these, the reagents are added to the 2D cultures, and the cultures analyzed directly using a microplate reader. To fully take advantage of the transparent hydrogel ICCs, it should be explored whether current assays can be performed directly within ICC scaffolds. This would greatly add to the value of the scaffolds and their ease of use.

BIBLIOGRAPHY

[1] W L McKeehan, D Barnes, L Reid, E Stanbridge, H Murakami, and G H Sato. Frontiers in mammalian cell culture. *In Vitro Cell Dev Biol*, 26(1):9–23, 1990.

[2] A B Sabin. Oral poliovirus vaccine: history of its development and use and current challenge to eliminate poliomyelitis from the world. *J Infect Dis*, 151(3):420–36, 1985.

[3] L P Gartner and J L Hiatt. *Color Textbook of Histology*. Philadelphia: Saunders, Philadelphia, 2001.

[4] M C Poznansky, R H Evans, R B Foxall, I T Olszak, A H Piascik, K E Hartman, C Brander, T H Meyer, M J Pykett, K T Chabner, S A Kalams, M Rosenzweig, and D T Scadden. Efficient generation of human t cells from a tissue-engineered thymic organoid. *Nat Biotechnol*, 18(7):729–34, 2000.

[5] V M Weaver, O W Petersen, F Wang, C A Larabell, P Briand, C Damsky, and M J Bissell. Reversion of the malignant phenotype of human breast cells in three-dimensional culture and in vivo by integrin blocking antibodies. *J Cell Biol*, 137(1):231–45, 1997.

[6] S A Pangas, H Saudye, L D Shea, and T K Woodruff. Novel approach for the three-dimensional culture of granulosa cell-oocyte complexes. *Tissue Eng*, 9(5):1013–21, 2003.

[7] T Elsdale and J Bard. Collagen substrata for studies on cell behavior. *J Cell Biol*, 54:626–637, 1972.

[8] J Lee, M J Cuddihy, and N A Kotov. Three-dimensional cell culture matrices: state of the art. *Tissue Eng Part B*, 14(1):61–86, 2008.

[9] Janeway CA, Travers P, Walport M, and Shlomchik MJ. *ImmunoBiology*. Garland Science Publishing, 2005.

[10] C A Simmons, E A, S H, W J Kim, and D J Mooney. Dual growth factor delivery and controlled scaffold degradation enhance in vivo bone formation by transplanted bone marrow stromal cells. *Bone*, 35(2):562–9, Aug 2004.

[11] T Elkayam, S Amitay-Shaprut, Mona Dvir-Ginzberg, Tamar Harel, and Smadar Cohen. Enhancing the drug metabolism activities of c3a–a human hepatocyte

cell line–by tissue engineering within alginate scaffolds. *Tissue Eng*, 12(5):1357–68, 2006.

[12] J Lee and N A Kotov. Notch ligand presenting acellular 3d microenvironments for ex vivo human hematopoietic stem-cell culture made by layer-by-layer assembly. *Small*, 5(9):1008–1013, 2009.

[13] D R Albrecht, G H Underhill, T B Wassermann, R L Sah, and S N Bhatia. Probing the role of multicellular organization in three-dimensional microenvironments. *Nat Methods*, 3(5):369–75, 2006.

[14] M J Bissell, A Rizki, and I S Mian. Tissue architecture: the ultimate regulator of breast epithelial function. *Curr Opin Cell Biol*, 15(6):753–62, 2003.

[15] D E Discher, P J, and Y-L Wang. Tissue cells feel and respond to the stiffness of their substrate. *Science*, 310(5751):1139–43, 2005.

[16] A J Engler, S Sen, H L Sweeney, and D E Discher. Matrix elasticity directs stem cell lineage specification. *Cell*, 126(4):677–89, 2006.

[17] J Lee, M J Cuddihy, G M Cater, and N A Kotov. Engineering liver tissue spheroids with inverted colloidal crystal scaffolds. *Biomaterials*, 30:4687–4694, 2009.

[18] R Langer and J P Vacanti. Tissue engineering. *Science*, 260(5110):920–6, 1993.

[19] S MacNeil. Progress and opportunities for tissue-engineered skin. *Nature*, 445(7130):874–80, 2007.

[20] X Liu, L A Smith, J Hu, and P X Ma. Biomimetic nanofibrous gelatin/apatite composite scaffolds for bone tissue engineering. *Biomaterials*, 30(12):2252–8, 2009.

[21] J M Kemppainen and S J Hollister. Tailoring the mechanical properties of 3d-designed poly(glycerol sebacate) scaffolds for cartilage applications. *J Biomed Mater Res A*, 94(1):9–18, 2010.

[22] N W Choi, M Cabodi, B Held, J P Gleghorn, L J Bonassar, and Abraham D Stroock. Microfluidic scaffolds for tissue engineering. *Nat Mater*, 6(11):908–15, 2007.

[23] C Fischbach, R Chen, T Matsumoto, T Schmelzle, J S Brugge, P J Polverini, and D J Mooney. Engineering tumors with 3d scaffolds. *Nat Methods*, 4(10):855–60, 2007.

[24] K B Hotary, E D Allen, P C Brooks, N S Datta, M W Long, and S J Weiss. Membrane type i matrix metalloproteinase usurps tumor growth control imposed by the three-dimensional extracellular matrix. *Cell*, 114(1):33–45, 2003.

[25] M J Cuddihy and N A Kotov. Poly(lactic-co-glycolic acid) bone scaffolds with inverted colloidal crystal geometry. *Tissue Eng Part A*, 14(10):1639–1649, 2008.

[26] N A Kotov, Y Liu, S Wang, C Cumming, M Eghtedari, G Vargas, M Motamedi, J Nichols, and Joaquin Cortiella. Inverted colloidal crystals as three-dimensional cell scaffolds. *Langmuir*, 20(19):7887–7892, 2004.

[27] J Lee, S Shanbhag, and N Kotov. Inverted colloidal crystals as three-dimensional microenvironments for cellular co-cultures. *Journal of Materials Chemistry*, 16:3558–3564, 2006.

[28] Y Liu, S Wang, J Lee, and N Kotov. A floating self-assembly route to colloidal crystal templates for 3d cell scaffolds. *Chem. Mater*, 17(20):4918–4924, 2005.

[29] Y Zhang, S Wang, M Eghtedari, M Motamedi, and NA Kotov. Inverted-colloidal-crystal hydrogel matrices as three-dimensional cell scaffolds. *Adv Funct Mater*, 15(5):725–731, 2005.

[30] J E Nichols, J Cortiella, J Lee, J A Niles, M Cuddihy, S Wang, J Bielitzki, A Cantu, R Mlcak, E Valdivia, R Yancy, M L McClure, and N A Kotov. In vitro analog of human bone marrow from 3d scaffolds with biomimetic inverted colloidal crystal geometry. *Biomaterials*, 30(6):1071–9, 2009.

[31] J Lee, G D Lilly, R C Doty, P Podsiadlo, and N A Kotov. In vitro toxicity testing of nanoparticles in 3d cell culture. *Small*, 5(10):1213–1221, 2009.

[32] J H Bahng, E Elliott, P Podsiadlo, K Critchley, J W Lee, C Doty, and N A Kotov. 3d scaffolds with inverted colloidal crystal geometry from expandable cationic poly(dmaa-co-amtac) hydrogel for well-plate format. *In preparation*, pages 1–39, 2010.

[33] J P Vacanti and R Langer. Tissue engineering: the design and fabrication of living replacement devices for surgical reconstruction and transplantation. *Lancet*, 354 Suppl 1:SI32–4, 1999.

[34] L G Griffith and G Naughton. Tissue engineering–current challenges and expanding opportunities. *Science*, 295(5557):1009–14, 2002.

[35] L G Griffith and M A Swartz. Capturing complex 3d tissue physiology in vitro. *Nat Rev Mol Cell Biol*, 7:211–224, 2006.

[36] J Nyman, M Reyes, and X Wang. Effect of ultrastructural changes on the toughness of bone. *Micron*, 36(7–8):566–582, 2005.

[37] S J Hollister, R A Levy, T M Chu, J W Halloran, and S E Feinberg. An image-based approach for designing and manufacturing craniofacial scaffolds. *Int J Oral Maxillofac Surg*, 29(1):67–71, 2000.

[38] S Hollister. Porous scaffold design for tissue engineering. *Nat mater*, 4:518–524, 2005.

[39] A Atala, S B Bauer, S Soker, J J Yoo, and A B Retik. Tissue-engineered autologous bladders for patients needing cystoplasty. *Lancet*, 367(9518):1241–6, 2006.

[40] J Cesarano and J Dellinger. Customization of load-bearing hydroxyapatite lattice scaffolds. *International Journal of Applied Ceramic Technology*, 2(3):212–220, 2005.

[41] P H Warnke, I N G Springer, J Wiltfang, Y Acil, H Eufinger, M Wehmöller, P A J Russo, H Bolte, E Sherry, E Behrens, and H Terheyden. Growth and transplantation of a custom vascularised bone graft in a man. *Lancet*, 364(9436):766–70, 2004.

[42] J J A Barry, D Howard, K M Shakesheff, S M Howdle, and M R Alexander. Using a core–sheath distribution of surface chemistry through 3d tissue engineering scaffolds to control cell ingress. *Adv Mater*, 18:1406–1410, 2006.

[43] K Li, M J Mondrinos, X Chen, M R Gandhi, F K Ko, and P I Lelkes. Co-electrospun poly(lactide-co-glycolide), gelatin, and elastin blends for tissue engineering scaffolds. *J Biomed Mater Res A*, 79(4):963–73, 2006.

[44] G Wei and P X Ma. Macroporous and nanofibrous polymer scaffolds and polymer/bone-like apatite composite scaffolds generated by sugar spheres. *Journal of biomedical materials research Part A*, 78(2):306–15, Aug 2006.

[45] S Vauthey, S Santoso, H Gong, N Watson, and S Zhang. Molecular self-assembly of surfactant-like peptides to form nanotubes and nanovesicles. *Proc Natl Acad Sci USA*, 99(8):5355–60, 2002.

[46] E Sachlos, D Gotora, and J T Czernuszka. Collagen scaffolds reinforced with biomimetic composite nano-sized carbonate-substituted hydroxyapatite crystals and shaped by rapid prototyping to contain internal microchannels. *Tissue Eng*, 12(9):2479–87, 2006.

[47] G E Park, M A Pattison, K Park, and T J Webster. Accelerated chondrocyte functions on naoh-treated plga scaffolds. *Biomaterials*, 26(16):3075–82, 2005.

[48] N Gomez, Y Lu, S Chen, and C E Schmidt. Immobilized nerve growth factor and microtopography have distinct effects on polarization versus axon elongation in hippocampal cells in culture. *Biomaterials*, 28(2):271–84, 2007.

[49] X Zhu, K L Mills, P R Peters, J H Bahng, E H Liu, J Shim, K Naruse, M E Csete, M D Thouless, and S Takayama. Fabrication of reconfigurable protein matrices by cracking. *Nat Mater*, 4(5):403–6, 2005.

[50] J C Y Dunn, W-Y Chan, V Cristini, J S Kim, J Lowengrub, S Singh, and B M Wu. Analysis of cell growth in three-dimensional scaffolds. *Tissue Eng*, 12(4):705–16, 2006.

[51] J R Jones, L M Ehrenfried, and L L Hench. Optimising bioactive glass scaffolds for bone tissue engineering. *Biomaterials*, 27(7):964–73, 2006.

[52] W-J Li, R Tuli, C Okafor, A Derfoul, K G Danielson, D J Hall, and R S Tuan. A three-dimensional nanofibrous scaffold for cartilage tissue engineering using human mesenchymal stem cells. *Biomaterials*, 26(6):599–609, 2005.

[53] A Mikos and J Temenoff. Formation of highly porous biodegradable scaffolds for tissue engineering. *Electron J Biotechnol*, 3(2):1–6, 2000.

[54] Y Nam and T Park. Biodegradable polymeric microcellular foams by modified thermally induced phase separation method. *Biomaterials*, 20(19):1783–1790, 1999.

[55] C-Y Lin, R M Schek, A S Mistry, X Shi, A G Mikos, P H Krebsbach, and S J Hollister. Functional bone engineering using ex vivo gene therapy and topology-optimized, biodegradable polymer composite scaffolds. *Tissue Eng*, 11(9-10):1589–98, 2005.

[56] J Williams, A Adewunmi, R Schek, and C Flanagan. Bone tissue engineering using polycaprolactone scaffolds fabricated via selective laser sintering. *Biomaterials*, 26(23):4817–4827, 2005.

[57] K F Leong, C M Cheah, and C K Chua. Solid freeform fabrication of three-dimensional scaffolds for engineering replacement tissues and organs. *Biomaterials*, 24(13):2363–78, 2003.

[58] F P W Melchels, J Feijen, and D W Grijpma. A review on stereolithography and its applications in biomedical engineering. *Biomaterials*, 31(24):6121–6130, 2010.

[59] S Yang, K-F Leong, Z Du, and C-K Chua. The design of scaffolds for use in tissue engineering. part ii. rapid prototyping techniques. *Tissue Eng*, 8(1):1–11, Feb 2002.

[60] J Taboas, R Maddox, P Krebsbach, and S Hollister. Indirect solid free form fabrication of local and global porous, biomimetic and composite 3d polymer-ceramic scaffolds. *Biomaterials*, 24(1):181–194, 2003.

[61] T Wei, G Hildebrand, R Schade, and K Liefeith. Two-photon polymerization for microfabrication of three-dimensional scaffolds for tissue engineering application. *Eng. Life Sci.*, 9(5):384–390, 2009.

[62] S Shanbhag, W Lee, and N Kotov. Diffusion in three-dimensionally ordered scaffolds with inverted colloidal crystal geometry. *Biomaterials*, 26(27):5581–5585, 2005.

[63] A Stachowiak, A Bershteyn, E Tzatzalos, and D J Irvine. Bioactive hydrogels with an ordered cellular structure combine interconnected macroporosity and robust mechanical properties. *Adv Mater*, 17(4):399–403, 2004.

[64] M M Stevens and J H George. Exploring and engineering the cell surface interface. *Science*, 310(5751):1135–8, 2005.

[65] J D Hartgerink, E Beniash, and S I Stupp. Self-assembly and mineralization of peptide-amphiphile nanofibers. *Science*, 294(5547):1684–8, 2001.

[66] G Wei and P X Ma. Structure and properties of nano-hydroxyapatite/polymer composite scaffolds for bone tissue engineering. *Biomaterials*, 25(19):4749–57, 2004.

[67] P X Ma and R Zhang. Synthetic nano-scale fibrous extracellular matrix. *J Biomed Mater Res*, 46(1):60–72, 1999.

[68] W-J Li, R Tuli, X Huang, P Laquerriere, and R S Tuan. Multilineage differentiation of human mesenchymal stem cells in a three-dimensional nanofibrous scaffold. *Biomaterials*, 26(25):5158–66, 2005.

[69] S Kay, A Thapa, K M Haberstroh, and T J Webster. Nanostructured polymer/nanophase ceramic composites enhance osteoblast and chondrocyte adhesion. *Tissue Eng*, 8(5):753–61, 2002.

[70] S Bhatia, U Balis, M Yarmush, and M Toner. Effect of cell-cell interactions in preservation of cellular phenotype: cocultivation of hepatocytes and nonparenchymal cells. *The FASEB Journal*, 13:1883–1900, 1999.

[71] J L Drury and D J Mooney. Hydrogels for tissue engineering: scaffold design variables and applications. *Biomaterials*, 24(24):4337–51, 2003.

[72] K Y Lee and D J Mooney. Hydrogels for tissue engineering. *Chem Rev*, 101(7):1869–79, 2001.

[73] S Zhang. Hydrogels: Wet or let die. *Nat Mater*, 3(1):7–8, 2004.

[74] J Elisseeff, K Anseth, D Sims, W McIntosh, M Randolph, and R Langer. Transdermal photopolymerization for minimally invasive implantation. *Proc Natl Acad Sci USA*, 96(6):3104–7, 1999.

[75] R G Ellis-Behnke, Y-X Liang, S-W You, D K C Tay, S Zhang, K-F So, and G E Schneider. Nano neuro knitting: peptide nanofiber scaffold for brain repair and axon regeneration with functional return of vision. *Proc Natl Acad Sci USA*, 103(13):5054–9, 2006.

[76] G A Silva, C Czeisler, K L Niece, E Beniash, D A Harrington, J A Kessler, and S I Stupp. Selective differentiation of neural progenitor cells by high-epitope density nanofibers. *Science*, 303(5662):1352–5, 2004.

[77] Y Li, Y D Tseng, S Y Kwon, L D'Espaux, J S Bunch, P L McEuen, and D Luo. Controlled assembly of dendrimer-like dna. *Nat Mater*, 3(1):38–42, 2004.

[78] S H Um, J B Lee, N Park, S Y Kwon, C C Umbach, and D Luo. Enzyme-catalysed assembly of dna hydrogel. *Nat Mater*, 5(10):797–801, 2006.

[79] D L Hern and J A Hubbell. Incorporation of adhesion peptides into nonadhesive hydrogels useful for tissue resurfacing. *J Biomed Mater Res*, 39(2):266–76, 1998.

[80] D S Grant, H K Kleinman, C P Leblond, S Inoue, A E Chung, and G R Martin. The basement-membrane-like matrix of the mouse ehs tumor: Ii. immunohistochemical quantitation of six of its components. *Am J Anat*, 174(4):387–98, 1985.

[81] J Miki, B Furusato, H Li, Y Gu, H Takahashi, S Egawa, I A Sesterhenn, D G McLeod, S Srivastava, and J S Rhim. Identification of putative stem cell markers, cd133 and cxcr4, in htert-immortalized primary nonmalignant and malignant tumor-derived human prostate epithelial cell lines and in prostate cancer specimens. *Cancer Res*, 67(7):3153–61, 2007.

[82] H K Kleinman and G R Martin. Matrigel: basement membrane matrix with biological activity. *Semin Cancer Biol*, 15(5):378–86, 2005.

[83] A Rizki, V M Weaver, S-Y Lee, G I Rozenberg, K Chin, C A Myers, J L Bascom, J D Mott, J R Semeiks, L R Grate, I S Mian, A D Borowsky, R A Jensen, M O Idowu, F Chen, D J Chen, O W Petersen, J W Gray, and M J Bissell. A human breast cell model of preinvasive to invasive transition. *Cancer Res*, 68(5):1378–87, 2008.

[84] Z Tang, G Geng, Q Huang, G Xu, H Hu, J Chen, and J Li. Expression of tissue factor pathway inhibitor 2 in human pancreatic carcinoma and its effect on tumor growth, invasion, and migration in vitro and in vivo. *J Surg Res*, In press, 2009.

[85] C T Laurencin, A M Ambrosio, M D Borden, and J A Cooper. Tissue engineering: orthopedic applications. *Annu Rev Biomed Eng*, 1:19–46, 1999.

[86] G F Muschler, C Nakamoto, and L G Griffith. Engineering principles of clinical cell-based tissue engineering. *J Bone Joint Surg Am*, 86-A(7):1541–58, 2004.

[87] C-M Dong, Y-Z Guo, K-Y Qiu, Z-W Gu, and X-D Feng. In vitro degradation and controlled release behavior of d,l-plga50 and pcl-b-d,l-plga50 copolymer microspheres. *J Control Release*, 107(1):53–64, 2005.

[88] T Hoc, L Henry, M Verdier, D Aubry, L Sedel, and A Meunier. Effect of microstructure on the mechanical properties of haversian cortical bone. *Bone*, 38(4):466–74, 2006.

[89] D B Burr. The contribution of the organic matrix to bone's material properties. *Bone*, 31(1):8–11, 2002.

[90] M C van der Meulen, K J Jepsen, and B Mikić. Understanding bone strength: size isn't everything. *Bone*, 29(2):101–4, 2001.

[91] K Rezwan, Q Z Chen, J J Blaker, and Aldo Roberto Boccaccini. Biodegradable and bioactive porous polymer/inorganic composite scaffolds for bone tissue engineering. *Biomaterials*, 27(18):3413–31, 2006.

[92] J Andersson, S Areva, B Spliethoff, and M Lindén. Sol-gel synthesis of a multifunctional, hierarchically porous silica/apatite composite. *Biomaterials*, 26(34):6827–35, Dec 2005.

[93] L Guan and J E Davies. Preparation and characterization of a highly macroporous biodegradable composite tissue engineering scaffold. *J Biomed Mater Res A*, 71(3):480–7, 2004.

[94] P Q Ruhé, E L Hedberg-Dirk, N T Padron, P H M Spauwen, J A Jansen, and A G Mikos. Porous poly(dl-lactic-co-glycolic acid)/calcium phosphate cement composite for reconstruction of bone defects. *Tissue Eng*, 12(4):789–800, 2006.

[95] F Zhao, W L Grayson, T Ma, B Bunnell, and W W Lu. Effects of hydroxyapatite in 3-d chitosan-gelatin polymer network on human mesenchymal stem cell construct development. *Biomaterials*, 27(9):1859–67, 2006.

[96] K G Marra, J W Szem, P N Kumta, P A DiMilla, and L E Weiss. In vitro analysis of biodegradable polymer blend/hydroxyapatite composites for bone tissue engineering. *J Biomed Mater Res*, 47(3):324–35, 1999.

[97] S-S Kim, M S Park, O J, C Y Choi, and B-S Kim. Poly(lactide-co-glycolide)/hydroxyapatite composite scaffolds for bone tissue engineering. *Biomaterials*, 27(8):1399–409, 2006.

[98] G B Adams, K T Chabner, I R Alley, D P Olson, Z M Szczepiorkowski, M C Poznansky, Claudine H Kos, Martin R Pollak, Edward M Brown, and David T Scadden. Stem cell engraftment at the endosteal niche is specified by the calcium-sensing receptor. *Nature*, 439(7076):599–603, 2006.

[99] F Arai, A Hirao, M Ohmura, H Sato, S Matsuoka, K Takubo, K Ito, G Y Koh, and T Suda. Tie2/angiopoietin-1 signaling regulates hematopoietic stem cell quiescence in the bone marrow niche. *Cell*, 118(2):149–61, 2004.

[100] M J Kiel and S J Morrison. Uncertainty in the niches that maintain haematopoietic stem cells. *Nat Rev Immunol*, 8(4):290–301, 2008.

[101] R S Taichman and S G Emerson. The role of osteoblasts in the hematopoietic microenvironment. *Stem Cells*, 16(1):7–15, Jan 1998.

[102] T Sugiyama, H Kohara, M Noda, and T Nagasawa. Maintenance of the hematopoietic stem cell pool by cxcl12-cxcr4 chemokine signaling in bone marrow stromal cell niches. *Immunity*, 25(6):977–88, 2006.

[103] G B Adams and D T Scadden. The hematopoietic stem cell in its place. *Nat Immunol*, 7(4):333–7, 2006.

[104] D T Scadden. The stem-cell niche as an entity of action. *Nature*, 441(7097):1075–9, 2006.

[105] K-N Chua, C Chai, P-C Lee, S Ramakrishna, K W Leong, and H-Q Mao. Functional nanofiber scaffolds with different spacers modulate adhesion and expansion of cryopreserved umbilical cord blood hematopoietic stem/progenitor cells. *Exp Hematol*, 35(5):771–81, 2007.

[106] M R Doran, B D Markway, I A Aird, A S Rowlands, P A George, L K Nielsen, and J J Cooper-White. Surface-bound stem cell factor and the promotion of hematopoietic cell expansion. *Biomaterials*, 30(25):4047–52, 2009.

[107] L Hou, T Liu, J Tan, W Meng, L Deng, H Yu, X Zou, and Y Wang. Long-term culture of leukemic bone marrow primary cells in biomimetic osteoblast niche. *Int J Hematol*, 90(3):281–91, 2009.

[108] K Ma, C K Chan, S Liao, W Y K Hwang, Q Feng, and S Ramakrishna. Electrospun nanofiber scaffolds for rapid and rich capture of bone marrow-derived hematopoietic stem cells. *Biomaterials*, 29(13):2096–103, 2008.

[109] B A Roecklein and B Torok-Storb. Functionally distinct human marrow stromal cell lines immortalized by transduction with the human papilloma virus e6/e7 genes. *Blood*, 85(4):997–1005, 1995.

[110] B A Roecklein, J Reems, S Rowley, and B Torok-Storb. Ex vivo expansion of immature 4-hydroperoxycyclophosphamide-resistant progenitor cells from g-csf-mobilized peripheral blood. *Biol Blood Marrow Transplant*, 4(2):61–8, 1998.

[111] C Rofani, L Luchetti, G Testa, R Lasorella, G Isacchi, G F Bottazzo, and A C Berardi. Il-16 can synergize with early acting cytokines to expand ex vivo cd34+isolated from cord blood. *Stem Cells Dev*, 18(4):671–682, 2009.

[112] P W Zandstra, E Conneally, A L Petzer, J M Piret, and C J Eaves. Cytokine manipulation of primitive human hematopoietic cell self-renewal. *Proc Natl Acad Sci USA*, 94(9):4698–703, 1997.

[113] C H Cho, J F Eliason, and H W T Matthew. Application of porous glycosaminoglycan-based scaffolds for expansion of human cord blood stem cells in perfusion culture. *J Biomed Mater Res A*, 86(1):98–107, 2008.

[114] Q Feng, C Chai, X-S Jiang, K W Leong, and H-Q Mao. Expansion of engrafting human hematopoietic stem/progenitor cells in three-dimensional scaffolds with surface-immobilized fibronectin. *J Biomed Mater Res A*, 78(4):781–91, 2006.

[115] Y Li, T Ma, D A Kniss, S T Yang, and L C Lasky. Human cord cell hematopoiesis in three-dimensional nonwoven fibrous matrices: in vitro simulation of the marrow microenvironment. *J Hematother Stem Cell Res*, 10(3):355–68, 2001.

[116] G Mehta, M J Kiel, J W Lee, N A Kotov, J J Linderman, and S Takayama. Polyelectrolyte-clay-protein layer films on microfluidic pdms bioreactor surfaces for primary murine bone marrow culture. *Adv Funct Mater*, 17:2701–2709, 2007.

[117] K Chadwick, L Wang, L Li, P Menendez, B Murdoch, A Rouleau, and M Bhatia. Cytokines and bmp-4 promote hematopoietic differentiation of human embryonic stem cells. *Blood*, 102(3):906–15, 2003.

[118] B Heissig, K Hattori, S Dias, M Friedrich, B Ferris, Neil R Hackett, R G Crystal, P Besmer, D Lyden, M A S Moore, Z Werb, and S Rafii. Recruitment of stem and progenitor cells from the bone marrow niche requires mmp-9 mediated release of kit-ligand. *Cell*, 109(5):625–37, 2002.

[119] X Liu and P Ma. Polymeric scaffolds for bone tissue engineering. *Ann Biomed Eng*, 32(3):477–486, 2004.

[120] Y S Nam and T G Park. Porous biodegradable polymeric scaffolds prepared by thermally induced phase separation. *J Biomed Mater Res*, 47(1):8–17, Oct 1999.

[121] C Song, P Wang, and H A Makse. A phase diagram for jammed matter. *Nature*, 453:629–632, 2008.

[122] E Jan and N Kotov. Successful differentiation of mouse neural stem cells on layer-by-layer assembled single-walled carbon nanotube composite. *Nano Lett*, 7(5):1123–1128, 2007.

[123] S Manolagas, D Burton, and L Deftos. 1, 25-dihydroxyvitamin d3 stimulates the alkaline phosphatase activity of osteoblast-like cells. *Journal of Biological Chemistry*, 256(14):7115–7, 1981.

[124] M Gomes, H Holtorf, R Reis, and A Mikos. Influence of the porosity of starch-based fiber mesh scaffolds on the proliferation and osteogenic differentiation of bone marrow stromal cells cultured in a flow perfusion bioreactor. *Tissue Eng*, 12(4):801–9, 2006.

[125] H Holtorf, N Datta, and J Jansen. Scaffold mesh size affects the osteoblastic differentiation of seeded marrow stromal cells cultured in a flow perfusion bioreactor. *J Biomed Mater Res A*, 74(2):171–80, 2005.

[126] L Mathieu, T Mueller, P Bourban, and D Pioletti. Architecture and properties of anisotropic polymer composite scaffolds for bone tissue engineering. *Biomaterials*, 27(6):905–16, 2006.

[127] Y Cao, G Mitchell, A Messina, L Price, and E Thompson. The influence of architecture on degradation and tissue ingrowth into three-dimensional poly (lactic-co-glycolic acid) scaffolds in vitro and in vivo. *Biomaterials*, 27(14):2854–64, 2006.

[128] V Chen and P Ma. The effect of surface area on the degradation rate of nanofibrous poly (l-lactic acid) foams. *Biomaterials*, 27(20):3708–15, 2006.

[129] V Karageorgiou and D Kaplan. Porosity of 3d biomaterial scaffolds and osteogenesis. *Biomaterials*, 26(27):5474–91, 2005.

[130] J Zeltinger, J Sherwood, and D Graham. Effect of pore size and void fraction on cellular adhesion, proliferation, and matrix deposition. *Tissue Eng*, 7(5):557–72, 2001.

[131] S Hulbert, F Young, and R Mathews. Potential of ceramic materials as permanently implantable skeletal prostheses. *J Biomed Mater Res A*, 4(3):433–56, 1970.

[132] F Klenke, Y Liu, and H Yuan. Impact of pore size on the vascularization and osseointegration of ceramic bone substitutes in vivo. *J Biomed Mater Res A*, 85(3):777–86, 2008.

[133] A Itala, H Ylanen, C Ekholm, and K Karlsson. Pore diameter of more than 100 micro m is not requisite for bone ingrowth in rabbits. *J Biomed Mater Res A*, 58(6):679–83, 2001.

[134] B Flautre, M Descamps, C Delecourt, and M Blary. Porous ha ceramic for bone replacement: Role of the pores and interconnections–experimental study in the rabbit. *J Mater Sci Mater Med*, 12(8):679–82, 2001.

[135] Y Kuboki, Q Jin, and H Takita. Geometry of carriers controlling phenotypic expression in bmp-induced osteogenesis and chondrogenesis. *J Bone Joint Surg Am*, 83-A Suppl 1(Pt2):S105–15, 2001.

[136] Y Kuboki, Q Jin, and M Kikuchi. Geometry of artificial ecm: sizes of pores controlling phenotype expression in bmp-induced osteogenesis and chondrogenesis. *Connective tissue research*, 43(2-3):529–34, 2002.

[137] O Zinger, G Zhao, Z Schwartz, J Simpson, and M Wieland. Differential regulation of osteoblasts by substrate microstructural features. *Biomaterials*, 26(14):1837–47, 2005.

[138] S Goldstein. Tissue engineering. *Ann NY Acad Sci*, 961(Reparative Medicine):183–192, 2006.

[139] P Ma and J Choi. Biodegradable polymer scaffolds with well-defined interconnected spherical pore network. *Tissue Eng*, 7(1):23–33, 2001.

[140] L Shea, D Wang, and R Franceschi. Engineered bone development from a pre-osteoblast cell line on three-dimensional scaffolds. *Tissue Eng*, 6(6):605–17, 2000.

[141] M Mondrinos, R Dembzynski, L Lu, and V Byrapogu. Porogen-based solid freeform fabrication of polycaprolactone-calcium phosphate scaffolds for tissue engineering. *Biomaterials*, 27(25):4399–408, 2006.

[142] T Hildebrand, A Laib, and R Müller. Direct three-dimensional morphometric analysis of human cancellous bone: microstructural data from spine, femur, iliac crest, and calcaneus. *J Bone Miner Res*, 14(7):1167–74, 1999.

[143] M Kang, W Lee, K Oh, J Han, K Song, and B Cha. The short-term changes of bone mineral metabolism following bone marrow transplantation. *Bone*, 26(3):275–9, 2000.

[144] H Wang, Y Li, Y Zuo, J Li, S Ma, and L Cheng. Biocompatibility and osteogenesis of biomimetic nano-hydroxyapatite/polyamide composite scaffolds for bone tissue engineering. *Biomaterials*, 28(22):3338–48, 2007.

[145] S A Harris, R J Enger, B L Riggs, and T C Spelsberg. Development and characterization of a conditionally immortalized human fetal osteoblastic cell line. *J Bone Miner Res*, 10(2):178–86, 1995.

[146] A Wilson and A Trumpp. Bone-marrow haematopoietic-stem-cell niches. *Nat Rev Immunol*, 6(2):93–106, 2006.

[147] J Barker and C M Verfaillie. A novel in vitro model of early human adult b lymphopoiesis that allows proliferation of pro-b cells and differentiation to mature b lymphocytes. *Leukemia*, 14(9):1614–20, 2000.

[148] J Chen, J S Brandt, F M Ellison, R T Calado, and N S Young. Defective stromal cell function in a mouse model of infusion-induced bone marrow failure. *Exp Hematol*, 33(8):901–8, Aug 2005.

[149] S X Hsiong and D J Mooney. Regeneration of vascularized bone. *Periodontol 2000*, 41:109–22, 2006.

[150] A Islam, D Catovsky, J M Goldman, and D A Galton. Histomorphological study of cellular interactions between stromal and haemopoietic stem cells in normal and leukaemic bone marrow. *Histopathology*, 8(2):293–313, 1984.

[151] M J Kiel, O H Yilmaz, T Iwashita, O H Yilmaz, C Terhorst, and S J Morrison. Slam family receptors distinguish hematopoietic stem and progenitor cells and reveal endothelial niches for stem cells. *Cell*, 121(7):1109–21, 2005.

[152] L Kobari, F Pflumio, M Giarratana, X Li, M Titeux, B Izac, F Leteurtre, L Coulombel, and L Douay. In vitro and in vivo evidence for the long-term multilineage (myeloid, b, nk, and t) reconstitution capacity of ex vivo expanded human cd34(+) cord blood cells. *Exp Hematol*, 28(12):1470–80, 2000.

[153] M Punzel, K A Moore, I R Lemischka, and C M Verfaillie. The type of stromal feeder used in limiting dilution assays influences frequency and maintenance assessment of human long-term culture initiating cells. *Leukemia*, 13(1):92–7, 1999.

[154] Z Tang, N A Kotov, S Magonov, and B Ozturk. Nanostructured artificial nacre. *Nat Mater*, 2(6):413–8, 2003.

[155] C I Civin, T Trischmann, N S Kadan, J Davis, S Noga, K Cohen, B Duffy, I Groenewegen, J Wiley, P Law, A Hardwick, F Oldham, and A Gee. Highly purified cd34-positive cells reconstitute hematopoiesis. *J Clin Oncol*, 14(8):2224–33, 1996.

[156] K G Murti, P S Brown, M a Kumagai, and D Campana. Molecular interactions between human b-cell progenitors and the bone marrow microenvironment. *Exp Cell Res*, 226(1):47–58, 1996.

[157] L M Calvi, G B Adams, K W Weibrecht, J M Weber, D P Olson, M C Knight, R P Martin, E Schipani, P Divieti, F R Bringhurst, L A Milner, H M Kronenberg, and D T Scadden. Osteoblastic cells regulate the haematopoietic stem cell niche. *Nature*, 425(6960):841–6, 2003.

[158] F Djouad, B Delorme, M Maurice, C Bony, F Apparailly, P Louis-Plence, F Canovas, P Charbord, D Noël, and C Jorgensen. Microenvironmental changes during differentiation of mesenchymal stem cells towards chondrocytes. *Arthritis Res Ther*, 9(2):R33, 2007.

[159] H Geiger, A Koehler, and M Gunzer. Stem cells, aging, niche, adhesion and cdc42: a model for changes in cell-cell interactions and hematopoietic stem cell aging. *Cell Cycle*, 6(8):884–7, 2007.

[160] M T Thompson, M C Berg, I S Tobias, M F Rubner, and K J Van Vliet. Tuning compliance of nanoscale polyelectrolyte multilayers to modulate cell adhesion. *Biomaterials*, 26(34):6836–45, 2005.

[161] N Q Balaban, U S Schwarz, D Riveline, P Goichberg, G Tzur, I Sabanay, D Mahalu, S Safran, A Bershadsky, L Addadi, and B Geiger. Force and focal adhesion assembly: a close relationship studied using elastic micropatterned substrates. *Nat Cell Biol*, 3(5):466–72, 2001.

[162] A Schneider, G Francius, R Obeid, P Schwinté, J Hemmerlé, B Frisch, P Schaaf, J-C Voegel, B Senger, and C Picart. Polyelectrolyte multilayers with a tunable young's modulus: influence of film stiffness on cell adhesion. *Langmuir*, 22(3):1193–200, 2006.

[163] N Berthelemy, H Kerdjoudj, C Gaucher, P Schaaf, J-F Stoltz, P Lacolley, J-C Voegel, and P Menu. Polyelectrolyte films boost progenitor cell differentiation into endothelium-like monolayers. *Adv Mater*, 20:2674–2678, 2008.

[164] A Dierich, Erell Le Guen, Nadia Messaddeq, Jean-Francois Stoltz, Patrick Netter, Pierre Schaaf, Jean-Claude Voegel, and Nadia Benkirane-Jessel. Bone formation mediated by synergy-acting growth factors embedded in a polyelectrolyte multilayer film. *Adv Mater*, 19:693–697, 2007.

[165] H A Minges Wols, G H Underhill, G S Kansas, and P L Witte. The role of bone marrow-derived stromal cells in the maintenance of plasma cell longevity. *J Immunol*, 169(8):4213–21, 2002.

[166] S M Graham, H G Jørgensen, E Allan, C Pearson, M J Alcorn, L Richmond, and T L Holyoake. Primitive, quiescent, philadelphia-positive stem cells from patients with chronic myeloid leukemia are insensitive to sti571 in vitro. *Blood*, 99(1):319–25, 2002.

[167] T Holyoake, X Jiang, C Eaves, and A Eaves. Isolation of a highly quiescent subpopulation of primitive leukemic cells in chronic myeloid leukemia. *Blood*, 94(6):2056–64, 1999.

[168] J Larsson, M Ohishi, B Garrison, M Aspling, V Janzen, G B Adams, M Curto, A I McClatchey, E Schipani, and D T Scadden. Nf2/merlin regulates hematopoietic stem cell behavior by altering microenvironmental architecture. *Cell Stem Cell*, 3(2):221–7, 2008.

[169] S K Nilsson, H M Johnston, G A Whitty, B Williams, R J Webb, D T Denhardt, I Bertoncello, L J Bendall, P J Simmons, and D N Haylock. Osteopontin, a key component of the hematopoietic stem cell niche and regulator of primitive hematopoietic progenitor cells. *Blood*, 106(4):1232–9, 2005.

[170] M C Puri and A Bernstein. Requirement for the tie family of receptor tyrosine kinases in adult but not fetal hematopoiesis. *Proc Natl Acad Sci USA*, 100(22):12753–8, 2003.

[171] S M Garrido, F R Appelbaum, C L Willman, and D E Banker. Acute myeloid leukemia cells are protected from spontaneous and drug-induced apoptosis by direct contact with a human bone marrow stromal cell line (hs-5). *Exp Hematol*, 29(4):448–57, 2001.

[172] P Laneuville, C Dilea, O Q P Yin, R C Woodman, J Mestan, and P W Manley. Comparative in vitro cellular data alone are insufficient to predict clinical responses and guide the choice of bcr-abl inhibitor for treating imatinib-resistant chronic myeloid leukemia. *J Clin Oncol*, 28(11):169–71, 2010.

[173] G Benton, J George, H.K Kleinman, and I.P Arnaoutova. Advancing science and technology via 3d culture on basement membrane matrix. *J Cell Physiol*, 221(1):18–25, 2009.

[174] G Y Lee, P A Kenny, E H Lee, and M J Bissell. Three-dimensional culture models of normal and malignant breast epithelial cells. *Nat Methods*, 4(4):359–65, 2007.

[175] M M P Zegers, L E O'Brien, W Yu, A Datta, and K E Mostov. Epithelial polarity and tubulogenesis in vitro. *Trends Cell Biol*, 13(4):169–76, 2003.

[176] I Guest and J Uetrecht. Drugs toxic to the bone marrow that target the stromal cells. *Immunopharmacology*, 46(2):103–12, 2000.

[177] M J Kiel, G L Radice, and S J Morrison. Lack of evidence that hematopoietic stem cells depend on n-cadherin-mediated adhesion to osteoblasts for their maintenance. *Cell Stem Cell*, 1(2):204–17, 2007.

[178] M J Kiel and S J Morrison. Maintaining hematopoietic stem cells in the vascular niche. *Immunity*, 25(6):862–4, 2006.

[179] J A DiMasi, R W Hansen, and H G Grabowski. The price of innovation: new estimates of drug development costs. *J Health Econ*, 22:151–185, 2003.

[180] M Pickl and CH Ries. Comparison of 3d and 2d tumor models reveals enhanced her2 activation in 3d associated with an increased response to trastuzumab. *Oncogene*, 28(3):461–8, 2008.

[181] M Wozniak, R Desai, P Solski, and C Der. Rock-generated contractility regulates breast epithelial cell differentiation in response to the physical properties of a three-dimensional collagen matrix. *J Cell Biol*, 163(3):583–95, 2003.

[182] M Xu, S Barrett, E West-Farrell, and L Kondapalli. In vitro grown human ovarian follicles from cancer patients support oocyte growth. *Hum Reprod*, 24(10):2531–40, 2009.

[183] A Gutierrez-Barrera and D Menter. Establishment of three-dimensional cultures of human pancreatic duct epithelial cells. *Biochem Biophys Res Commun*, 358(3):698–703, 2007.

[184] E Rosines, R Sampogna, K Johkura, D A Vaughn, Y Choi, H Sakurai, M M Shah, and S K Nigam. Staged in vitro reconstitution and implantation of engineered rat kidney tissue. *Proc Natl Acad Sci USA*, 104(52):20938–43, 2007.

[185] A Abbott. Cell culture: biology's new dimension. *Nature*, 424(6951):870–2, 2003.

[186] J Kim. Three-dimensional tissue culture models in cancer biology. *Semin Cancer Biol*, 15(5):365–77, 2005.

[187] S Zhang. Beyond the petri dish. *Nat Biotechnol*, 22(2):151–2, 2004.

[188] M Talpaz, N P Shah, H Kantarjian, N Donato, J Nicoll, R Paquette, J Cortes, S O'Brien, C Nicaise, E Bleickardt, M A Blackwood-Chirchir, V Iyer, T-T Chen, F Huang, A P Decillis, and C L Sawyers. Dasatinib in imatinib-resistant philadelphia chromosome-positive leukemias. *N Engl J Med*, 354(24):2531–41, 2006.

[189] Y Jiang, R C Zhao, and C M Verfaillie. Abnormal integrin-mediated regulation of chronic myelogenous leukemia cd34+ cell proliferation: Bcr/abl up-regulates the cyclin-dependent kinase inhibitor, p27kip, which is relocated to the cell cytoplasm and incapable of regulating cdk2 activity. *Proc Natl Acad Sci USA*, 97(19):10538–43, 2000.

[190] M Savona and M Talpaz. Getting to the stem of chronic myeloid leukaemia. *Nat Rev Cancer*, 8(5):341–50, 2008.

[191] J Zhang, C Niu, L Ye, H Huang, X He, W-G Tong, J Ross, J Haug, T Johnson, J Q Feng, S Harris, L M Wiedemann, Y Mishina, and L Li. Identification of the haematopoietic stem cell niche and control of the niche size. *Nature*, 425(6960):836–41, 2003.

[192] S C Bailey, R Spangler, and A J Sytkowski. Erythropoietin induces cytosolic protein phosphorylation and dephosphorylation in erythroid cells. *J Biol Chem*, 266(35):24121–5, 1991.

[193] T D Richmond, M Chohan, and D L Barber. Turning cells red: signal transduction mediated by erythropoietin. *Trends Cell Biol*, 15(3):146–55, 2005.

[194] E J Baek, H-S Kim, S Kim, H Jin, T-Y Choi, and H O Kim. In vitro clinical-grade generation of red blood cells from human umbilical cord blood cd34+ cells. *Transfusion*, 48(10):2235–2245, 2008.

[195] I Dorn, P Lazar-Karsten, S Boie, J Ribbat, D Hartwig, B Driller, H Kirchner, and P Schlenke. In vitro proliferation and differentiation of human cd34+ cells from peripheral blood into mature red blood cells with two different cell culture systems. *Transfusion*, 48(6):1122–32, 2008.

[196] J Bertino. Cancer research: from folate antagonism to molecular targets. *Best Pract Res Clin Haematol*, 22(4):577–82, 2009.

[197] S Hauser, K Udupa, and David Lipschitz. Murine marrow stromal response to myelotoxic agents in vitro. *Br J Haematol*, 95(4):596–604, 1996.

[198] A Olaharski, H Uppal, M Cooper, S Platz, and T Zabka. In vitro to in vivo concordance of a high throughput assay of bone marrow toxicity. *Toxicol Lett*, 188(2):98–103, 2009.

[199] V C Broudy. Stem cell factor and hematopoiesis. *Blood*, 90(4):1345–64, 1997.

[200] S J Peter, M J Miller, A W Yasko, M J Yaszemski, and A G Mikos. Polymer concepts in tissue engineering. *Journal of Biomedical Materials Research Part B: Applied Biomaterials*, 43(4):422–427, 1999.

[201] D W Hutmacher. Scaffolds in tissue engineering bone and cartilage. *Biomaterials*, 21(24):2529–2543, 2000.

[202] C Andres, V Sinani, D Lee, Y Gun'ko, and N Kotov. Anisotropic calcium phosphate nanoparticles coated with 2-carboxyethylphosphonic acid. *Journal of Materials Chemistry*, 16(3964-3968), 2006.

[203] T M Blanco, A Mantalaris, A Bismarck, and N Panoskaltsis. The development of a three-dimensional scaffold for ex vivo biomimicry of human acute myeloid leukaemia. *Biomaterials*, 31(8):2243–51, 2010.